Permeability and Mechanotransduction in Aging Endothelial Cells

by

Tracy Melissa Cheung

Department of Biomedical Engineering
Duke University

Date:_____
Approved:

_____
George Truskey, Supervisor

_____
Fan Yuan

_____
David Katz

_____
Brenton Hoffman

_____
Eleni Tzima

Dissertation submitted in partial fulfillment of
the requirements for the degree of Doctor
of Philosophy in the Department of
Biomedical Engineering in the Graduate School
of Duke University

2014

ABSTRACT

Permeability and Mechanotransduction in Aging Endothelial Cells

by

Tracy Melissa Cheung

Department of Biomedical Engineering
Duke University

Date:_____
Approved:

_____
George Truskey, Supervisor

_____
Fan Yuan

_____
David Katz

_____
Brenton Hoffman

_____
Eleni Tzima

An abstract of a dissertation submitted in partial
fulfillment of the requirements for the degree
of Doctor of Philosophy in the Department of
Biomedical Engineering in the Graduate School
of Duke University

2014

Abstract

Complications from cardiovascular disease, such as a heart attack or a stroke, represent the leading cause of death in the United States and many developed and developing countries. Atherosclerosis is the primary pathology underlying cardiovascular disease. It is caused by an increase in endothelial cell (EC) permeability, leading to the buildup of cholesterol and lipids which form the atherosclerotic plaque. Accelerated aging in regions of atherosclerosis contribute to the development and progression of the disease. The global hypothesis that motivated this research was that activation of deacetylase antioxidant regulator, Sirtuin1 (SIRT1), improved function in senescent ECs by increasing the integrity of cell-cell junctions. In turn, this led to elevated EC permeability, a decline in the response to shear stress, and elevated traction forces.

Aging of hCB-ECs significantly increased permeability due to changes in tight junction protein localization and phosphorylation. Activation of SIRT1 significantly reduced permeability in aged hCB-ECs and restored junction integrity. ECs under flow also exhibited changes in cell junctions with increasing age. Aged hCB-ECs were less responsive to shear stress, exhibiting lower levels of atheroprotective genes, KLF2 and eNOS. Activation of SIRT1 in aged hCB-ECs restored the response to shear stress by altering localization and phosphorylation of adherens junction protein, VE-cadherin.

The endothelial glycocalyx is a layer of proteoglycans and glycoproteins on the surface of ECs that is important in maintaining EC barrier function. In aging ECs, the glycocalyx was thinner and less dense. However, activation of SIRT1 restored the structure of the glycocalyx, suggesting that the positive effect of SIRT1 on elevated permeability in aged hCB-ECs may also be due to restoration of the glycocalyx. Aged hCB-ECs also exhibited elevated traction forces for measurements done with single cells, cell clusters (2 to 3 cells), and cell monolayers (20 to 30 cells). The elevated traction forces correlated with altered actin localization and increased actin filament thickness. Activation of SIRT1 reduced traction forces and decreased actin stress fiber thickness in aged hCB-ECs, suggesting that the effects of SIRT1 on cell-cell junctions alters binding of junction proteins to the actin cytoskeleton and generation of cell traction forces. Together, these results implicate an important role for SIRT1 in regulating permeability and mechanotransduction in aging endothelium.

Contents

List of Tables

List of Figures

Acknowledgements

Several collaborators have also helped to make this work possible. I would like to thank Dr. Jianyong Huang for his help with traction force microscopy. I would also like to acknowledge all of the undergraduates that I have had the pleasure of working with. Mansi Ganatra, Justin Fu, and Jessica Yan are all undergraduates that have contributed work to this thesis and to my manuscripts. I am grateful for the opportunity to mentor and train these talented individuals.

Finally, I would like to acknowledge my family. I thank my parents, Winnie and Francis, and my brother, Kevin, for supporting me in my decision to go to graduate school to pursue a career in Biomedical Engineering. Thank you for teaching me the values of hard work, integrity, and kindness. I would also like to acknowledge my fiancé James for his support of me throughout our undergraduate and graduate careers. I am excited to see what the future holds for us.

Chapter 1. Introduction.

1.1 Research Overview

Complications from cardiovascular disease, such as heart attack and stroke, represent the leading cause of death in the United States and many developed and developing countries. In 2008, approximately 672,000 people died of heart disease or stroke, which accounts for about 27% of all deaths.[148] While mortality and morbidity is decreasing in the United States,[148] the incidence of the disease is increasing in developed countries such as China and India. Atherosclerosis is the primary pathology underlying heart disease and stroke. The disease is localized to large and medium sized arteries and involves a complex sequence of events in which the accumulation of lipids and cholesterol in the arterial intima initiates an inflammatory response. The result is a thickened intima consisting of lipids, macrophages and smooth muscle cells. The thickened intima can compromise blood flow or rupture, causing a thrombus to form, blocking blood flow and precipitating a heart attack or stroke. The earliest events in the disease process involve changes to the function of endothelium leading to increased adhesion of leukocytes, altered permeability and decreased release of the vasodilator nitric oxide (NO). There are several risk factors for atherosclerosis including age, high cholesterol levels, diabetes, genetics, hypertension, and smoking.[35]

There is evidence of accelerated aging of endothelial cells (ECs) in regions of atherosclerosis. Senescent ECs in these lesion-prone areas exhibit elevated levels of

senescence-associated β-galactosidase [109] and telomere shortening.[123]   In

atherosclerotic regions in both animals and humans, ECs undergo high cell turnover and

are exposed to high levels of oxidative stress, which can lead to replicative senescence

[13, 123] or stress-induced senescence.[54] However, senescent ECs are not found in

arteries that are free of atherosclerosis, suggesting that development of cell senescence is

due to local, rather than systemic, changes.[109] The development of atherosclerosis is

also related to changes in EC function including decreased expression of endothelial

nitric oxide synthase (eNOS) [32, 102] and elevated EC permeability [26, 27], both of

which could be altered by cell senescence.

The major goal of this research was to understand the effect of cell aging on

permeability and mechanotransduction. Further, we sought to identify the role of

deacetylase antioxidant regulator SIRT1 in reversing age-associated phenotypes. SIRT1

levels have been shown to be low at vessel branches, which are regions of low and

oscillating shear stress.[24] These are also regions where the endothelial glycocalyx,

which plays an important role in EC barrier function and nitric oxide (NO) generation, is

degraded.[57, 192] This suggests a possible link between EC mechanosensing and

SIRT1. While the relationship between SIRT1 and cell aging has been well-studied, its

impact on age-associated changes in endothelial cell function is not well understood. A

better understanding of endothelial cell aging and SIRT1 could lead to improved

treatments for atherosclerosis.

The specific aims for this project are to (1) evaluate the effect of cell senescence on albumin permeability of blood-derived endothelial cells, (2) determine a role for SIRT1 in regulating cell mechanotransduction in the aging endothelial cell response to shear stress, and (3) examine the effect of endothelial cell aging on cell traction forces for isolated cells and clusters.

In **Chapter 2**, we addressed Specific Aim 1 by measuring albumin permeability in aging endothelial cells. We used the Transwell permeability assay to measure permeability of young and old hCB-ECs and to compare these with values from human aortic ECs (HAECs). We then examined the role of cell proliferation and changes in cell junction protein expression and localization, as possible reasons for elevated permeability in aged cells. Lastly, we examined how activation of SIRT1 with several agents could alter permeability and cell junctions.

In **Chapter 3**, we addressed Specific Aim 2 by using qRT-PCR to measure change in gene expression as aging ECs were subjected to steady shear stress. Decreased responsiveness in aged ECs was attributed to changes in cell mechanotransduction. We assessed changes in both the structure and function of the glycocalyx and VE-cadherin using immunofluorescence and Western blots. We further established a role for SIRT1 in regulating cell mechanotransduction by using activators and inhibitors, as well as by using transient siRNA transfection to knockdown SIRT1. Upon altering SIRT1, we

subsequently examined changes in the response to shear stress as well as changes to the glycocalyx and VE-cadherin.

In **Chapter 4**, we addressed Specific Aim 3 by examining changes in isolated EC traction forces with increasing age. We then examined how increased traction forces in aged ECs correlated with changes in the actin cytoskeleton and elevated permeability. Furthermore, we examined the role of SIRT1 in reversal of age-associated increase in traction forces by treating ECs with activators and inhibitors of SIRT1 and then monitoring changes in traction forces and actin.

In **Chapter 5,** we further addressed Specific Aim 3 by examining changes in EC traction forces for clusters of cells and confluent monolayers. We compared these values with those obtained for isolated cells. The effect of different SIRT1 treatments was then evaluated for cell clusters. We further examined the role of actin and RhoA, a protein important in cell contractility, in age-associated changes in traction forces.

In **Chapter 6**, we summarize the main results and conclusions from this work. We also discuss future directions and implications of this work.

1.2 Role of Endothelium in Maintaining Tissue Homeostasis
1.2.1 Function of Endothelial Cells in Blood Vessel

Endothelial cells comprise the inner lining of blood vessels. They are surrounded by a layer of smooth muscle cells, which aid in vessel dilation and constriction. ECs form a barrier between the blood and other layers of the blood vessel,

thereby regulating transport of molecules across the endothelium. ECs are also important in blood clotting and inflammation responses. Specific cell surface markers including CD34, von Willebrand factor, and VE-cadherin can be used to characterize and identify ECs. The presence of these markers can be verified with either flow cytometry or immunofluorescence.

1.2.2 Influence of Vascular Geometry on Endothelial Cell Function and Atherogenesis

Vascular geometry influences the local flow properties and the initiation of atherosclerosis.[117] Atherogenesis tends to occur at specific locations, such as vessel branches and regions of curvature, in the blood vessel. In these areas, there is significant variation in flow fields and shear stress [91, 117] and lesion formation and intimal thickening are correlated with low and oscillating shear stresses that change direction.[92].. ECs in these regions are polygonal in shape and are prone to express adhesion molecules for leukocytes and release cytokines, which promotes the development of atherosclerosis.[33] In contrast, regions away from branches or regions of curvature are exposed to a unidirectional pulsatile shear stress.[117] The ECs are quiescent and express proteins that limit platelet and leukocyte adhesion and are anti-inflammatory.[38] A number of factors influence the development of atherosclerosis including biomechanical changes to the cell after exposure to uniform and laminar shear, fluid flow types, and the interaction of local hemodynamics and risk factors.

1.2.3 Transport in the Endothelium

The endothelium plays an important role in regulating water and macromolecular transport, leukocyte adhesion and transmigration, vessel remodeling, apoptosis, generation and metabolism of biochemical substances, and modulation of smooth muscle cell (SMC) function and proliferation [36]. Endothelial cells (ECs) respond to mechanical forces such as shear stress by modulating signaling pathways and overall cell function.[31] As a result, the local hemodynamics impact EC vascular homeostasis and influence the development of atherosclerosis. Transport of monocytes by arterial fluid dynamics and subsequent adhesion to activated endothelium may also influence the location of atherosclerotic lesions.[164]

An increase in the permeability of the endothelial layer to proteins influences the development and progression of atherosclerosis.[118, 157] Localized sites of elevated endothelial permeability occur at lesion-prone regions of arteries prior to the onset of atherosclerosis.[79] Such sites of increased permeability likely represent increased transport through endothelial cell junctions.[20, 79, 157]

1.2.4 EC Dysfunction Near Atherosclerotic Lesions

There are a number of changes that occur to blood vessel ECs during atherosclerosis including increased adhesion of leukocytes, altered permeability, disintegration of the glycocalyx,[57, 192] and decreased release of the vasodilator nitric oxide (NO). The glycocalyx plays an important role in maintaining the endothelial

6

barrier and regulating levels of NO, which are important in maintaining EC function.[57, 192] Additionally, ECs in regions prone to develop atherosclerosis experience high cell turnover and high oxidative stress, which leads to replicative senescence and stress-induced senescence. When ECs in the arterial endothelium undergo senescence, they become larger, are unable to divide, resist apoptosis, and contribute to a loss of tissue homeostasis,[17] which can ultimately lead to cardiovascular disease development.   In these regions, the glycocalyx is less abundant. While higher oxidative stress alters the glycocalyx in young ECs, changes to the glycocalyx during cell senescence are not understood.

1.2.5 Role of SIRT1 in Regulating EC Permeability

Both gene and protein expression levels of deacetylase SIRTUIN1 (SIRT1) have been shown to be reduced in senescent ECs [199]. In contrast, the protein levels of LKB1, a serine/threonine kinase and tumor suppressor, and the phosphorylation of its downstream target AMPK(Thr172) were are high in senescent cells. Overexpression of LKB1 or hyperphosphorylation of AMPK (Thr172) promoted cellular senescence and decreased endothelial proliferation.[199]

In primary porcine aortic endothelial cells [199], human embryonic kidney 293T cells [95], and mouse liver cells,[95] the deacetylase SIRTUIN1 (SIRT1) promoted proliferation and prevents senescence by downregulation and deacetylation of liver kinase B1 (LKB1), a serine/threonine kinase and tumor suppressor.   Senescence could be

7

reversed by knocking down LKB1 with siRNA or by downregulating LKB1 via activation of SIRT1 with Resveratrol.[199] Reversal of senescence via these pathways also increased EC proliferation.[199] Knocking down of SIRT1 induced senescence and elevated the protein levels of LKB1 and phosphorylated AMPK(Thr172).
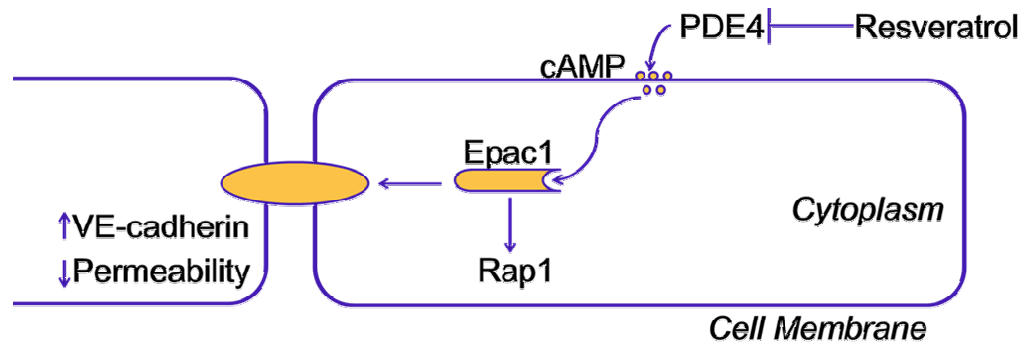
Figure 1: Resveratrol inhibits PDE4 to activate the Epac1-Rap1 pathway.   This increases junctional VE-cadherin and a subsequent decrease in permeability.

Resveratrol indirectly activates SIRT1 via competitive inhibition of cAMP-degrading phosphodiesterases.[128] Elevated levels of membrane-associated cAMP activate the cyclic AMP-regulated guanosine nucleotide exchange factor Epac1 which, in turn, leads to guanosine triphosphate (GTP) binding to the small G protein Rap1 [128]. GTP bound Rap1 activates SIRT1 but also causes changes to the cortical cytoskeleton and organization of VE-cadherin in the endothelial junctions [42], leading to reduced endothelial permeability.[59]   Thus, changes that occur during cell aging which affect the pathway leading to SIRT1 activity may also elevate permeability through endothelial junctions.

1.3 Blood-Derived Endothelial Cells

Late-outgrowth endothelial progenitor cells (EPCs) derived from umbilical cord blood (hCB-ECs) are a suitable model to study cell aging because these cells undergo a significant number of population doublings in vitro and their permeability is close to values for large artery permeability in vivo.[1, 11] Additionally, these cells express EC molecular markers and no markers for monocytes or macrophages, and respond to flow in the same manner as large vessel endothelium.[1, 11] ECs that possess the high proliferative potential of late-outgrowth EPCs can be isolated from arterial endothelium.[11, 80, 89] Progenitor cells from young animals injected into older animals preferentially localize to sites of endothelial dysfunction and reverse atherosclerosis in older animals.[138] This result suggests that a decline in progenitor cell adhesion, incorporation into the endothelium and function with age may influence the onset and progression of atherosclerosis. Further, endogenous bone marrow-derived circulating EPCs adhere to sites of acute endothelial injury, such as vein grafts.[190, 197]

1.4 Response of Endothelium to Steady Unidirectional Flow

1.4.1 Unidirectional Shear Stress Causes Rearrangement of Cell Cytoskeleton

In vitro, exposure of confluent endothelial cells to steady or unidirectional shear stress induces a change in shape and orientation such that the cells are elongated and aligned in the direction of flow.[44] Such EC organization is observed *in vivo* away from

vessel branches whereas around vessel branches, ECs exhibit a rounder shape without any preferred orientation.[44] The endothelial cell actin cytoskeleton reorganizes in response to shear stress, aligning in the direction of flow. Prominent actin stress fibers appear [58] and cell proliferation is inhibited.

The dynamic response to shear stress reflects the different signaling pathways activated by fluid shear stress. Within 15 seconds of application of shear stress, a complex is formed in endothelial cell junctions involving VE-cadherin, platelet-endothelial cell adhesion molecule (PECAM) and vascular endothelial growth factor receptor 2 (VEGFR2).[166] After binding VEGF, VEGFR2, as part of the mechanotransduction complex, binds to phosphatidylinositol-3-OH kinase (PI(3)K) which activates integrins initiating responses such as Jun NH2-terminal kinase (JNK) activation, nuclear factor κB (NFκB) activation and nuclear translocation [68] which then leads to expression of adhesion molecules for leukocytes and secretion of MCP-1. PI(3)K also activates the protein kinase B or Akt which leads to activation of NOS III and other early anti-inflammatory responses. In addition to transient pro-inflammatory activity, JNK is phosphorylated and localizes to focal adhesions. There, the JNK focal adhesion complex promotes EC alignment under unidirectional shear stress.[70]

The longer-term response to shear stress takes several hours or days and involves activation of the mitogen activated protein kinase 5 (MEK5) by transient increases in reactive oxygen species. In turn, MEK5 phosphorylates extracellular signal-

regulated kinase 5 (ERK5) which then activates the transcription factor myocyte

enhancement factor 2(MEF2).[130]   In turn, MEF2 promotes KLF2 expression. Further,

KLF2 expression and Nuclear Factor-like 2 (Nrf2) produce antioxidants that control the

intracellular levels of ROS, limiting activation of NFκB.[119] The PECAM/VE-

Cadherin/PI(3)K and MEK/ERK5/MEF2 pathways activated by shear stress intersect in

several ways to modulate the response to flow. Shear mediated activation of PI(3)K and

Akt leads to the activation of Nrf2[43] which influences KLF2 activation.[84]   KLF2

regulates actin cytoskeleton organization which regulate the level of JNK and its

downstream mediators, thereby limiting the pro-inflammatory response of steady and

pulsatile shear stress.[8]

1.4.2 Unidirectional Flow and Shear Stress Promote an Anti-Thrombotic and Anti-Inflammatory Phenotype

A key physiological response to flow *in vivo* is the release of NO, which causes

vessel dilation. NO is produced in ECs by endothelial nitric oxide synthase (eNOS or

NOS III) [15]. NO diffuses to smooth muscle where it acts upon soluble guanylate

cyclase to alter production of cyclic GMP that decreases the activity of myosin light

chain kinase, causing relaxation of the muscle. When ECs are exposed to steady or

pulsatile unidirectional shear stress, NO production increases due to a change in the

activity of NOS III followed by a sustained increase in NOS III levels.[75] Changes in

brachial artery dilation are used to assess endothelial dysfunction in early

atherosclerosis.[71] In addition to serving as a potent vasodilator, NO inhibits

expression of monocyte chemoattractant protein-1 (MCP-1) and vascular cell adhesion

molecule-1 (VCAM-1), prevents SMC proliferation, and decreases platelet

aggregation.[127]

The zinc-finger transcription factor Kruppel-like factor 2 (KLF-2) is a key

regulator of oxidative and inflammatory responses to shear stress.[46, 130] This

transcription factor is expressed by endothelial cells but not expressed by SMC in

mature blood vessels.[46] KLF-2 exhibits continued high levels of expression after 7 days

exposure to a pulsatile shear stress of 1.2 Pa in vitro [46] due to stabilization of mRNA

levels by shear stress [171] and down-regulation of microRNA-92 which inhibits KLF-2

protein levels.[187] KLF-2 induces NOS III and the anti-thrombotic molecule

thrombomodulin, and inhibits cytokine-induced expression of VCAM-1 and E-selectin,

but does not affect cyclooxygenase 2, which is involved in PGI_2 production.[152] KLF-2

overexpression blocks VCAM-1 and E-selectin expression by blocking activation of

NFκB.

1.4.3 Shear Stress Regulates Metabolic Activity

A key regulator of metabolic activity sensitive to shear stress is SIRTUIN1

(SIRT1) that deacetylates proteins that regulate antioxidant activity and energy balance,

promotes proliferation, and prevents senescence. Steady and pulsatile shear stress of 1.2

Pa increase SIRT1 levels and mitochondrial biosynthesis.[23] Shear stress also elevates

adenosine monophosphate (AMP)-activated protein kinase (AMPK), which regulates

energy metabolism and facilitates the ability of SIRT1 to activate NOS III [23].

Interestingly, SIRT1 elevates KLF2 levels providing an important regulatory loop that

promotes an anti-oxidative environment and limit cell aging when ECs are exposed to

unidirectional shear stress.[65]

The application of shear stress causes a number of very rapid changes including

ion channel opening, production of reactive oxygen species (ROS), activation of G

proteins and focal adhesion movement.[44]   Potential mechanisms initiating these

processes likely involve the glycocalyx, a soft layer of proteoglycan on the cell surface;

primary cilia which extend from the endothelial cell surface; cytoskeleton deformation

and focal adhesions.[45] However, the manner by which the applied stress is translated

into a chemical signal has yet to be established.

1.5 Response of Aged ECs to Fluid Shear Stress

Aging at the cellular level is associated with replicative senescence or stress-

induced senescence. For replicative senescence, the cell doubling time increases and

ultimately ceases with increasing cell age due to telomere shortening which protects

against genetic mutation.[53] Stress-induced senescence is primarily caused by

environmental stresses such as intracellular oxidative stress, DNA damage by radiation,

or chromatin decondensation. Endothelium at lesion-prone sites and on advanced

lesions show signs of advanced aging, including elevated levels of β-galactosidase, a

histochemical marker for senescence,[108] and telomere shortening.[122] ECs near

atherosclerotic lesions often experience high cell turnover and high levels of oxidative stress, induced by a combination of the reversing oscillatory flow and presence of risk factors for cardiovascular disease.

Cell energy metabolism is altered during senescence. In particular, levels of SIRT1 are reduced which also reduces a number of anti-thrombotic and anti-inflammatory genes.[53] NO release is impaired as ECs age and NOS III production induced by shear stress is reduced in senescent human ECs [102]. Following exposure to TNFα or short periods of shear stress, senescent ECs exhibit greater monocyte adhesion than do younger ECs.[102] When levels of human telomerase, a reverse transcriptase, are elevated in late passage human ECs, NOS III levels are increased and monocyte adhesion is reduced. Previous studies have shown that drugs that activate the Sirtuins activate eNOS through a cAMP/PKA- and PI3K/Akt-dependent pathway by inducing the phosphorylation of eNOS at Ser1177.[125, 134] NO has also been shown to activate the SIRT1 promoter in white adipose tissue.[120] Additionally, SIRT1 deacetylates and activates the eNOS enzyme [103], indicating that a positive feedback mechanism exists between these two key signaling molecules.

Elevating SIRT1 levels reverses EC senescence. Resveratrol has been used to reduce age-associated metabolic phenotypes [129] and it may mitigate symptoms associated with atherogenesis. Resveratrol acts upon SIRT1 via competitive inhibition of phosphodiesterase 4 which causes elevated cAMP levels.[129] The resulting elevation of

cAMP activates effector protein Epac1, and sequentially increases Rap1, intracellular

Ca^{2+} and activates the CamKKβ-AMPK pathway to activate SIRT1.[129] Elevated cAMP

levels cause a decrease in endothelial permeability by activation of protein kinase A

which then inactivates myosin light chain kinase [105] or activates Epac-mediated

Rap1.[59] Further, membrane associated cAMP bound to Epac1 interacts with

phosphodiesterase 4, to bind to VE-cadherin [137] and regulates endothelial

permeability by redistributing tight junction molecules to cell junctions.[42] Given the

shear stress sensitivity of SIRT1 and VE-cadherin, shear stress should influence EC

senescence.

Studies suggest that there are similarities between exposure to shear stress and

aging.   Cyclin-dependent kinase inhibitor 2A and 2B, which reduce cell proliferation,

are elevated by both aging and exposure to 1.2 Pa shear stress for 24 hours.[114]

Expression of NADPH oxidase 4 is reduced by unidirectional shear stress and aging.

NADPH oxidase 4 promotes production of oxygen radicals, and a reduction in the level

of this enzyme protects the aging ECs from oxidative damage. This is offset by a

reduction in aging cells of NOS III and argininosuccinate synthetase 1; the levels of these

enzymes are elevated by shear stress in older ECs, although to a less extent than

younger cells.[114] Argininosuccinate synthetase 1 catalyzes the rate-limiting step of

arginine biosynthesis and can regulate NO release and monocyte adhesion independent

of NOS III levels.[113] Increased monocyte adhesion in older ECs exposed to TNFα is

due to a reduction in NO release and an increase in the expression of CD44, which can

bind to leukocytes, but not to changes in the levels of leukocyte adhesion molecules

VCAM-1, ICAM-1and E-selectin.[112] Interestingly, CD44 levels are not affected by

exposure of older ECs to shear stress.[112]

There is evidence that EPCs from elderly patients can become more responsive to

shear stress through activation of specific pathways, such as the CXCR4/Janus kinase

pathway.[189] Peripheral blood late-outgrowth EPCs that are isolated from elderly

patients have decreased migration and adhesion *in vitro* and reduced reendothelization

in vivo in nude mice with carotid artery denudation injury.[189] However, when the

EPCs are pretreated with 15 dynes/cm^2 shear stress for 12 hours, there is enhanced

migration, adhesion, and reendothelization. The authors show that upregulation of the

CXCR4/Janus kinase pathway under shear stress may play a role in the improved

function of the EPCs from elderly individuals.[189] Additionally, loss of function of

transient receptor potential cation channel subfamily V member 4 (TRPV4) gene in ECs

has also been shown to decrease response to shear stress by decreasing vasodilation.

TRPV4 is involved in the synthesis of nitric oxide and in endothelium-derived

hyperpolarizing factor (EDHF) signaling.[76]

16

1.6 Endothelial Glycocalyx

1.6.1 Composition

The glycocalyx is composed of membrane-bound glycoproteins on the surface of endothelial cells and is important in regulating the endothelial barrier [78, 183] and the response to shear stress.[57, 111, 192] The glycocalyx consists of glycoproteins bearing acidic oligosaccharides with terminal sialic acids (SA), and proteoglycans with associated glycosaminoglycans of heparan sulfate, chondroitin sulfate, and hyaluronic acid.

1.6.2 Endothelial Glycocalyx in Disease Development

Changes in the glycocalyx in both microvasculature and microvasculature have been shown to lead affect disease development. Disruption of the glycocalyx in capillaries will increase the permeability of capillary beds.[150] If this occurs in the glomerulus of the kidneys, it can lead to albuminuria.[150] Increased systemic microvascular permeability, which can lead to ischemia and diabetes, is also a possible consequence of endothelial glycocalyx disruption.[150] Disintegration of the glycocalyx also leads to cardiovascular pathologies, including atherosclerosis.[168]

1.6.3 Role of Glycocalyx in Mechanosensing

Nature Reviews | Molecular Cell Biology
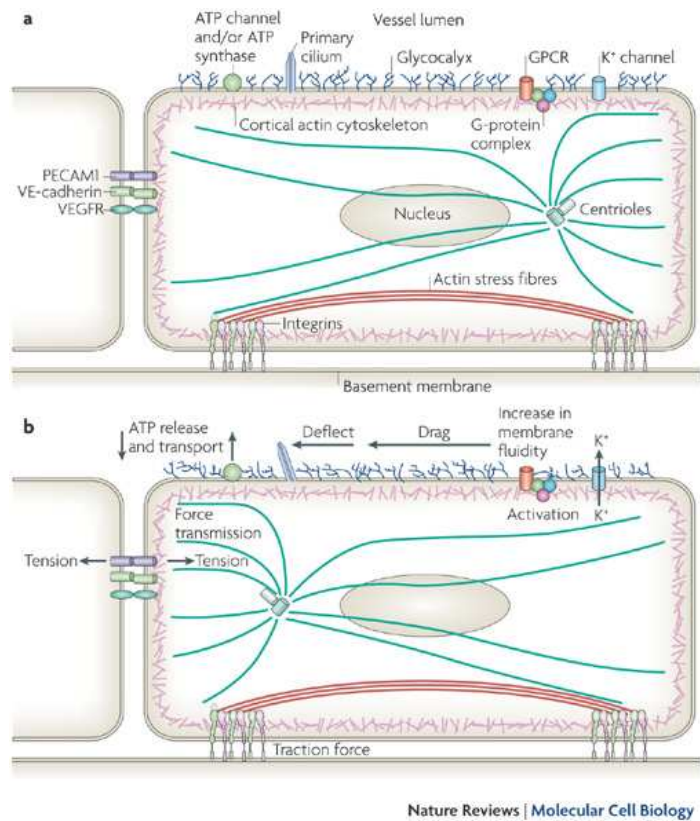
Figure 2: Cell under A) static and B) flow conditions. Glycocalyx experiences drag under flow conditions, which also affect ATP generation. Tension is transmitted to the lateral borders and basal membrane, where adhesion receptors, such as VE-cadherin or integrins, experience changes in tension. Adapted from Hahn et al (2009).

Heparan sulfate has been previously shown to co-localize with VE-cadherin at the periphery of the cell for ECs exposed to shear stress.[192] Degradation of heparan sulfate blocked shear-induced VE-cadherin junctional localization and led to an increase in cell migration and proliferation.[192] Enzymatic degradation of sialic acid, heparan sulfate, and hyaluronic acid from the surface of bovine aortic endothelial cells blocked shear-induced NO production.[126] Heparan sulfate is a primary component of the

18

glycocalyx and acts as a mechanosensor by mediating NO production in response to

shear stress.[57] Furthermore, heparan sulfate-matrix interactions are involved in

regulating cell migration when cells are exposed to shear stress.[111] Other components

of the glycocalyx, including syndecan-1 and glypican-1, have been shown to be

important in mechanotransduction. Syndecan-1 is a transmembrane protein linked to

the cytoskeleton. Knockdown of syndecan-1 induces a pro-inflammatory state [172] and

prevents activation of RhoA.[172]. Glypican-1 is a protein present on the surface of the

ECs that regulates the activation of eNOS by fluid shear stress.[50] For ECs under flow,

the cell experiences drag from the glycocalyx. This tension at the surface of the cell is

transmitted to the lateral borders and the basal membrane, where adhesion receptors,

such as PECAM, VE-cadherin, or integrins, experience changes in tension.[69] ECs

exposed to laminar, uniform, unidirectional shear stress for at least 24 hours are known

to realign and elongate along the direction of fluid flow.[48, 144] When ECs are treated

with heparinase, an enzyme that degrades heparan sulfate, there is no realignment of

ECs in the direction of flow.[192] Knockdown of syndecan-1 also prevents cytoskeleton-

dependent alignment of ECs after exposure to shear stress.[50] Furthermore, VE-

cadherin does not redistribute to cell-cell junctions after treatment with heparinase

suggesting that heparan sulfate and VE-cadherin interact for cytoskeletal rearrangement

after EC exposure to flow.[192] It is likely that the role of the endothelial glycocalyx in

aging endothelial cells is important because of its function as a mechanosensor and its role in regulating permeability.

1.6.4 Visualization of Glycocalyx

Visualization of the glycocalyx is important to establish its presence and exact role in disease development. There are several methods that have been used to detect the glycocalyx including immunofluorescence staining and transmission electron microscopy (TEM).[143] Components of the glycocalyx, such as heparan sulfate, can be labeled with antibodies and visualized on the confocal microscope. One drawback to this technique is the dehydration of the tissue during aldehyde fixation, limited resolution of the confocal microscope to tenths of micrometers, and glare from fluorescent labels.[51] Another drawback of immunofluorescence staining is that antibodies label specific components of the glycocalyx and the antibodies used varies in the literature.[51] Heparan sulfate antibodies (US Biological) are commonly used to measure the glycocalyx thickness and density. However, antibodies for heparan sulfate core proteins, such as perlecan, have also been used as a measure of glycocalyx thickness and density.[77] While perlecan is a basement membrane protein, it has been shown to be secreted to the luminal endothelial cell surface.[72] Methods for immunofluorescence of the glycocalyx typically use low percentages (~2%) of formaldehyde for fixation to minimize damage to the glycocalyx.[50, 192, 195]

In conventional TEM, live cells or tissue are prepared for microscopy by aldehyde fixation followed by alcohol dehydration. Because the glycocalyx is very delicate and easily disturbed, this type of sample preparation can compromise the integrity of the layer leading to discrepancies in results.[51] Ebong et al have described measurement of the endothelial glycocalyx using rapid freezing/freeze substitution (RF/FS) TEM to preserve the structure.[51] This technique involves aldehyde fixation and then rapid freezing using a liquid nitrogen slam freezer. The frozen vitrified liquid is then replaced with acetone. Thin 80nm sections are then cut in the sample and imaged with TEM. The group measured a glycocalyx thickness of 11µm in the macrovascular bovine aortic endothelial cells.[51] This value is much closer to values reported for large arteries *in vivo*. Results from the work indicate that the elimination of the alcohol dehydration steps traditionally used in TEM leads to a better preserved glycocalyx. A drawback of RF/FS TEM is that individual components of the glycocalyx cannot yet be labeled. However, it is possible that a technique could be developed to use a metal, like gold, to label components for imaging on the TEM that would allow researchers to better study individual glycocalyx components.

Another promising technique to visualize the glycocalyx, especially for *ex vivo* and *in vivo* samples, is two-photon microscopy. The use of two photons of longer wavelengths, will allow for better penetration depth of the tissue, better resolution,

optical sectioning, and low phototoxicity. Additionally, the technique can be used *in vivo* to visualize dynamic changes in the glycocalyx in large vessels.[104]

1.7 Endothelial Cell Traction Forces

The spatial distribution of forces a cell exerts on its substrate can be measured using Traction Force Microscopy. To measure these forces, cells are seeded onto either gels containing fluorescent beads [141] or PDMS microposts.[154] Confocal images are taken of the cells before and after cell removal by trypsin. The displacement of either the beads or microposts is used to calculate the spatial distribution of tractions across the cell.

Traction forces in endothelial cells play a role in cell migration and adhesion with forces being highest at the ends of the pseudopodia.[141] Age-related intimal stiffening of bovine aortic endothelial cells has been shown to increase cell traction forces. This result also correlated with increased actomyosin cell contractility. Traction forces were also higher for stiffer substrates, which correlated with an elevated permeability of stiff substrates. This suggests that cell stiffening can alter traction forces and permeability.[87]

Endothelial cells exert stress on the substrate and on neighboring cells through the linkages formed by the cytoskeleton connections to integrins bound to their extracellular matrix protein ligands. Stresses between individual cells and substrate depend upon the type and amount of extracellular matrix ligand and the elasticity of the

substrate. In spite of the nonuniform distribution of traction stresses, confluent layers of

ECs exhibit a uniform distribution of intracellular tension.[86] After exposure to flow

for 16 hours, the EC traction force was slightly greater for cells exposed to steady shear

stress than for cells under static conditions or exposed to a recirculating flow.[161]

Steady flow also caused the surface traction force vectors to align in the direction of

flow, whereas the surface traction force vectors exhibited no preferred direction for cells

under static conditions or exposed to the recirculating flow. These differences in the

traction forces in response to unidirectional shear stress led to greater intercellular forces

that were associated with increased levels of endothelial junction proteins. After 24

hours exposure to unidirectional flow, significant anisotropy in intracellular tension

arose, with higher values normal to the direction of flow, possibly reflecting the

reorganization of the cytoskeleton.[86] Interestingly, the tension induced by shear stress

is much less than the intracellular tension, suggesting that while changes to the

intracellular tension are initiated by shear stress, the magnitude of the intracellular

tension reflects biochemical changes within the cell [86] as well as cell-cell and cell-

substrate interactions.

1.8 Motivation and Significance

There are several important risk factors for the development of atherosclerosis

and cardiovascular disease, including age, genetics, and lifestyle. While regions of

atherosclerosis contain cells that have undergone accelerated aging, the relationship

between the two remains unclear. The motivation of this work is to better understand

how cell senescence affects both the structure and function of different components of

the cell. Furthermore, we seek to find feasible targets that can reverse age-associated

phenotypes in aging ECs. Current models for studying vascular endothelium include

aortic ECs from either human or bovine sources. However, these cell sources are limited

by the number of population doublings they can undergo. Human cord blood-derived

endothelial cells (hCB-ECs) represent a promising source for studying cell aging because

of their high proliferative potential in subconfluent cultures and their low, physiological

permeability. Development of this aging model will allow others to studying EC aging

and treatments for age-associated diseases. In this work, we also elucidate the role of

SIRT1 in regulating permeability, cell mechanotransduction, and cell contractility.

SIRT1 may be a potential target for therapies that aim to reduce or reverse age-

associated pathologies.

1.9 Specific Aims

This research aims to better understand the effect of cell aging on EC

permeability and mechanotransduction. We hypothesize that 1) aged ECs will exhibit

increased permeability due to changes in tight junction protein expression and

localization, and increased senescence, 2) aged ECs have a decreased expression of

atheroprotective genes KLF2 and eNOS due to altered mechanotransduction, and 3)

aged ECs exhibit increased cell traction forces caused by alterations to actin. Specific

Aims to address this hypothesis are:

Specific Aim 1: Evaluate effect of cellular senescence on albumin permeability of blood-derived endothelial cells

The goal of this aim is was to measure permeability in aging cord blood-derived

endothelial cells and to compare these values with those from human aortic endothelial

cells. We hypothesized that increased cell age would lead to increased permeability due

to changes in cell junctions. Albumin permeability across low passage hCB-EC and

human aortic endothelial cells (HAECs) monolayers were be measured using Transwell

membranes. The expression and localization of tight junction protein occludin, ZO-1,

and ZO-2, and tyrosine phosphorylation of occludin in hCB-ECs and HAECs were

investigated as the basis for the difference in permeability. Rates of proliferation and

mitosis were also be determined in both cell types. To age the cells in culture, hCB-ECs

will be passaged (1:10 split). hCB-ECs of >44 population doublings will be compared to

hCB-ECs of < 31 population doublings in terms of permeability measurements and

junction protein expression.   Cell age was confirmed using a telomerase assay. High

passage hCB-ECs were treated with activators SIRT1 to determine whether the elevated

permeability levels can be reduced by reducing cellular senescence.

Specific Aim 2: Evaluate effect of glycocalyx on aged cell response to flow.

The goal of this aim is to determine how EC aging affects cell

mechanotransducers and the response to shear stress. We hypothesized that EC aging

and senescence alters both the structure and function of the glycocalyx and VE-cadherin

to alter the response of ECs to shear stress. Young and old ECs derived from late

outgrowth hCB-ECs in umbilical cord blood were subjected to unidirectional,

physiological shear stress. Using immunofluorescence, we determined whether changes

in glycocalyx composition affect VE-cadherin localization and VE-cadherin organization.

We also assessed whether changes to the glycocalyx are associated with the altered

response to shear stress in aged ECs. qRT-PCR for KLF2 and eNOS gene expression

levels were used to show whether treatment with how treatments that affect SIRT1 alter

the response to flow. We used immunofluorescence and Western blots to further

investigate whether improvements in the response to flow are due to changes in the

glycocalyx or VE-cadherin organization.

Specific Aim 3: Examine the effect of aging on cell traction forces.

The goal of this aim is to determine how cell aging alters EC traction forces for

isolated ECs and clusters of ECs. We hypothesize that aging will have increased traction

forces due to changes in actin. Traction force microscopy was used to measure cell

traction forces and immunofluorescence will be used to measure changes in actin.

Western blots will be used to detect changes in RhoA with increased cell age. We will

also use different activators and inhibitors, as well as knockdown, of SIRT1 to determine

its role on cell traction forces and actin. We will further determine the role of the

endothelial glycocalyx on regulating cell traction forces, because both are important in

maintaining low permeability levels in endothelial monolayers.

Chapter 2. Effect of Cellular Senescence on Albumin Permeability of Blood-Derived Endothelial Cells.

2.1 Introduction

The vascular endothelium plays a key role in the regulation of transport of macromolecules and water into tissues and blood vessels. An increase in the permeability of the endothelial layer to proteins influences the development and progression of atherosclerosis [118, 157]. Localized sites of elevated endothelial permeability occur at lesion-prone regions of arteries prior to the onset of atherosclerosis [79]. Such sites of increased permeability likely represent increased transport through endothelial cell junctions [20, 79, 157].

As cells age, morphological and physiological changes occur that may alter macromolecular transport and subsequent disease development. Aging at the cellular level is associated with replicative senescence or stress-induced senescence [54]. Senescent cells become more frequent in aging individuals, exhibit an altered phenotype, contribute to a loss of tissue homeostasis, and play a role in the development of age-associated pathologies [17]. Elevated levels of β-galactosidase, a histochemical marker for senescence, have been found in atherosclerotic lesions [109]. Because endothelial cells at sites that develop atherosclerosis often experience high cell turnover, endothelial cells in these regions exhibit greater replicative senescence [13, 123] that may be linked to altered permeability. Additionally, environmental stresses in atheroprone regions of blood vessels may induce premature senescence [54].

The deacetylase SIRTUIN1 (SIRT1) promotes proliferation and prevents senescence by targeting liver kinase B1 (LKB1), a serine/threonine kinase and tumor suppressor, in primary porcine aortic endothelial cells [199]. Senescence can be reversed by knocking down LKB1 with siRNA or by downregulating LKB1 via activation of SIRT1 with Resveratrol [199]. Resveratrol indirectly activates SIRT1 via competitive inhibition of cAMP-degrading phosphodiesterases [128]. Elevated levels of membrane-associated cAMP activate the cyclic AMP-regulated guanosine nucleotide exchange factor Epac1 which, in turn, leads to guanosine triphosphate (GTP) binding to the small G protein Rap1 [128]. GTP bound Rap1 activates SIRT1 but also causes changes to the cortical cytoskeleton and organization of VE-cadherin in the endothelial junctions [42], leading to reduced endothelial permeability [59]. Thus, changes that occur during cell aging which affect the pathway leading to SIRT1 activity may also elevate permeability through endothelial junctions.

Endothelial cells (ECs) derived from late outgrowth endothelial progenitor cells (EPCs) in human umbilical cord or adult blood represent a promising source of endothelium for applications in regenerative medicine [1, 11, 12]. These cells express many of the molecular markers found on large vessel endothelium [11, 80, 89], and respond to flow in the same manner as large vessel endothelium [1, 11]. ECs that possess the high proliferative potential of late-outgrowth EPCs can be isolated from arterial endothelium [88]. Circulating EPCs do not appear to contribute significantly to the

endothelium overlying atherosclerotic lesions [67]. Progenitor cells from young animals

injected into older animals preferentially localize to sites of endothelial dysfunction and

can reverse atherosclerosis in older animals [138]. This result suggests that a decline in

progenitor cell adhesion, incorporation into the endothelium and function with age may

influence the onset and progression of atherosclerosis. Further, endogenous bone

marrow-derived circulating EPCs adhere to sites of acute endothelial injury, such as vein

grafts [190, 197].

In this study, we tested the hypotheses that (1) human endothelial cells derived

from endothelial progenitor cells isolated from umbilical cord blood (hCB-ECs) (hCB-

ECs) exhibited low permeability which increased as the hCB-ECs age and undergo

senescence and that (2) the change in permeability of hCB-ECs is due to changes in tight

junction protein localization and the activity of Epac1 [59]. To address these hypotheses,

we determined the permeability to the serum protein albumin of hCB-ECs, and assessed

the extent to which cell replication, occludin expression and phosphorylation, and cell

age influence permeability differences of hCB-ECs and human aortic ECs (HAECs). We

also examined the effect of agents that specifically activate Epac1 and SIRT1 upon the

permeability in late passage hCB-ECs.

2.2 Methods and Materials

2.2.1 Cell Culture

Human umbilical cord blood derived endothelial cells (hCB-ECs) and human

adult peripheral blood derived endothelial cells (hPB-ECs) were isolated from blood as

previously described by Ingram et al [89]. For isolation of hCB-ECs, umbilical cord blood

was obtained from the Carolina Cord Blood Bank (n=5). Prior to receipt, all patient

identifiers were removed. For isolation of hPB-ECs, peripheral blood samples were

obtained from young healthy, non-smoking volunteers taking no medicine (n=1). The

Duke University Institutional Review Board approved the protocol for collection and

use of human blood employed in this study.

After collection, blood was diluted 1:1 with Hanks Balanced Salt Solution (HBSS,

Invitrogen), placed onto Histopaque 1077 (Sigma), and centrifuged at 740x*g* for 30

minutes. Buffy coat mononuclear cells were collected and washed three times with

"complete EC growth medium," comprising 8% (vol/vol) fetal bovine serum (FBS)

added to Endothelial Basal Media-2 (Cambrex) supplemented with Endothelial Growth

Media-2 SingleQuots (containing 2% FBS plus growth factors, Cambrex), and 1%

antibiotic/antimycotic solution (Invitrogen). Mononuclear cells were plated on plastic 6

well 35 mm diameter plates coated with collagen I (rat tail, BD Biosciences) in complete

EC growth medium. Medium was exchanged every 24 hours for the first week in

culture, to remove non-adherent cells. Colonies of EPC-derived ECs appeared 7-10 days

after the initial isolation. The colonies were trypsinized and 200 cells were plated onto a collagen-coated T-25 and labeled passage 1.

Human aortic endothelial cells (HAECs) were obtained from Cambrex/Lonza. HAECs were obtained at passage 3 and, as noted by the supplier, had undergone 17 total population doublings at the time of purchase. HAECs were also cultivated in complete EC growth medium.

The hCB-ECs, hPB-ECs and HAECs were grown separately in T75 flasks using MCDB131 growth media supplemented with L-glutamine, penicillin/streptomycin, EGM2 Singlequots Kit, and 10% Fetal Bovine Serum (10% complete media). Media was changed every other day until the time of experiment. The hCB-ECs, hPB-ECs and HAECs were passaged 1:10 into new T75 flasks upon reaching confluence. Cells were then subsequently split 1:10. The number of population doublings that occurred between each passage was adjusted based upon a 75% attachment rate and calculated according to the formula $\ln(10)/\ln(2)*(4/3) = 4.43$ as previously described [169].

2.2.2 Flow Cytometry

To characterize the hCB-ECs used in this study, flow cytometry was performed for surface markers CD31, CD34, CD45, and CD115 (10μL antibody per 100,000 cell sample, pre-conjugated with FITC and PE, Biolegend). The hCB-ECs were passaged using 0.025% trypsin-EDTA (Invitrogen) at 80% confluence. Approximately 100,000 hCB-ECs were resuspended in 1% BSA buffered with DPBS with calcium and

magnesium (GIBCO). The hCB-ECs were incubated at room temperature in the dark for

30 minutes with 2 μg of pre-conjugated antibody prior to a wash step with 1% BSA

solution buffered in DPBS with calcium and magnesium (GIBCO). The cells were

collected after centrifugation at 400 g for 7 minutes and fixed using 0.5%

paraformaldehyde (J.T. Baker) before storage at -20°C until analysis. For each sample,

9000 events were collected. Mouse IgG1 was used as the control (Biolegend).

2.2.3 Permeability Experiments

hCB-ECs or HAECs were seeded with 10% complete FBS media onto the luminal

(top) chambers of 0.4◦m pore diameter, polyester, 12-well Transwell plates (Corning) at

a density of 100,000 cells/cm² which ensured the development of a confluent monolayer

1 to 2 days post-plating. The abluminal (bottom) chamber contained serum-free media.

The permeability was measured 2, 3, and 7 days post-plating. Prior to the experiment,

the cells were incubated with serum-free media for 1 hour. 1 mg/mL of unlabeled

bovine serum albumin (BSA) was added to the abluminal chamber and 1mg/mL of

FITC-BSA was added to the luminal chamber at volumes that would ensure no

differences in hydrostatic or osmotic pressure. 10μL samples were taken from the

abluminal chamber every 20 minutes for 2 hours. The change in hydrostatic pressure

due to a decrease in the volume of the abluminal chamber was 1.5 Pa, a level that would

generate a very low fluid flow relative to physiological pressure drops between 1333 and

6667 Pa. There was no change in osmotic pressure during the experiment because the

albumin concentration did not change with sampling. Albumin content of the sample

was determined by a fluorimeter using a calibration curve. Permeability coefficients

were determined using the following expression previously described by Albelda et

al.[2]

$$V_1 \ln\left[\frac{c_1}{c_0}\left(1+\frac{V_1}{V_2}\right) - \frac{V_1}{V_2}\right] = -A_m P\left(1+\frac{V_1}{V_2}\right)t \qquad (1)$$

Where V_1 and V_2 are the volumes in the luminal and abluminal chamber,

respectively. C_0 is the concentration of labeled albumin initially in the luminal chamber.

C_1 is the concentration of labeled albumin in the luminal chamber at time t. P is the

diffusive permeability and A_m is the area of the membrane. The permeability P was

obtained from the slope of a linear regression of the natural logarithm of the bracketed

term in equation (1) versus time for a given experiment. The R^2 value of the trendline

ranged from 0.94 to 0.99 and was used to assess goodness of fit. Figure 3 contains a

representative plot. The permeability coefficients were calculated from the slope of the

trendline. This permeability term represents contributions from both the cells and the

membrane. To calculate the permeability of the cells alone, the permeability of the cell

layer and the membrane were treated as resistances in series.

$$\frac{1}{P_{Cell+Membrane}} = \frac{1}{P_{Cell}} + \frac{1}{P_{Membrane}} \qquad (2)$$

The permeability of the Transwell membrane alone was $3.1\pm0.2 \times 10^{-5}$ cm/s (n=9),

13-100 times greater than the endothelial permeability.

The plot shows data points with the linear fit:

$$y = -1.75E\text{-}04x + 3.8E\text{-}05$$
$$R^2 = 0.99$$

with y-axis labeled $V_1 \ln(c_1/c_0(1+V_1/V_2)-V_1/V_2)$ and x-axis labeled Time (minutes).

The equation shown on the plot:

$$V_1 \ln\left[\frac{c_1}{c_0}\left(1+\frac{V_1}{V_2}\right)-\frac{V_1}{V_2}\right] = -A_m P\left(1+\frac{V_1}{V_2}\right)t$$
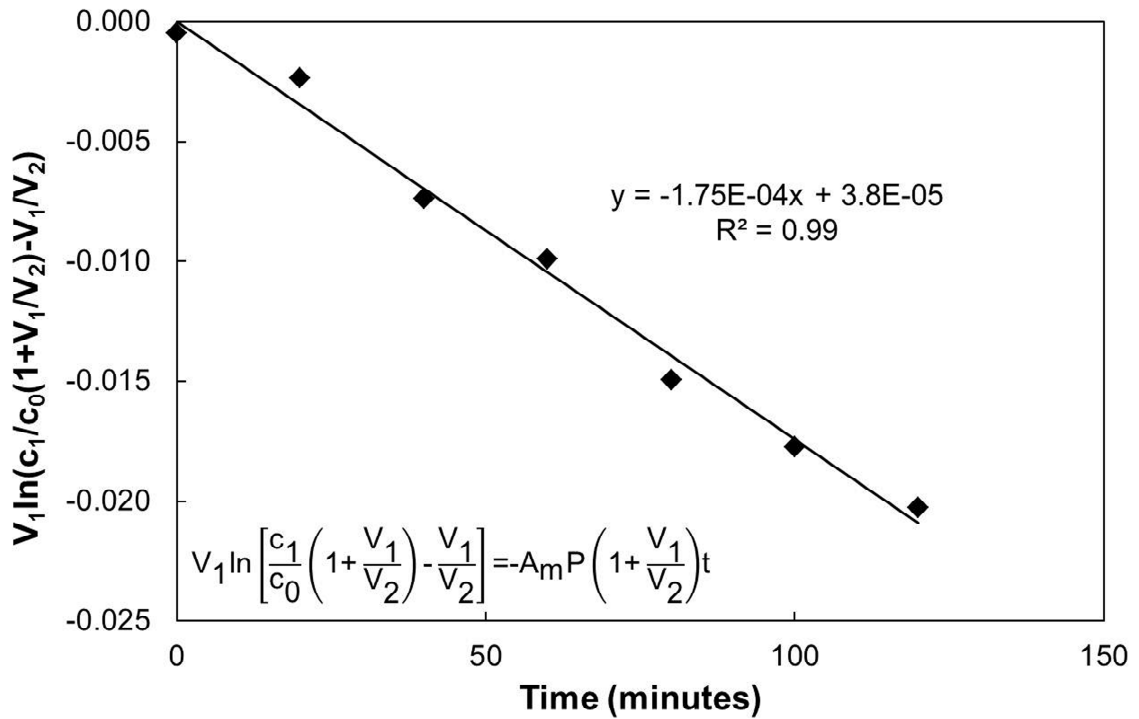
Figure 3: Representative plot of data from the Transwell permeability experiments. A semi-log plot of the albumin concentration versus time using equation (1) was used to calculate the permeability. This permeability coefficient represents contributions from both the membrane and the cells, which were treated as resistances in series (equation (2)) to determine the permeability of the cell layer alone.

2.2.4 Proliferation Assays

The Click-iT EdU Alexa Fluor 488 Imaging Kit (Invitrogen) was used to measure the number of cells in the S-phase. Cells were plated on Transwell plates as described in the permeability experiments. The EdU label was incubated with the cells for 2 hours. Detection of the label was performed as described in the manufacturer's protocol. The Hoechst 33342 stain was used to detect all nuclei. The membrane of the Transwell insert was cut out and mounted on a glass slide for imaging. The stain was visualized with a

Nikon© Eclipse Inverted Microscope system. Cells in the M-phase of mitosis were distinguished based on typical morphological features including condensed and segregating chromosomes [97]. The percentage of cells in S-phase or M-phase was reported as the total number respectively of EdU labeled cells or M-phase cells divided by the total number of cells that contained the Hoechst 33342 stain.

2.2.5 Western Blotting

Western blots were performed to determine the expression of tight junction proteins occludin and ZO-2 in both cell types. Cells were grown on T25 flasks for 4 days post-confluence. Cells were harvested with a cell scraper and subjected to a solution of CellLytic-M (Sigma) and Protease Inhibitor Cocktail (Sigma). Protein quantification was performed with the BCA Protein Assay Kit (Pierce). 10 µg of protein was loaded into each well for the SDS-polyacrylamide gel electrophoresis (10% gel, Biorad). Afterwards, the protein bands were transferred to PVDF membranes. The membranes were blocked with a Tris-Buffered Saline with 0.1% Tween 20 (TBST) solution containing 5% milk at room temperature for 1 hour. Primary antibodies for mouse-ZO-2 (1:1000 dilution, clone 3E8D9, Invitrogen), mouse-occludin (1:2000 dilution, clone OC-3F10, Invitrogen), and mouse-β-actin (1:1000 dilution, clone AC-15, Invitrogen) were diluted in a TBST solution containing 1% milk and incubated with the membrane overnight at 4°C. The goat-anti-mouse secondary antibody (1:2500 dilution, Invitrogen) was incubated with the membrane for 45 minutes at room temperature. After washing, immunoreactive bands

were detected by luminography using Supersignal chemiluminescent substrate (Pierce). Subsequently, expression of phosphorylated occludin was detected by stripping the immunoblot and then reprobing with anti-mouse-β-actin (1:1000 dilution, Invitrogen) and mouse-anti-phosphotyrosine (1:500 dilution, clone PY-7E1, PY20, Invitrogen) diluted in a TBST solution containing 1% milk. The secondary antibody and chemiluminescent substrates were added in the normal manner. Integrated band density was determined by densitometry after scanning onto autoradiographic films (Kodak) and evaluated by ImageJ (NIH). Protein expression was reported as a normalized intensity of the band of interest compared to the band of the housekeeping protein, β-actin.

2.2.6 Immunofluorescence

hCB-ECs and HAECs were seeded at a density of 100,000 cells/cm^2 on 35 mm glass dishes. At 6 days post plating, cells were fixed and permeabilized for 3 minutes with methanol. Samples were then blocked with PBS/0.02% Tween 20 (Biorad)/10%goat serum (Gibco) for 1 hour at room temperature. The samples were then incubated with antibodies to the mouse-occludin (1:250 dilution, clone OC-3F10, Invitrogen), mouse-ZO-1 (1:250 dilution, clone ZO1-1A12, Invitrogen), or mouse-ZO-2 (1:250 dilution, clone 3E8D9, Invitrogen) overnight at 4°C. This was followed by appropriate secondary antibody incubation with goat anti-mouse Alexa Fluor 488 (1:250 dilution, Invitrogen) or goat anti-mouse Alexa Fluor 546 (1:250 dilution, Invitrogen) for 1 hour at room

temperature. All antibodies were diluted in PBS/10% goat serum. The stains were

visualized with a Leica SP5 Confocal Microscope (Zeiss).

2.2.7 β-Galactosidase Staining

hCB-ECs were plated at 100,000 cells/cm^2 on 24-well plates. The cells were then

fixed at 4 days post-plating. For Resveratrol experiments, hCB-ECs were plated at

100,000 cells/cm^2 and cells were treated with 2 μM or 20 μM Resveratrol [66] 1 day post-

plating and were fixed 4 days post-plating. The senescence β-galactosidase Staining Kit

(Cell Signaling Technology) was used according to the manufacturer's protocol to stain

for senescent cells. The stain was visualized with a Nikon© Eclipse Inverted Microscope

system. The percentage of senescent cells was calculated as the total number of cells that

contained the blue β-galactosidase stain divided by the total number of cells in the field

of view.

2.2.8 Telomerase Activity

The TRAPEZE RT Telomerase Detection Kit (Millipore/Chemicon) was used to

measure telomerase activity in cell samples. 100μL of lysis buffer was incubated with

500,000 cells for 30 minutes. The tube was then centrifuged at 4°C for 20 minutes. The

supernatant was removed and the protein was quantified using the BCA Assay Kit

(Pierce). 200ng of protein was used in each sample and the samples were performed in

triplicate. A no template control of PCR grade water, minus telomerase control of lysis

buffer, positive telomerase control cell line, and heat-inactivated samples were used as

controls. The assay was completed according to the manufacturer's protocol. According

to the manufacturer, the sensitivity of the assay is 0.004 attomoles.

2.2.9 Statistical Analysis

Values of n represent the number of cell donors. For Figures 4, 5, 6, and 8,

ANOVA tests were performed to compare different data sets. Post-hoc Tukey tests were

performed for additional comparisons. For Figure 9, a 2-factor repeated measures

ANOVA for cell age and treatment followed by a post-hoc Tukey test was used. For

Tables 2 and 3, a repeated measures ANOVA followed by a post-hoc Tukey test was

used. All data presented represent mean ± SE. A $p<0.05$ was interpreted to denote

statistical significance.

2.3 Results

2.3.1 hCB-EC Characterization

Flow cytometry showed that hCB-ECs and hPB-ECs were positive for the

endothelial-specific CD31 and CD34, and negative for CD14, CD45 and CD115 found on

monocytes or hematopoietic cells. Immunofluorescence indicated that CD-31, platelet-

endothelial cell adhesion molecule, was present at the cell borders of hCB-ECs, HAECs,

and hPB-ECs. We previously characterized hCB-ECs and found that they expressed von

Willebrand factor, CD31 and VE-cadherin [11]. Following exposure to 15 dyne/cm² for

24 or 48 hours, hCB-ECs aligned with the direction of flow [11, 20], increased nitric oxide

production, and increased mRNA for endothelial cell specific genes sensitive to flow,

39

Kruppel-like factor 2, nitric oxide synthase III, cyclo-oxygenase 2, and thrombomodulin [11]. The level and organization of actin filaments are similar in hCB-ECs and HAECs as are the associated values of cell stiffness [20].

2.3.2 Low Passage hCB-ECs Have Lower Permeability than HAECs

The *in vitro* permeability of HAECs to BSA 7 days post plating ($2.4 \pm 0.6 \times 10^{-6}$ cm/s (n=3)) agrees with published values of $3.2 \pm 0.4 \times 10^{-6}$ cm/s for bovine aortic endothelial cells (BAECs) [18] and 1.9×10^{-6} cm/s for human umbilical vein endothelial cells [21]. For hCB-ECs that underwent less than 44 population doublings since passage 1, the average permeability 7 days post-plating ($3.1 \pm 0.5 \times 10^{-7}$ cm/s (n=3)) was significantly less than the value obtained with HAECs that underwent less than 35 population doublings (Figure 4A) ($p < 0.01$). For hPB-ECs (P-11, 44 population doublings), the average permeability ($5.3 \pm 0.2 \times 10^{-7}$ cm/s (n=2)) 7 days post-plating was between values for hCB-ECs and HAECs. Differences in permeability between EC type are significant for each day ($p < 0.01$), but, for each cell type, the permeability did not change significantly over time and was not dependent upon donor ($p < 0.60$).

2.3.3 Expression of Occludin and ZO-2 in Low Passage hCB-ECs and HAECs Does Not Explain Difference in Permeability

Elevated occludin levels have been correlated with reduced permeability to [14][C]sucrose in bovine brain microvascular endothelial cells [37]. To assess the degree of tight junction protein expression in low passage hCB-ECs and HAECs, Western blots were performed for the tight junction proteins zonula occludens 2 (ZO-2) (molecular

weight: 160kDa) [5] and occludin (molecular weight: 66 kDa) [4]. β-actin (molecular

weight: 37kDa) served as a control (Figure 4B). The relative intensity for ZO-2 was

virtually identical for hCB-ECs (0.3±0.2) and HAECs (0.4±0.2) (n=4). Surprisingly, the

relative intensity of occludin was less for hCB-ECs (1.4±0.1) than HAECs (2.5±0.6)

($p<0.05$) (n=4).

2.3.4 Less Phosphorylated Occludin in Low Passage hCB-ECs than HAECs

Although the amount of functional occludin is important in maintaining tight

junction integrity, phosphorylation of occludin causes disruption of tight junctions [39].

Therefore, cells with a lower permeability will have less phosphorylated occludin.

Western blot and associated densitometry (Figure 4C) showed that the relative intensity

of antiphosphotyrosine antibody colocalized to occludin was 25% lower for hCB-ECs

than for the HAECs ($p<0.01$). Consistent with the lower level of occludin tyrosine

phosphorylation in hCB-ECs than HAECs, immunofluorescence showed greater

occludin localization at the periphery of hCB-ECs than HAECs (Figure 4D). Although

ZO-1 staining was not intense enough to permit quantification via densitometry, we

could visualize ZO-1 by immunofluorescence. The greater localization of ZO-1 (Figure

4E) to the periphery of hCB-ECs relative to HAECs is consistent with the role of occludin

and ZO-1 at EC junctions in contributing to the reduced permeability of the hCB-ECs. In

contrast, (ZO-2) (Figure 4F) was not localized to the periphery in either hCB-ECs or

HAECs suggesting additional mechanisms are involved in regulating permeability.
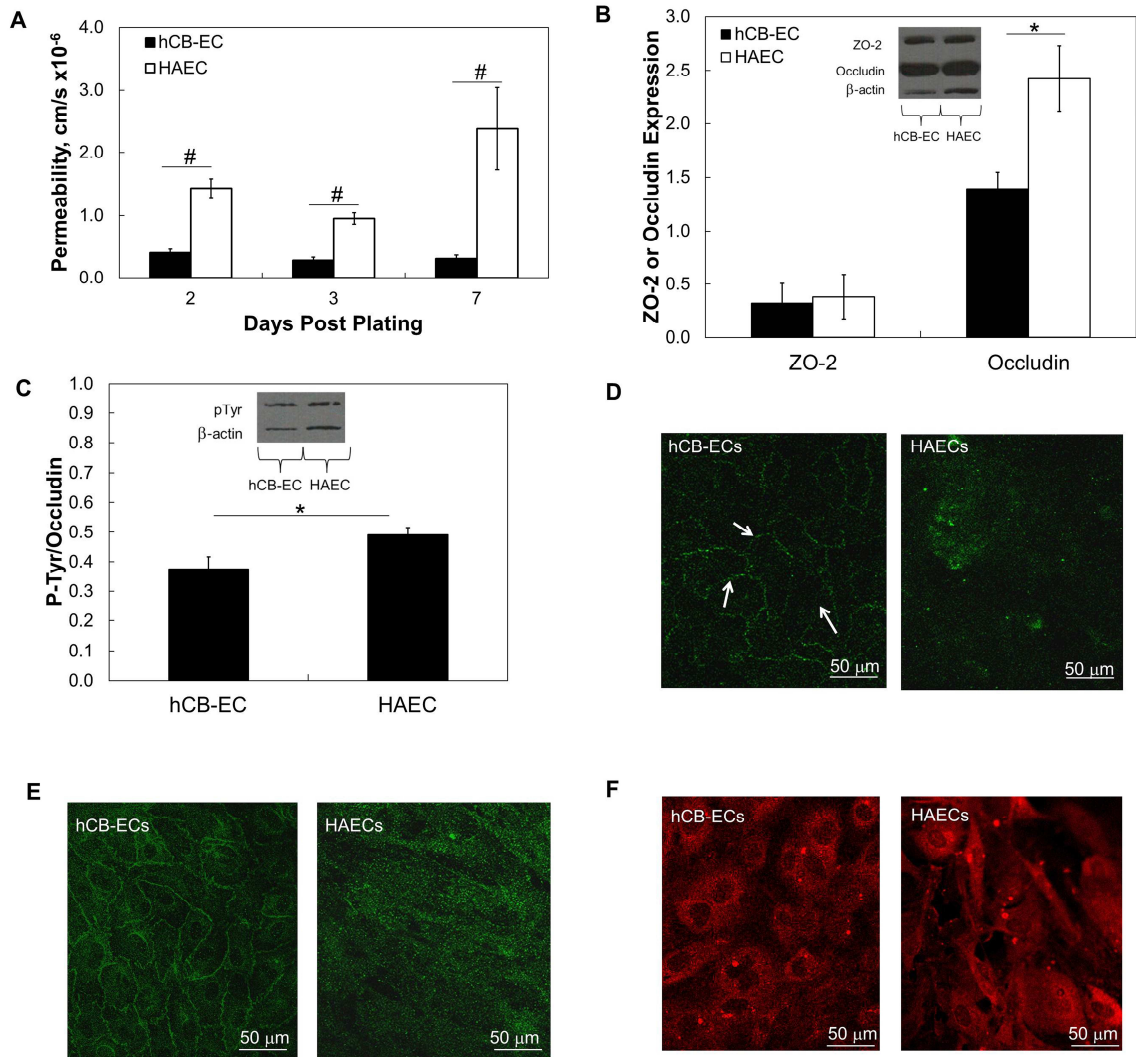
Figure 4: hCB-ECs that underwent less than 44 population doublings have lower permeability than HAECs that underwent less than 35 population doublings due to changes in phosphorylated occludin. A) The albumin permeability of the hCB-ECs is significantly lower than that of the HAECs; B) Western Blot and quantitative analysis of occludin and ZO-2 protein expression normalized to β-actin; C) Western Blot and quantitative analysis of phosphorylated occludin. D) Occludin localization in hCB-ECs and HAECs; E) ZO-1 localization in hCB-ECs and HAECs; F) ZO-2 localization in hCB-ECs and HAECs. Data are presented as mean ± SE. n=3-4; *: p-value < 0.05 #: p-value < 0.01.

2.3.5 Low Passage hCB-ECs Proliferate More than HAECs

Since cells must break their junctions in order to divide [157], we hypothesized that a monolayer with a higher permeability would have more cells dividing at any one time. However, on days 2, 3 and 7 after plating, hCB-ECs that underwent less than 44 population doublings had a higher percentage of cells in the S-phase of mitosis than did HAECs that underwent fewer than 35 population doublings (Figure 5). Differences in the percent of cells in S-phase between cell type were statistically significant for each day, but for each cell type, the percent of cells in S-phase did not change significantly over time.
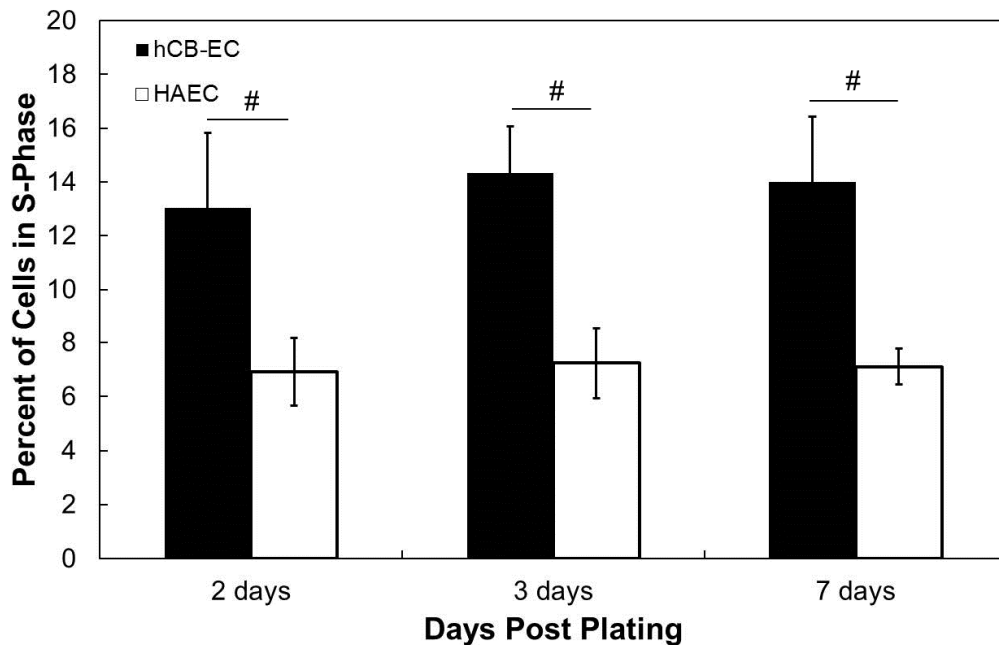
Figure 5: Percent of hCB-ECs that underwent less than 44 population doublings and HAECs that underwent less than 35 population doublings in S-phase for 2, 3, and 7 Days Post Plating. hCB-ECs proliferate at a higher rate than HAECs. n=6-8; #: p-value<0.017

43

While the percentage of cells in S-phase provides some indication of cell turnover, cells divide during the M-phase of mitosis, creating leaky junctions and enhancing permeability [97]. The percentage of cells in the M-phase significantly decreased over time after plating for low passage hCB-ECs and HAECs ($p<0.017$), but on each day, there was no difference between each cell type in the fraction of cells in the M-phase (Figure 6). The higher percentage of hCB-ECs in the S-phase can be attributed to the shorter doubling time of the hCB-ECs relative to the HAECs [11]. The low mitotic frequency of mitosis relative to cells in the S-phase reflects the duration of labeling and the relative amounts of time in the S and M phases. Because there are similar numbers of hCB-ECs and HAECs dividing, cell mitosis cannot explain the difference in permeability between the two cell types.
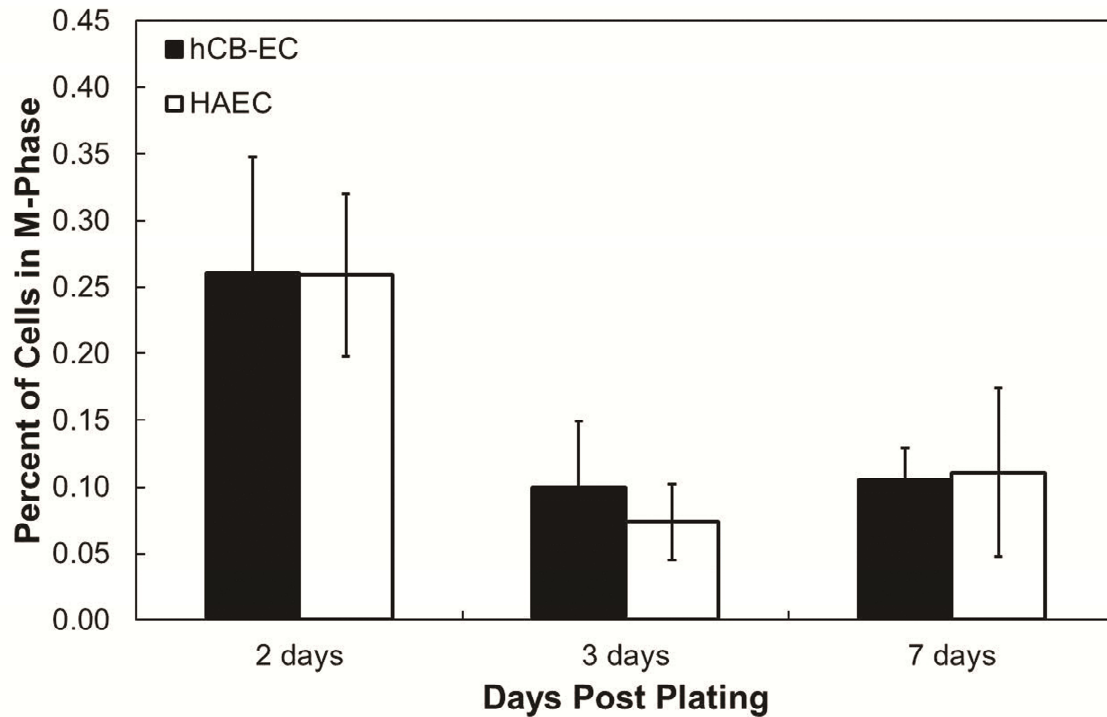
Figure 6: Similar M-Phase Mitosis Rates in hCB-ECs that underwent less than 31 population doublings and HAECs that underwent less than 35 population doublings. The percentage of cells in the M-phase was determined for HAECs and hCB-ECs 2,3 and 7 days after plating.   n=3.

2.3.6 Changes in hCB-EC Proliferation and Permeability with Cell Aging

To characterize aging of hCB-ECs and HAECs, preliminary experiments were

performed to measure the amount of telomerase in cells at different numbers of

population doublings after the first passage. Telomerase is a specialized reverse

transcriptase that is necessary for the synthesis of telomeric DNA at the ends of

chromosomes [54]. A lack of telomerase hinders the ability of the DNA polymerase to

replicate the end of the lagging strand, causing the DNA to shorten by 25-100 base pairs

with each round of cell division. Thus, younger cells exhibit higher concentrations of

telomerase [54]. In general, the amount of telomerase decreased with increasing cell age

in hCB-ECs (Table 1). The amount of telomerase in HAECs at 35 population doublings

was equivalent to the value of hCB-ECs at later passages, suggesting that HAECs are

older than any of the hCB-ECs tested.

Table 1: Telomerase Activity Decreases with Increasing Population Doublings in Culture. **The average telomerase level generally decreases with increasing population doublings. The HAECs exhibit less telomerase than any of the hCB-ECs tested indicating that their relative age is higher than that of the hCB-ECs. Samples were run in triplicate.**

Cell Type	Population Doublings	Telomerase (amoles/10^6 cells)
hCB-EC	31	1.200
hCB-EC	44	≤0.004
hCB-EC	71	≤0.004
hCB-EC	31	0.220
hCB-EC	44	0.0280
hCB-EC	71	0.0194
HAEC	35	≤0.004

Next, we examined the effect of aging on hCB-EC permeability. Proliferation

studies done in parallel with the permeability measurements indicate that the percent of

cells in S-phase decreased with increasing cell age (Table 2), a result expected as cells

become senescent [109].

Table 2: Percent of hCB-ECs in S-Phase With Increasing Population Doublings. The percent of hCB-ECs in S-phase decreases as the population doublings increases. Data are presented as mean±SE. n=3. *: p-value < 0.05 compared to 50 population doublings since passage 1.

Population Doublings Since Passage 1	Percent of Cells in S-phase
44	9.6±2.6
58	6.4±1.2
71*	4.5±1.8

Consistent with the lower level of proliferation of older cells, β-galactosidase staining was greater in hCB-ECs that underwent 71 doublings since passage 1 than in hCB-ECs that underwent fewer doublings (Figure 7).
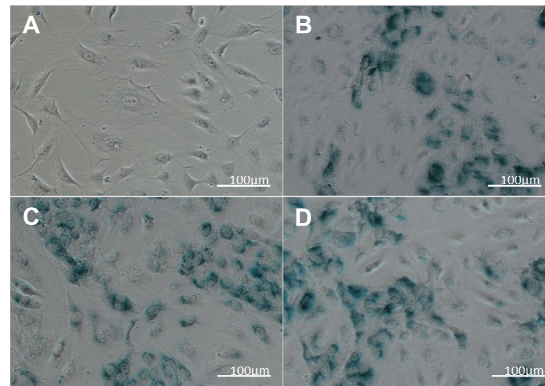
Figure 7: Senescence associated-β-galactosidase staining of aging hCB-ECs. A) hCB-ECs at 18 doublings since passage 1; B) hCB-ECs at 71 doublings since passage 1; C) hCB-ECs at 71 doublings since passage 1 with 20µM Resveratrol; D) hCB-ECs at 71 doublings since passage 1 with 2 µM Resveratrol.

For hCB-ECs that had undergone 84 population doublings, the permeability was 1.5±0.9 x 10^{-6} cm/s (mean ±SE, n = 3 donors), almost five times the value at lower passage (Figure 4).   In a study with hCB-ECs from an additional donor, the permeability of hCB-ECs

47

increased monotonically with increasing age (Figure 8). The mean value for late passage

hCB-ECs was lower than values obtained with the lower passage HAECs.

Cell Type	HAEC	hCB-EC					
Age (doublings)	<35	<44	62	66	72	75	79
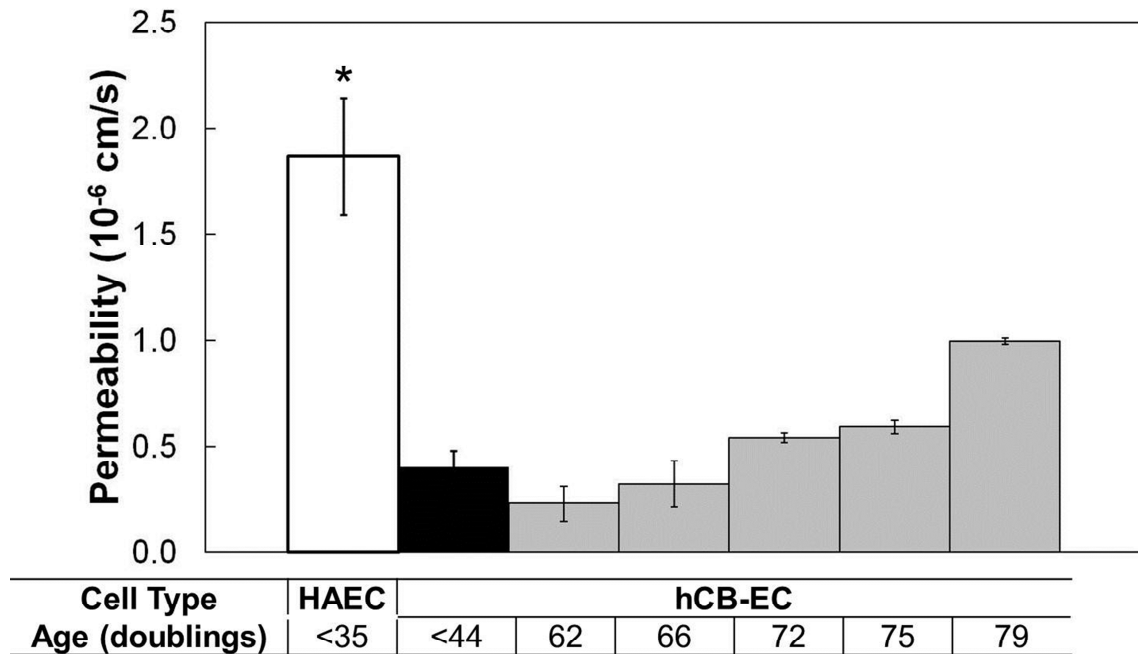
Figure 8: Albumin Permeability of Cells Increases with Increasing Population Doublings. Age is defined as population doublings since passage 1. The permeability of the hCB-ECs from 1 isolation increases with increasing population doublings. The permeability approaches that of the HAECs. n=3; *: p-value <0.05 compared to hCB-EC (<31 doublings) #: p-value < 0.01 compared to hCB-EC (<31 doublings)

2.3.7 Resveratrol Treatment Decreases hCB-EC Permeability

SIRT1 deacetylates proteins involved in regulating antioxidant activity.[25]

SIRT1 levels decline with aging whereas elevation of SIRT1 improves endothelial cell

function [41, 167]. To test the effect of SIRT1 levels on endothelial permeability in aging

cells, we treated ECs with Resveratrol, which increases expression levels of SIRT1

indirectly [41, 167].

While porcine aortic ECs [199] and human umbilical vein ECs [25] tolerated a dose of 100 µM Resveratrol for 16 hours, this dose was toxic to hCB-ECs after 48 hours. We found that hCB-ECs could tolerate doses less than or equal to 20 µM for 48 hours. Addition of 20 µM Resveratrol for two days prior to measurement decreased the permeability of hCB-ECs that underwent at least 57 population doublings by approximately 28% (p<0.05) while incubation of hCB-ECs monolayers with 2 µM Resveratrol, decreased the permeability of hCB-ECs by approximately 41% (p<0.05) (Table 3). HAECs incubated with 2µM Resveratrol decreased the permeability by approximately 22%. Doses of 2 µM and 20 µM Resveratrol had no significant effect on the percentage of cells in the S-phase or on β-galactosidase staining (Figure 7C, Figure 7D).

2.3.8 Activation of the Epac1-Rap1 Pathway Reduces Permeability in Late Passage Cells

The compound 8-pCPT-2'-O-Me-cAMP (007) is a membrane permanent activator of the exchange factor activated by cAMP, Epac1, which exerts the same effect on cell function as Resveratrol [128]. Treatment of cells with 100µM 8-pCPT-2'-O-Me-cAMP during the permeability experiment decreased the permeability of hCB-ECs that underwent at least 57 population doublings by approximately 26% (p<0.01) (Table 3).

Table 3: Resveratrol, 007 and Rolipram decrease hCB-EC Permeability. Data are presented as mean±SE for n = 3, * p<0.05 and # p<0.01 relative to untreated control.

Treatment	Concentration	Permeability Decrease (%)
Resveratrol	20μM	28±7*
Resveratrol	2μM	41±5*
007	100μM	26±5#
Rolipram	25μM	30±1#

To confirm that the change in permeability is due to phosphodiestarase 4 which has been proposed as the mode of action of Resveratrol, we examined the permeability of hCB-ECs after treatment with Rolipram is a specific PDE4 inhibitor that increases cAMP levels at the membrane which then activates the Epac1-Rap1 pathway. Consistent with the role of Resveratrol as a phosphodiesterase 4 (PDE4) inhibitor [128], treatment of hCB-ECs that underwent at least 57 population doublings with 25 μM Rolipram caused the permeability to decrease about 30% (Table 3). Taken together, these results suggest that Resveratrol alters permeability in aging cells by increasing membrane associated cAMP.

2.3.9 Increased Expression of ZO-2 and Phosphorylated Occludin in Aging hCB-ECs

Because addition of Resveratrol decreased the permeability of the aged hCB-ECs (Table 3), we examined the tight junction protein expression and localization for cells treated with 2 μM Resveratrol for 48 hours. Both occludin and phosphorylated occludin levels decreased significantly as hCB-ECs went from population doubling 35 to 71, but

then increased between population doubling 71 and 84 (Figure 9A and Figure 9B) ($p<0.01$). Cells that underwent 84 population doublings and were treated with 2 μM Resveratrol had decreased levels of occludin and phosphorylated occludin ($p<0.05$) (Figure 9D and Figure 9E). The change in phosphorylated occludin is consistent with the increase in hCB-EC permeability with increasing cell age and the reduced permeability of hCB-ECs after treatment with Resveratrol.

Like occludin, ZO-2 levels increased for hCB-EC population doublings between 71 and 84 (Figure 9C) ($p<0.01$). Treatment with Resveratrol did not significantly affect levels of ZO-2 expression (Figure 9C). From these results, we conclude that higher levels of tyrosine phosphorylation of occludin are associated with the elevated permeability of the aging hCB-ECs and Resveratrol decreases permeability, in part, by reducing the level of tyrosine phosphorylated occludin.

Unlike early passage hCB-ECs (Figure 4D, Figure 4E, and Figure 4F) localization of occludin, ZO-1, and ZO-2 in hCB-ECs that underwent 57 population doublings since passage 1 was not at the cell junctions (Figure 9F). The tight junction proteins were diffusely distributed in the cells and the staining resembled that of the HAECs (Figure 2.2). In contrast, the hCB-ECs that underwent fewer than 44 population doublings exhibited localization of occludin and ZO-1 to cell junctions (Figure 4D). The results indicate that there is a change in localization of tight junction protein in hCB-ECs of

increasing age, which correlates with the increase in permeability with increasing cell

age.
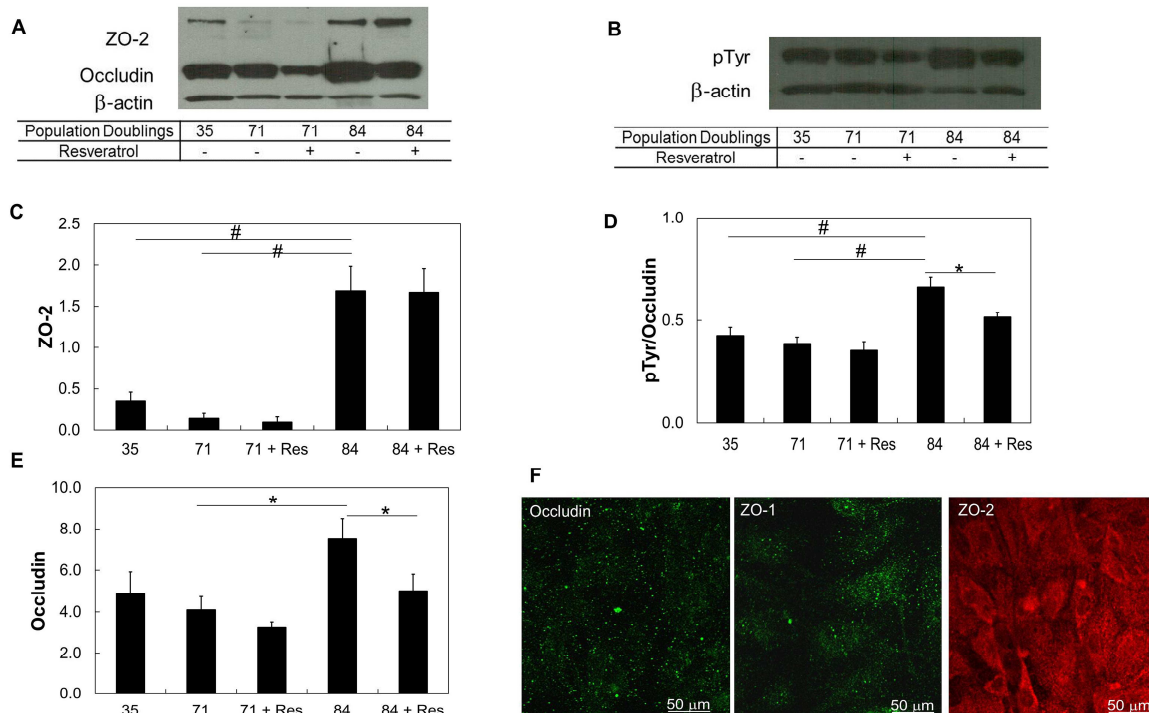
Figure 9: Change in occludin, ZO-2 and phosphorylated occludin with increasing cell age. The increase is mitigated with the addition of 2 μM Resveratrol for 48 hours. A) Western Blot of tight junction proteins probed with antibodies for occludin and ZO-2; B) Western blot of phosphotyrosine with control β-actin; C) Quantitative analysis ofZO-2. Values are the band intensity normalized by the intensity of the β-actin band; D) Quantitative analysis of phosphorylated occludin; E) Quantitative analysis of occludin. F) Immunofluorescence of tight junction proteins occludin, ZO-1 and ZO-2 in hCB-ECS after 44 population doublings. Data are presented as mean ± SE. n=3; *: p-value < 0.05 #: p-value < 0.01

2.4 Discussion

To our knowledge, these studies demonstrate for the first time that the

permeability of low passage hCB-ECs is significantly lower than that of HAECs and that

the permeability of hCB-ECs increases with increasing population doublings due to

52

elevation of tyrosine phosphorylation of occludin and alteration of Epac1 activity.

Additionally, the early passage hCB-EC permeability values are close to those reported

for large vessel endothelium permeability to serum albumin *in vivo* [6, 10]. For instance,

the permeability of the porcine abdominal aorta to albumin ranges from 8.6 x 10^{-7} to 27 x

10^{-7} cm/s [6] and the permeability of the rabbit aorta to albumin is reported as 0.6 x 10^{-7}

cm/s [10] and 0.8 x 10^{-7} cm/s [106]. This is the first type of cultured endothelial cell for

which *in vitro* permeability to macromolecules is close to *in vivo* values for large vessels.

The permeability values measured in this study were obtained under diffusive

conditions, whereas *in vivo* values represent the combined effect of diffusion and

convection. Albumin is transported across endothelium by a vesicular pathway, through

endothelial junctions, and across leaky endothelium. *In vitro*, about 80% of water

transport occurs through the junctions and 20% across leaky junctions [18]. For

transport through the junctions and across the leaky endothelium, convection and

diffusion modify the endothelial permeability through each pathway P_e as follows [18]:

$$P_e = \frac{P_o Pe}{e^{Pe} - 1} + J_v\left(1 - \sigma\right)$$

(3)

where P_o is the diffusive permeability, J_v is the fluid flux, σ is the osmotic reflection

coefficient and Pe is the Peclet number, Pe = $J_v(1-\sigma)/P_o$. Convective transport is

dependent upon J_v and $(1-\sigma)$, which represents the drag exerted upon the

macromolecule by interaction with the junction proteins. For a given macromolecule, the

value of σ is sensitive to the radius and volume fraction of junction fibers. A value of J_v =

1.8 x 10^{-6} cm/s was measured in the rabbit aorta [106]. For this value of J_v and an in vitro value of σ = 0.49 for albumin [18], Pe = 2.6 for early passage hCB-ECs and 0.6 for late passage hCB-ECs. Convection would have a more significant effect upon P_e for early passage hCB-ECs than for late passage hCB-ECs, although P_e is smaller for early passage ECs (9.9 x 10^{-7} cm/s) than late passage ECs (2.0 x 10^{-6} cm/s). Future studies will need to examine the relative importance of each of these pathways in early and late passage hCB-ECs and the manner in which transport is affected by applied pressures across the endothelium.

We examined several possible reasons for the lower permeability of the hCB-ECs: increased levels and tyrosine phosphorylation of tight junction proteins, reduced levels of cell mitosis and alterations in Epac1 activity. Occludin, when linked to ZO-1 and ZO-2 regulates transport through the endothelial cell tight junctions [157]. While we found that expression of ZO-2 and occludin were not reduced in hCB-ECs relative to HAECs, occludin exhibited reduced levels of tyrosine phosphorylation and was redistributed to the cell junctions in the hCB-ECs. Mitosis levels also did not correlate with the reduced permeability of the hCB-ECs, which is consistent with published results and indicates that cell mitosis is less important than other factors, such as apoptosis, in raising EC permeability [19].

The amount of functional occludin, in the form of non-phosphorylated occludin, as well as its localization to junctions between ECs are important to maintain the tight

junction barrier in hCB-ECs [39]. Ser-490 phosphorylation and ubiquination of occludin is associated with increased permeability of primary bovine retinal endothelial cells due to a loss of occludin from EC-EC junctions and its movement towards lysosomes [116]. Elevated albumin permeability was associated with increased occludin tyrosine phosphorylation and the elevation in permeability was blocked with tyrosine phosphatase and protein kinase inhibitors [39]. This finding was further supported by the result that activation of c-Src by oxidative stress increased phosphorylation of tyrosine residues 398 and 402, which prevented occludin from assembling in the tight junctions and led to an increase in permeability [52]. Treatment of human umbilical vein endothelial cells with tyrosine phosphatase inhibitors led to selective occludin proteolysis and redistribution and increased permeability[173]. When bovine brain microvascular ECs were exposed to shear stress for just a few hours, hydraulic permeability and phosphorylation of tyrosine sites in occludin increased [178]. Correspondingly, exposure of confluent monolayers to shear stress for 24 hours, led to a decrease in tyrosine phosphorylation and an associated decrease in permeability [178]. Incubation of ECs with the protein tyrosine phosphatase activity inhibitor dephostatin led to smaller reductions in endothelial permeability after exposure to shear stress [178]. In the current study, we found that there was significantly less phosphorylated occludin in the hCB-ECs compared to the HAECs, which is consistent with the reduced permeability of the hCB-ECs. While our results are consistent with published studies

which show that increased occludin tyrosine phosphorylation causes the permeability to increase, phosphorylation of serine and threonine residues on occludin and other junction proteins could also affect permeability [47].

The amount of phosphorylated occludin increased as hCB-ECs underwent more population doublings and this was associated with an increase in hCB-EC permeability. Treatment with Resveratrol decreased hCB-EC permeability and produced a decrease in expression of phosphorylated occludin. However, significant increases in occludin tyrosine phosphorylation were not observed until the hCB-ECs underwent 71 population doublings (Figure 9D), while permeability increased at earlier passages (Figure 8). Because the changes in permeability precede the changes in phosphorylated occludin, additional pathways, such as transport through leaky junctions and vesicular transport [18, 105], are likely to influence the permeability of hCB-ECs.

Other factors, besides occludin and ZO-1 localization and the extent of phosphorylated occludin in hCB-ECs, likely contribute to the lower permeability of the hCB-ECs. Apoptosis is known to be elevated in senescent cells [99], and would produce an increase in the number of leaky junctions and increase permeability [19]. The glycocalyx is composed of several membrane-bound macromolecules on the surface of ECs and may regulate transport of water and macromolecules. Actin-myosin contraction can cause the breakdown of intercellular junctions leading to elevations of permeability [105].

Aging at the cellular level is associated with replicative senescence or stress-induced senescence. For replicative senescence, after a certain number of population doublings, cells cease to replicate [17]. A leading theory for the cause of replicative senescence is telomere shortening. After the telomere is shortened to a certain degree, the cell becomes senescent and do not divide any further to protect against mutation of its genetic code [54]. Similarly, stress-induced senescence causes cells to cease to divide. It is primarily caused by environmental stresses such as intracellular oxidative stress, DNA damage by radiation, or chromatin decondensation. Our finding that hCB-EC permeability increasing with increasing population doublings indicates that cell aging and cell senescence play an important role in the regulation of albumin transport.

While the ECs divide more rapidly *in vitro* than *in vivo*, there is evidence that ECs at lesion prone sites have undergone replicative senescence by their size, shape and telomere length [13, 123]. The use of 44 or more population doublings to show an effect of cell replication on albumin is not an absolute number, but the data present a general trend at which cells become more susceptible to aging.

Resveratrol has been used to reduce age-associated metabolic phenotypes [128]. We found that addition of 2 µM Resveratrol for 48 hours was more effective than 20 µM Resveratrol at decreasing the permeability. Relative to 60 µM, Resveratrol at 1 µM was more effective at promoting adhesion and migration of early outgrowth EPCs and low doses of resveratrol promoted reendothelization [66]. Incubation of early outgrowth

EPCs with Resveratrol doses between 10 and 50 μM for three days reduced β-galactosidase staining, and increased migration, proliferation and telomerase activity, suggesting a reversal of senescence, while a dose of 100 μM increased apoptosis [188]. While endothelial cells can tolerate 100 μM Resveratrol for short periods of time, our results suggest that lower doses of Resveratrol can reduce permeability without necessarily reducing senescence.

Resveratrol acts upon SIRT1 via competitive inhibition of phosphodiesterase 4 which causes elevated cAMP levels [128]. Park et al. showed that the resulting elevation of cAMP activates effector protein Epac1, and sequentially increases Rap1, intracellular Ca^{2+} and activates the CamKKβ-AMPK pathway to activate SIRT1 [128]. Interestingly, elevated cAMP levels cause a decrease in endothelial permeability by activation of protein kinase A which then inactivates myosin light chain kinase [105] or through Epac-mediated Rap1 activation [59]. Further, membrane associated cAMP bound to Epac1 interacts with phosphodiesterase 4, to bind to VE-cadherin [137] and regulates endothelial permeability by redistributing tight junction molecules to cell junctions [42]. Thus, in addition to regulating occludin phosphorylation, Resveratrol may influence permeability through Epac1-Rap1 interactions with VE-cadherin. We showed that 8-pCPT-2'-O-Me-cAMP, a cAMP analog which specifically activates the Epac1-Rap1 pathway, and Rolipram, a specific PDE4 inhibitor, both decrease hCB-EC permeability in a manner similar to Resveratrol. These results, along with results in Park et al.,

indicate that Resveratrol is acting as a PDE4 inhibitor, which activates membrane-bound cAMP, which stimulates the Epac1-Rap1 pathway, which ultimately upregulates SIRT1 levels.

The incidence of cerebral vascular disease increases with increasing age and can ultimately lead to stroke or dementia [55]. Increases in blood-brain barrier permeability play an important role in the pathophysiology of the diseases due to leakage of blood components into white matter and the vessel wall [162]. These age-related white matter changes are associated with increased incidence of stroke [90]. Levels of circulating EPCs are decreased in patients with these age-related white matter changes. Taken together, these results indicate that increases in age-associated permeability can lead to cerebral vascular disease development.

Using EPCs *in vitro* as a model of cell aging may be a useful tool for studying the development and progression of atherosclerosis and cerebrovascular diseases. We have found that when ECs are cultured on quiescent vascular smooth muscle cells that EC proliferation is greatly reduced [174]. This coculture system could then be used to mimic the vessel wall structure and reduce hCB-EC proliferation towards in vivo values.

2.5 Conclusion

The results of these studies suggest that cell age may be a key biological mechanism for the observed permeability differences between hCB-ECs and HAECs. The study also shows that hCB-ECs may be a suitable model for cell aging as they can be

used to represent very young cells after isolation and they can be passaged a significant number of times until they can be used as a model for older, senescent cells. This is important as the permeability of the endothelium is higher in regions prone to the initiation of atherosclerosis. Additionally, senescent cells are known to be present in areas with atherosclerosis. ECs in these regions undergo more cycles of replication and, due to the local hemodynamics, are more sensitive to extracellular stresses. These environmental conditions can ultimately lead to senescence that increases permeability, either due to alterations in signaling pathways within individual ECs or increased apoptosis leading to leaky junctions.

2.6 Chapter Acknowledgements

Chapter 3. SIRT1 Regulates Glycocalyx and VE-Cadherin to Modulate Response of Senescent Endothelial Cells to Shear Stress

3.1. Introduction

Endothelium at lesion-prone sites and on atherosclerotic lesions show signs of senescence, including evidence of giant cells,[13] elevated levels of β-galactosidase,[108] and telomere shortening.[123] In atherosclerotic regions in both humans and animals, endothelial cells (ECs) experience high cell turnover and high oxidative stress, leading to replicative[13, 123] and stress-induced senescence.[54] Interestingly, senescent ECs were not found in arteries from the same individuals which were free of atherosclerosis, suggesting that senescence was not systemic and was due to local changes to ECs.[108] Senescence affects several EC functions including decreased expression of endothelial nitric oxide synthase (eNOS)[32, 102] and increased permeability.[26, 27] In ECs, changes in eNOS mRNA expression levels from shear stress results from alterations in the EC response to mechanical forces, leading to modifications in signaling pathways and overall cell function.[31] Increased EC permeability with increased cell age likely results from disruptions in tight junction protein localization and phosphorylation.[27]

While replicative and stress induced senescence arise by different mechanisms, the two pathways converge in ECs by elevating the tumor suppressor p53,[108] which is negatively regulated by the deacetylase SIRTUIN1 (SIRT1). Further, senescent cells exhibit reduced cell replication and SIRT1 levels. In LDL receptor deficient mice fed a

cholesterol diet, p53 positive senescent ECs are present at higher levels at lesion-prone sites.[182] Activation of SIRT1 reverses several senescent-associated cell phenotypes.[26, 27, 128, 199] SIRT1 overexpression in ECs decreased atherosclerosis in ApoE-knockout mice.[198] SIRT1 expression is also sensitive to changes in shear stress.[24] When ECs were subjected to atheroprotective flow, SIRT1 expression levels increased and led to a corresponding increase in nitric oxide (NO) production and availability.[24] SIRT1 may regulate key ECs functions such as permeability and response to flow through cell junctions, including occludin[27] and VE-cadherin.[42]

VE-cadherin[40] and the glycocalyx[57, 192] are mechanosensors which regulate the response to fluid shear stress. Myosin-dependent tension across VE-cadherin is decreased after exposure to shear stress.[40] Disturbed flow alters VE-cadherin localization and expression.[32] VE-cadherin phosphorylation elevates permeability through uncoupling of p120-catenin or β-catenin.[135] The glycocalyx is associated with reduced endothelial permeability and increased NO production in response to shear stress.[57, 192] In regions of disturbed flow and atherogenesis, the glycocalyx is disintegrated.[168] Interestingly, SIRT1 levels are reduced by low and oscillating shear stresses present at vessel branches,[24] suggesting a possible link between mechanosensing and SIRT1.

While changes in endothelial structure and function lead to the development of atherosclerosis, it is unclear whether EC senescence is a cause or effect of these EC

functional changes. In this study, we tested the hypothesis that the response to steady

shear stress is decreased in aging-induced senescent ECs due to impairment of

antioxidant regulator SIRT1, which leads to alteration in the abundance and thickness of

the glycocalyx and phosphorylation of VE-cadherin. We use human cord blood-derived

ECs (hCB-ECs) as a model for cell aging because of their low, physiological permeability

at low population doublings, high proliferative potential in subconfluent cultures,[27]

and similarity to arterial ECs.[11] We examined the response of aging hCB-ECs to shear

stress with and without activators and inhibitors of SIRT1. We also examined the effect

of SIRT1 on mechanotransducers, glycocalyx and VE-cadherin.

3.2 Methods

3.2.1 Cell Culture

Human umbilical cord blood derived endothelial cells (hCB-ECs) were isolated

from blood as previously described by Ingram et al.[89] For isolation of hCB-ECs,

umbilical cord blood was obtained from the Carolina Cord Blood Bank (n=3 donors).

Prior to receipt, all patient identifiers were removed. The Duke University Institutional

Review Board approved the protocol for collection and use of human blood employed in

this study. For all experiments, we found no statistically significant effect of the donor

on the results.

After collection, blood was diluted 1:1 with Hanks Balanced Salt Solution (HBSS,

Invitrogen), placed onto Histopaque 1077 (Sigma), and centrifuged at 740x*g* for 30

minutes. Buffy coat mononuclear cells were collected and washed three times with "complete EC growth medium," comprising 8% (vol/vol) fetal bovine serum (FBS) added to Endothelial Basal Media-2 (Cambrex) supplemented with Endothelial Growth Media-2 SingleQuots (containing 2% FBS plus growth factors, Cambrex), and 1% antibiotic/antimycotic solution (Invitrogen). Mononuclear cells were plated on plastic 6 well 35 mm diameter plates coated with collagen I (rat tail, BD Biosciences) in complete EC growth medium. Medium was exchanged every 24 hours for the first week in culture, to remove non-adherent cells. Colonies of EPC-derived ECs appeared 7-10 days after the initial isolation. The colonies were trypsinized and cells were plated onto a collagen-coated T25 and labeled passage 1.

The hCB-ECs were grown in T75 flasks using EBM2 basal media supplemented with penicillin/streptomycin, EGM2 Singlequots Kit, and 10% Fetal Bovine Serum (10% complete media). Media was changed every other day until the time of experiment. The hCB-ECs were passaged 1:10 into new T75 flasks upon reaching confluence. Cells were then subsequently split 1:10. The number of population doublings (PDLs) that occurred between each passage was adjusted based upon a 75% attachment rate and calculated according to the formula $\ln(10)/\ln(2)*(4/3) = 4.43$ as previously described.[169]

3.2.2 EC Characterization

The hCB-ECs with fewer than 31 population doublings (PDL) have been extensively studied and function very similar to vascular ECs.[11, 20, 27, 88, 89] The

hCB-ECs are positive for the endothelial-specific CD31 and CD34, and negative for

CD14, CD45 and CD115 found on monocytes or hematopoietic cells.[27] We previously

characterized hCB-ECs and found that they also expressed von Willebrand factor and

VE-cadherin.[11] Following exposure to 15 dyne/cm^2 for 24 or 48 hours, hCB-ECs

aligned with the direction of flow,[11, 20] increased nitric oxide production, and

increased mRNA for endothelial cell specific genes sensitive to flow, KLF2, eNOS, cyclo-

oxygenase 2, and thrombomodulin.[11] The level and organization of actin filaments are

similar in hCB-ECs and human aortic ECs (HAECs) as are the associated values of cell

stiffness[20]. hCB-ECs < 31 PDL had high levels of telomerase and low levels of

senescence-associated β-galactosidase staining, so we refer to them as "young" ECs.[27]

hCB-ECs > 44 PDL had low levels of telomerase and high levels of senescence-associated

β-galactosidase staining compared to hCB-ECs < 31 PDL, so we refer to them as "aged"

ECs.[27]

3.2.3 Flow Experiments

hCB-ECs were plated at a density of about 50,000 cells/cm^2 in slide flasks

(Thermo Scientific) for flow experiments and in 6-well plates (BD) for static controls.

hCB-ECs were grown to confluence for 24 hours. The slides with cells were carefully

assembled into a parallel plate flow chamber and exposed to a steady wall shear stress

of 15 dyne/cm^2 for 24-48 hours before RNA isolation or immunofluorescence. At the

same time, control samples were maintained under static conditions in the incubator for

24-48 hours. All static and flow experiments were performed with flow medium

(DMEM/F12 with 15 mmol/L HEPES, 3.3% FBS, and 1× ITS).

3.2.4 Quantitative real-time RT-PCR

RNA purity and quantity were measured using a NanoDrop Spectrophotometer

(NanoDrop Technologies). Total RNA (50 ng) was reverse transcribed using the cDNA

Synthesis Kit (Bio-Rad) and a MyIQ Cycler (Bio-Rad) thermal cycler. One cycle of 5 min

at 25°C, 30 min at 43°C, and 5 min at 85°C was performed. Primers, RNAse-free water,

and IQ SYBR Green Supermix (Bio-Rad) were combined with the cDNA samples and

placed in a MyIQ single color real-time PCR detection system (Bio-Rad). A two-step

cycle configuration was performed with an initial denaturation for 3 min at 95°C and 50

cycles at 95°C for 15 s and 61°C for 1 min. All samples were performed in triplicate for

all genes. The $2^{-\Delta\Delta CT}$ method was used to determine the relative gene expression.[98]

Primers were selected based on the gene sequence (PubMed) of interest as previously

described.[177] The primers (IDT Technologies) used to complete the studies were *1*) β2-

microglobulin: 5′-GGC TAT CCA GCG TAC TCC AAA G-3′ and 5′-CAA CTT CAA TGT

CGG ATG GAT G-3′; *2*) KLF2: 5′-GCA CGC ACA CAG GTG AGA AG-3′ and 5′-ACC

AGT CAC AGT TTG GGA GGG-3′; and *3*) eNOS: 5′-GTG ATG GCG AAG CGA GTG

AAG-3′ and 5′-CCG AGC CCG AAC ACA CAG AAC-3′. Melting curves were plotted

following each reaction to verify that only the target cDNA was amplified. Reference

RNA, collected from a large batch of ECs at 18 population doubling, was used as a

common reference for all samples tested. The reference RNA was isolated, aliquoted, and stored at −80°C until needed.

3.2.5 Immunofluorescence

hCB-ECs were seeded at 50,000 cells/cm^2 on 6-well plates. At 2 days post plating, cells were fixed and permeabilized for 3 minutes with methanol or for 10 minutes with 2% paraformaldehyde. Samples were then blocked with PBS/0.02% Tween 20 (Biorad)/3% bovine serum albumin (Sigma) for 1 hour at room temperature. The samples were then incubated with antibodies to mouse-PECAM (1:250 dilution, lot #986831A, clone MEM-05, Invitrogen), goat-VE-cadherin (1:250 dilution, lot #D0312, Santa Cruz Biotechnology), or mouse-heparan sulfate proteoglycan (1:250 dilution, clone 7E12, Thermo Scientific), or mouse-heparan sulfate (1:100 dilution, clone 10E4, US Biological) for 1-2 hours at room temperature. This was followed by appropriate secondary antibody incubation with goat anti-mouse Alexa Fluor 546 (1:250 dilution, Invitrogen), or goat anti-mouse Alexa Fluor 488 (1:250 dilution, Invitrogen), or rabbit anti-goat Alexa Fluor 488 (1:250 dilution, Invitrogen) for 1 hour at room temperature. All antibodies were diluted in PBS/1% BSA. The stains were visualized with a Zeiss 510 Upright or Inverted Microscope.

3.2.6 Glycocalyx Thickness and Density Measurements

The heparan sulfate component of the glycocalyx and the nucleus were stained as described above. To measure glycocalyx thickness, z-stack images were taken on the Zeiss 510 Upright Confocal Microscope at 63x (for static samples) or on the Zeiss 510 Inverted Confocal Microscope at 40x (for flow samples) at 0.33μm intervals as previously described by others.[51] The Zeiss LSM Image Browser was used for generation of z-stack images, 3-D reconstructions, and cross-sectional images. With the cross-sectional images, heparan sulfate thickness was measured for each individual EC for the region over the center of the cell nucleus. Only cells that were completely in the field of view and whose surface glycocalyx was continuous were included in the data.[51] For each condition, at least 3 fields of view are analyzed. Within each field of view, at least 5 cells are analyzed.

To measure the glycocalyx density, images were taken on the Zeiss 510 Upright Confocal Microscope at 63x (for static samples) or on the Zeiss 510 Inverted Confocal Microscope at 40x (for flow samples). Fluorescence intensity of the samples was measured with ImageJ (NIH). An IgG isotype control was used to determine background fluorescence values. For each condition, at least 5 fields of view were analyzed. At least 2 replicates were performed for each sample.

3.2.7 Modulation of SIRT1 Activity

Modulation of SIRT1 activity was performed using an inhibitor, EX-527 (5µmol/L, Sigma) for 6 hours prior to the start of the experiment, or with an activator SRT1720 (0.16µmol/L, Sigma) for 1 hour prior to the start of the experiment. Indirect activation of SIRT1 through Epac1 was performed using 8-pCPT-2'-O-Me-cAMP ("007", 100µmol/L, Biolog) for 2 days prior to the start of the experiment. None of these agents are present when the cells are exposed to flow.

3.2.8 Knockdown of SIRT1

Transient transfection was performed as previously described[24] with Lipofectamine RNAiMAX (Invitrogen). The hCB-ECs were grown to 70% confluency in T-75 flasks. Flasks were then transfected with either SIRT1 (Qiagen, SI00098434) or scramble (negative control) siRNA (Qiagen, 1022076) at 20nM in Opti-MEM (Gibco). Untransfected cells were used as a control. Four hours after transfection, the medium was changed back to fresh 10% complete medium. The cells were then cultured for 24 hours before the start of the experiment.

3.2.9 Modulation of Glycocalyx

Degradation of the glycocalyx was performed with *Flavobacterium heparinum* heparinase III (Sigma) for 2 hours prior to the start of the experiment.[22, 64, 126, 192] Angiopoietin-1 (R&D Systems) was incubated at 100ng/mL for 30 minutes prior to the start of the experiment to increase the thickness of the glycocalyx.[149] Brefeldin A is a

specific Golgi translocation inhibit that works within minutes.[146] Co-perfusion of

Brefeldin A with angiopoietin-1 reduces angiopoietin-1 mediated increases in glycocalyx

thickness and mass.[149] Brefeldin A (Sigma) was incubated at 100 µmol/L for 30

minutes prior to the start of the experiment. None of these agents are present when the

cells are exposed to flow.

3.2.10 Inhibition of NADPH Oxidase

Inhibition of NADPH oxidase was performed incubating the cells with 5 µmol/L

of the specific inhibitor VAS2870 (Sigma)[185] for 30 minutes prior to the start of the

experiment. This agent was not present when the cells are exposed to flow.

3.2.11 Western Blotting

Western blots were performed to determine the expression of phosphorylated

VE-cadherin and SIRT1. Cells were seeded at a density of 50,000 cells/cm^2 on to slide

flasks and grown for 24 hours. The cells were then subjected to 15 dynes/cm^2 of steady

shear stress for 48 hours. For the SIRT1 knockdown experiments, cells were seeded at

50,000 cells/cm^2 on to 6-well plates and grown for 24 hours. Cells were harvested with a

cell scraper and subjected to a solution of CellLytic-M (Sigma) and Protease Inhibitor

Cocktail (Sigma). Protein quantification was performed with the A280 Protein

Quantification Method. For SIRT1 knockdown experiments, samples were boiled for 5

minutes at 100°C. 20 µg of protein was loaded into each well for the SDS-

polyacrylamide gel electrophoresis (10% gel, Biorad). Afterwards, the protein bands

were transferred to PVDF membranes. The membranes were blocked with a Tris-Buffered Saline with 0.1% Tween 20 (TBST) solution containing 1% BSA or 5% milk at room temperature for 1 hour. Primary antibodies for rabbit-SIRT1 (1:250, 120kDa, Santa Cruz Biotechnology), goat-VE-cadherin (1:2000 dilution, 132kDa, Santa Cruz Biotechnology) and mouse-β-actin (1:2000 dilution, 42kDa, Santa Cruz Biotechnology) were diluted in a TBST solution containing 1% milk or 1% BSA and incubated with the membrane overnight at 4°C. Goat-anti-mouse (1:2500 dilution, Invitrogen) goat-anti-rabbit (1:500 dilution, Invitrogen) and donkey anti-goat (1:2500 dilution, Santa Cruz Biotechnology) secondary antibodies were incubated with the membrane for 45 minutes at room temperature. After washing, immunoreactive bands were detected by luminography using Supersignal chemiluminescent substrate (Pierce). Subsequently, expression of phosphorylated VE-cadherin was detected by stripping the immunoblot and then reprobing with mouse-β-actin (1:2000 dilution, 42 kDa, Santa Cruz Biotechnology), rabbit-pTyr658-VE-cadherin (1:500 dilution, 120kDa, Millipore), diluted in a TBST solution containing 1% BSA overnight at 4°C. Goat-anti-mouse (1:2500 dilution, Invitrogen) or goat anti-rabbit (1:500 dilution, Invitrogen) secondary antibody diluted in TBST with 1% BSA was incubated with the membrane for 45 minutes at room temperature. Chemiluminescent solutions (Pierce) were added for 5 minutes to cover the membrane. Integrated band density was determined by densitometry after scanning onto autoradiographic films (GE Healthcare) and evaluated by ImageJ (NIH). Protein

expression was reported as a normalized intensity of the band of interest compared to the band of the housekeeping protein, β-actin. There was no significant effect of any of the conditions on the protein expression of loading control, β-actin.

3.2.12 Quantification of Cell Alignment

hCB-EC PECAM images were analyzed with ImageJ to quantify cell alignment. For each experiment, at least 4 fields of view were analyzed per well. The freehand trace tool was used to trace the perimeter of each cell. The orientation angle was determined using the fit ellipse analysis tool. This angle was converted to a first quadrant angle between 0 and 90 degrees. The direction of fluid flow was defined as 0 degrees, while the direction perpendicular to fluid flow was defined as 90 degrees.

3.2.13 Quantification of Trabecular VE-cadherin

hCB-EC VE-cadherin images were analyzed using ImageJ to quantify the amount of trabecular VE-cadherin as previously described.[56] Briefly, we traced the trabecular junction with the freehand tracing tool and calculated its area using the analysis tool. The percentage cell area covered by the reticular junction was measured and expressed as percentage of total cell perimeter area.

3.2.14 Permeability Experiments

Permeability experiments were performed as previously described.[27] Briefly, hCB-ECs or HAECs were seeded with 10% complete FBS media onto the luminal (top) chambers of 0.4μm pore, polyester, 12-well Transwell plates (Corning) at a density of

100,000 cells/cm² which ensured the development of a confluent monolayer 1 to 2 days

post-plating. The abluminal (bottom) chamber contained serum-free media. The

permeability was measured 7 days post-plating. Prior to the experiment, cells in some

wells were incubated with an agent that modifies the glycocalyx – heparinase or

angiopoietin-1. 1 mg/mL of unlabeled bovine serum albumin (BSA) was added to the

abluminal chamber and 1mg/mL of FITC-BSA was added to the luminal chamber at

volumes that would ensure no differences in hydrostatic or osmotic pressure. 10μL

samples were taken from the abluminal chamber every 20 minutes for 2 hours. Albumin

content of the sample was determined by a fluorimeter using a calibration curve.

Permeability coefficients were determined using the expression previously described by

Albelda et al.[2] The permeability term represents contributions from both the cells and

the membrane. To calculate the permeability of the cells alone, the permeability of the

cell layer and the membrane were treated as resistances in series.

3.2.15 Statistical Analysis

All data presented represent mean ± SE with the number of experiments (n)

noted in the legend. A $p < 0.05$ was interpreted to denote statistical significance. For

Figure 10A, a two-factor ANOVA for cell age and presence of flow was performed,

followed by a post-hoc Tukey test.   For Figure 10B, an ANOVA for cell age and flow,

followed by a post-hoc Tukey test was used to determine differences in gene expression

levels between young and old cells. For Figure 11, a 2-factor ANOVA for treatment

condition and age was performed. For Figure 12, a 2-factor ANOVA was used to determine the effect of flow and treatment on gene expression in hCB-ECs. For Figure 14, a 2-factor ANOVA for treatment condition and flow was performed, followed by a post-hoc Tukey test was used to determine differences in gene expression levels for the different treatment and control groups tested. For Figure 16, an ANOVA for cell age followed by a post-hoc Tukey test was performed to determine differences in glycocalyx thickness and intensity for each cell age. For Figure 17, an ANOVA followed by a post-hoc Tukey test was used to determine the influence of treatment groups.   In Figure 18, a 2-factor ANOVA for flow and treatment was performed followed by a post-hoc Tukey test. For Figure 20, a t-test was used to determine whether there was a significant difference of age (Figure 20D) or treatment (Figure 20E) on amount of trabecular VE-cadherin.   For Figure 21, an ANOVA was performed on log-normal data (to ensure a normal distribution) to determine the effect of age and treatment on protein expression. This was followed by a post-hoc Tukey test to discern the effect of different treatments. For Figure 22, a 2-factor ANOVA was performed on log-normal data (to ensure a normal distribution) to determine the effect of age and treatment. This was followed by a post-hoc Tukey test to discern the effect of different treatments. For Table 1, a paired t-test comparing treated ECs to untreated ECs was used to determine whether treatment affected the glycocalyx thickness or density. For Figure 23, a 2-factor ANOVA for flow and treatment was performed for each gene, followed by a post-hoc Tukey test. All

statistical analysis was performed using JMP (SAS). Results represent data from at least

3 different isolations of ECs. Values of n indicate the number of experiments performed.

Values of N represent the number of cells or fields of view analyzed.

3.3 Results

3.3.1 Less Alignment to Flow in Aged hCB-ECs than Young hCB-ECs

We previously found that hCB-ECs with fewer than 31 population doublings

(PDL) had high levels of telomerase and low levels of senescence-associated β-

galactosidase staining,[7] and refer to them as "young" ECs. In contrast, hCB-ECs with

more than 44 PDL had low levels of telomerase and high levels of senescence-associated

β-galactosidase staining compared to hCB-ECs < 31 PDL, and refer to them as "aged"

ECs, while noting the specific range of PDL examined.

Because early passage ECs align in the direction of flow,[96] we compared the

effect of 24 hours of 15 dynes/cm^2 steady uniform, laminar shear stress on alignment of

young and aged hCB-ECs. Both young (13 PDL) and aged (49 PDL) hCB-ECs aligned in

the direction of flow compared to static conditions (Figure 10A, p<0.05). Under static

conditions ECs were randomly oriented, averaging 47±5 degrees with respect to the flow

direction. Young hCB-ECs exposed to flow aligned at 10±1 degrees, whereas aged hCB-

ECs aligned to a lesser extent, 21±3 degrees (Figure 10A, p<0.05).
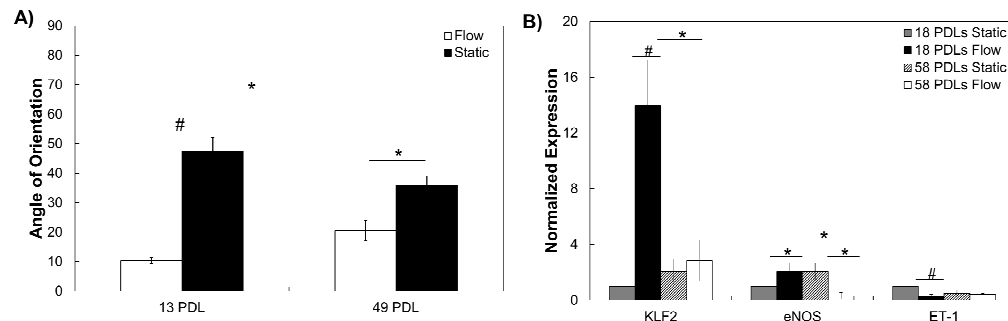
Figure 10: Aged hCB-ECs have a decreased response to shear stress. A) Young hCB-ECs (13 PDL) align more in the direction of fluid flow than aged hCB-ECs (49 PDL). (n=3, N= 27-59 cells per experiment); B) Under steady laminar, unidirectional shear (15 dynes/cm^2) old hCB-ECs (58 PDL) exhibit a smaller increase in eNOS and KLF2 mRNA levels compared to young hCB-ECs (18 PDL) under shear stress and aged hCB-ECs under static conditions *: p<0.05; #: p<0.01 (n=4).

3.3.2 Aged hCB-ECs Have Decreased Response to Steady Shear Stress

Next, we examined in young and aged ECs the flow-mediated enhancement of

KLF2, a transcription factor that mediates anti-inflammatory and anti-thrombotic

properties of ECs, and eNOS, an EC-specific isoform of nitric oxide synthase regulated

by KLF2. For young hCB-ECs (18 PDLs), KLF2 mRNA levels increased 14-fold in

response to 15 dynes/cm^2 for 24 hours compared to ECs exposed to static conditions for

the same duration (Figure 10B, p<0.01). In contrast, aged hCB-ECs (58 PDLs) exposed to

15 dyne/cm^2 for 24 hours exhibited no change in KLF2 compared to static conditions

(Figure 10B), indicating that these aged hCB-ECs are not responsive to shear stress.

Additionally, the KLF2 mRNA levels are 5 times lower for aged hCB-ECs than young

hCB-ECs under shear stress (Figure 10B, p<0.05). When pooling control samples from

all experiments, KLF2 was significantly lower in aged (> 44 PDL) compared to young (< 31 PDL) hCB-ECs under flow conditions (p<0.05).

While eNOS mRNA was upregulated 2-fold in young hCB-ECs exposed to shear stress compared to static controls (Figure 10B, p<0.05), eNOS levels were reduced in aged cells under flow compared to young cells under flow (Figure 10B, p<0.05). Furthermore, eNOS mRNA in aged hCB-ECs under flow is 7 times lower than that of the corresponding static conditions, indicating that eNOS generation is inhibited by flow in aged hCB-ECs (Figure 10B, p<0.05). When pooling control samples from all experiments, eNOS levels were significantly lower in aged (> 44 PDL) compared to young (< 31 PDL) hCB-ECs under flow conditions (p<0.05). ET-1, a vasoconstrictor, is not normally upregulated by shear stress and was used as a control. Its levels were downregulated for young hCB-ECs under shear stress compared to static controls (Figure 10B, p<0.01), but there was no significant effect of age. Thus, aged hCB-ECs exhibit a decreased response to steady shear stress due to little or no upregulation of atheroprotective genes KLF2 and eNOS.

3.3.3 SIRT1 Levels Are Reduced in Aging hCB-ECs

Because SIRT1 has been shown to be important in age-associated pathologies, we measured SIRT1 levels in aging hCB-ECs. We found that SIRT1 levels were high in young hCB-ECs and were significantly reduced in aged hCB-ECs (Figure 11). Because SIRT1 levels were high in young hCB-ECs, we investigated the effects of a SIRT1

inhibitor on young hCB-ECs. Treatment of young hCB-ECs with EX-527, a SIRT1

inhibitor, had no significant effect on SIRT1 protein levels (Figure 11). However, others

have shown that EX-527 does not alter protein levels, but does alter SIRT1 activity

levels.[155]   Because SIRT1 levels are low in aged hCB-ECs, we investigated the effects

of a SIRT1 activator on aged hCB-ECs. Activation of SIRT1 with SRT1720 in aged hCB-

ECs elevated SIRT1 levels compared to untreated controls (Figure 11).
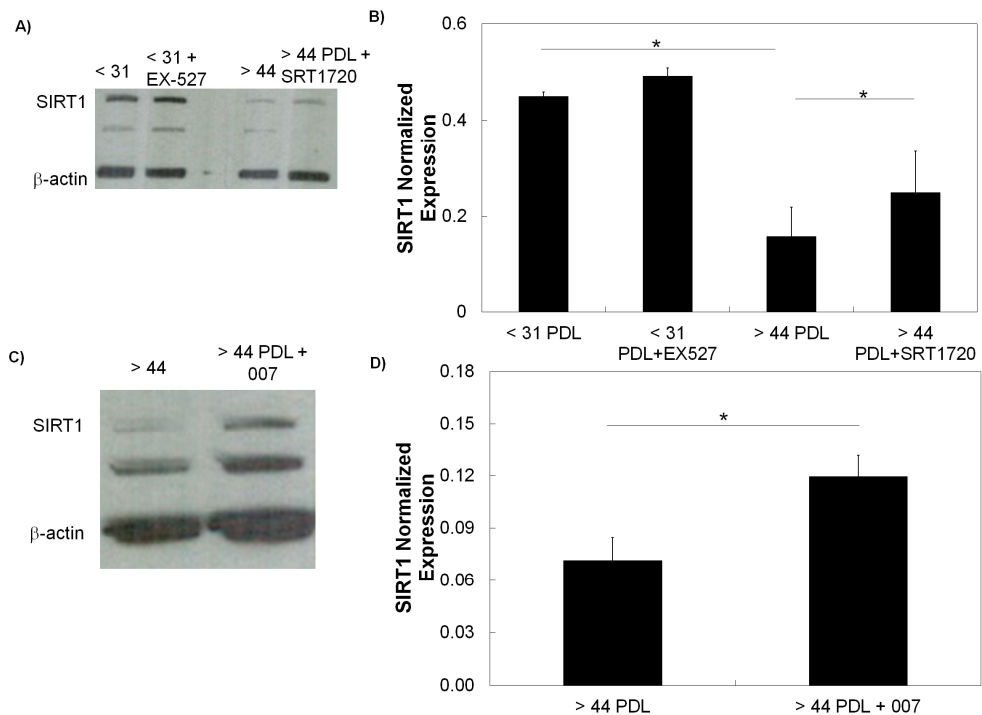
Figure 11: SIRT1 levels are reduced in aged hCB-ECs. A) Representative Western blot of SIRT1 with loading control β-actin. B) SIRT1 levels are significantly lower in aged hCB-ECs. Activation of SIRT1 with SRT1720 increases SIRT1 levels. However, there is no significant effect on SIRT1 levels when EX-527 is used to inhibit SIRT1. C) Representative Western blot of SIRT1 with loading control β-actin. D) SIRT1 levels are lower in aged hCB-ECs after activation with 007. *p<0.05. (n=3)

3.3.4 Modulation of SIRT1 Regulates hCB-EC Response to Shear Stress

The deacetylase antioxidant regulator SIRT1 decreases with increasing cell age[9, 136] and in regions of accelerated EC aging in the vasculature.[24] To determine whether inhibition of SIRT1 decreased the hCB-EC response to shear stress, young hCB-ECs were exposed to 5 µmol/L EX-527, a specific SIRT1 inhibitor,[63] for 6 hours prior to the start of flow experiments.[155, 191] For all flow experiments, flow media did not contain any pharmacological treatments. EX-527 led to a 5-fold decrease in KLF2 levels under static (Figure 12A, p<0.01) conditions and a 3-fold decrease under flow conditions (Figure 12A, p<0.05). Likewise, EX-527 treatment decreased eNOS levels under both static and flow conditions (Figure 12B).
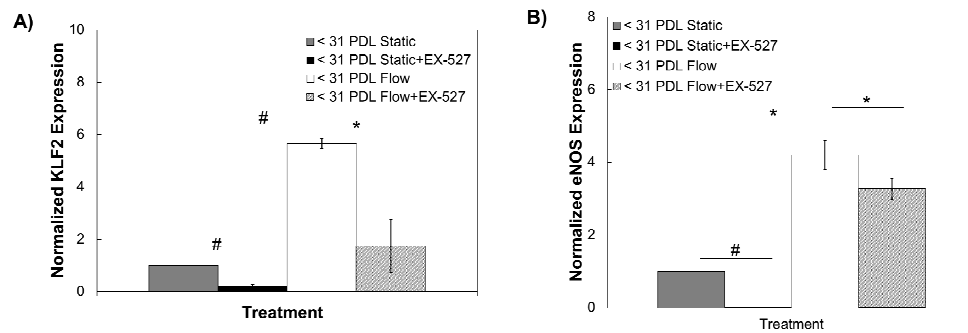
Figure 12: Inhibition of SIRT1 with 5 µmol/L EX-527 in < 31 PDL hCB-ECs reduces A) KLF2 and B) eNOS in response to shear stress. *: p<0.05; #: p<0.01 (n=3).

Treatment with siRNA to SIRT1 caused complete knockdown of SIRT1 protein (Figure 13) and reduced KLF2 levels under static conditions (Figure 14A), but KLF2 still

increased in response to flow. However, siRNA knockdown of SIRT1 completely

abolished eNOS mRNA under both static and flow conditions (Figure 14B).
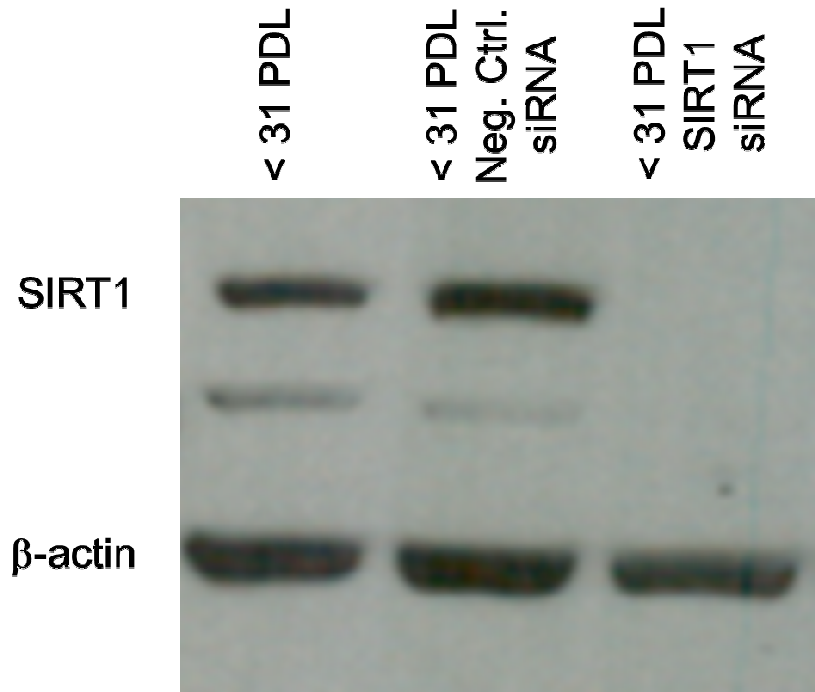
Figure 13: Representative Western blot to confirm knockdown of SIRT1 with siRNA.

To determine whether indirect activation of SIRT1 through Epac1 improves the

response to flow in aging hCB-ECs, we used cyclic AMP analog 007, which ameliorates

aging-related metabolic phenotypes[128] and increases VE-cadherin junctional

localization.[42] Treatment with 100 µmol/L 007 of aged hCB-ECs under static

conditions or after exposure of aged ECs to 15 dynes/cm² shear stress for 24 hours did

not significantly affect KLF2 levels (Figure 14C). However, addition of 007 to old hCB-

ECs under shear stress significantly increased KLF2 levels by 3-fold compared to flow

conditions (Figure 14C, p<0.01). Treatment with 007 had a similar effect on eNOS levels

(Figure 14D).
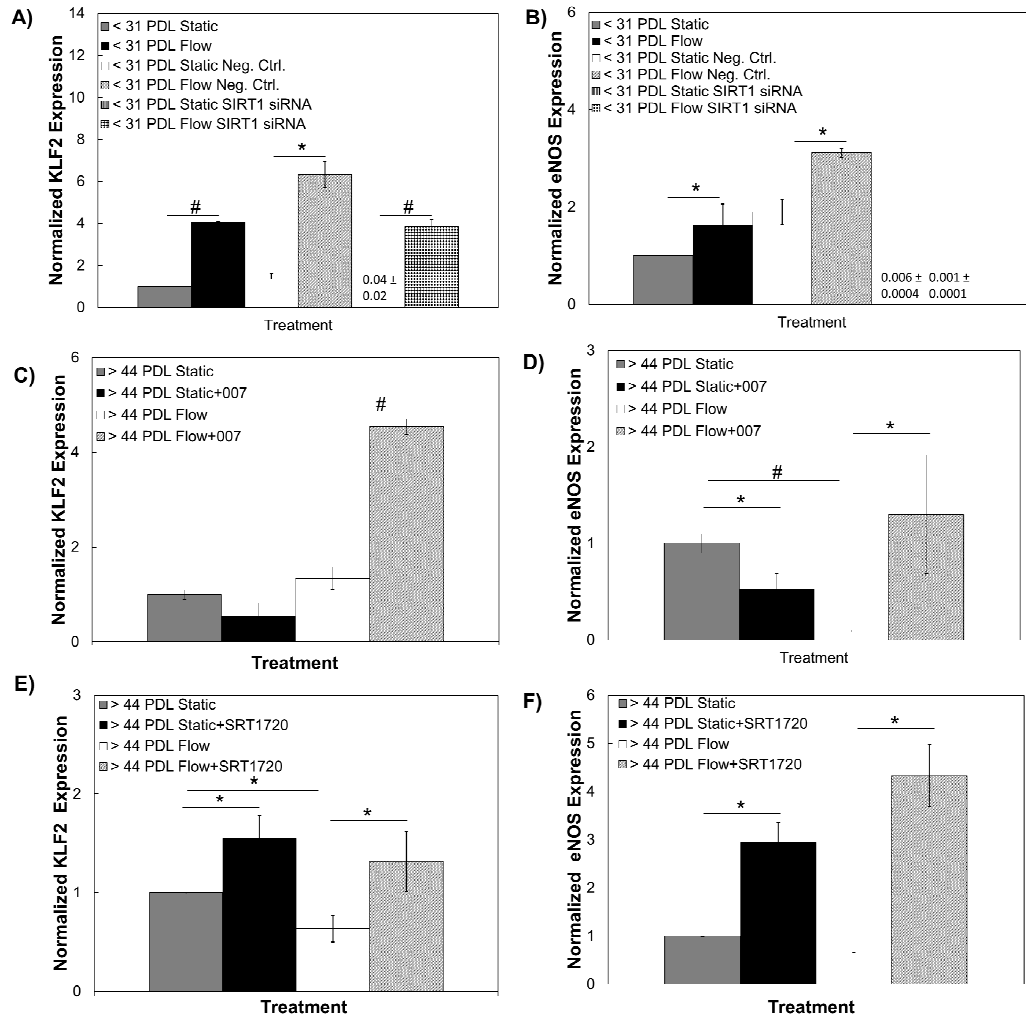
Figure 14: Modulation of SIRT1 regulates response to shear stress. Treatment of young hCB-ECs (< 31 PDL) with SIRT1 siRNA under static conditions caused a decrease in KLF2 (A) and B) eNOS mRNA levels; Treatment with 100 μmol/L 8-pCPT-2'-O-Me-cAMP (007) to indirectly activate SIRT1 increased KLF2 (C) and eNOS mRNA levels (D) for aged hCB-ECs (> 44 PDL); Directly activating SIRT1 with 0.16 ✿mol/L SRT1720 increased KLF2 (E) and eNOS (F) mRNA levels for aged hCB-ECs . *: p<0.05; #: p<0.01 (n=3).

Relative to untreated aged hCB-ECs, direct activation of SIRT1 with 0.16 μmol/L

SRT1720[107] led to an increase in KLF2 levels in aged hCB-ECs under both static

(Figure 3E, p<0.05) and flow (Figure 14E, p<0.05) conditions. However, levels of KLF2

with SRT1720 treatment under both static and flow conditions were not significantly

different indicating that SRT1720 was not sufficient in restoring the flow responsiveness.

SRT1720 had a similar effect on eNOS levels (Figure 14F).

3.3.5 Glycocalyx Thickness and Density Decrease with Increasing Cell Age

To determine whether age-related changes to the glycocalyx are a cause of

decreased response to shear stress in aged ECs, we examined the heparan sulfate

component and the perlecan core protein component of the glycocalyx with increasing

cell age for ECs from a single isolation. Although perlecan is a core protein, it has been

shown to be present in the glycocalyx[72] and has been used to measure glycocalyx

thickness.[77] Isotype control antibodies were used to assess background fluorescence

(Figure 15).
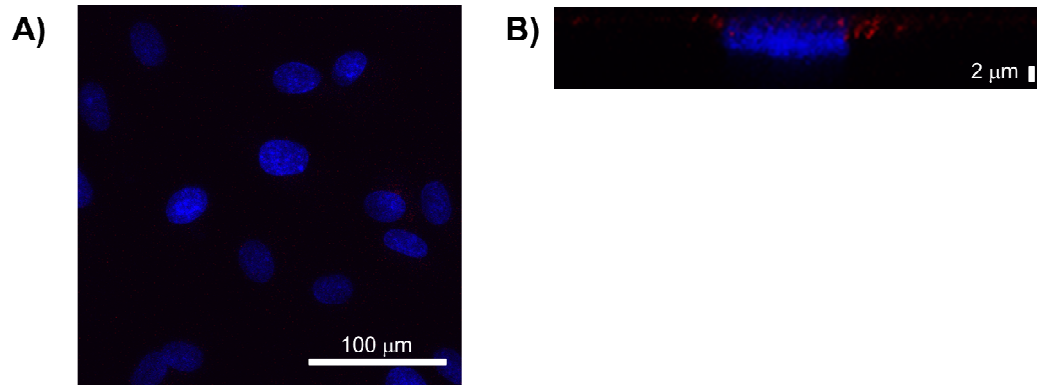
Figure 15: Representative image of fluorescence produced by treatment of hCB-ECs with IgG isotype control (red) and nuclei (blue) in A) planar and B) cross-sectional views.

Confocal images of perlecan immunofluorescence in 22 PDL (Figure 16A) and 49 PDL hCB-ECs (Figure 16B) under static conditions showed that the perlecan density, as measured by the fluorescence intensity, decreased significantly in aged ECs (Figure 16F, $p<0.01$). Likewise, perlecan thickness also decreased with increasing cell age (Figure 16E). Consistent with this trend, confocal images of heparan sulfate immunofluorescence in young hCB-ECs (Figure 16C) and aged hCB-ECs (Figure 16D) indicate an increased heparan sulfate density in young hCB-ECs.
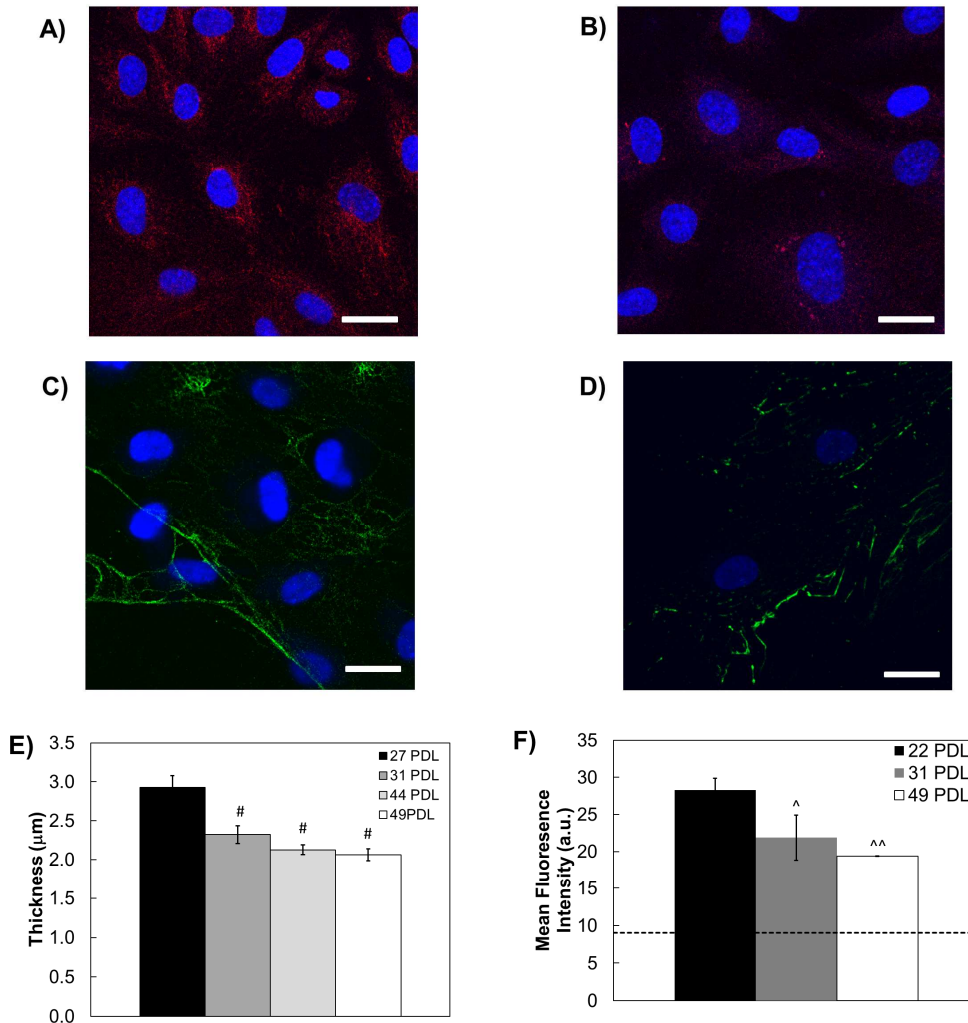
Figure 16: Confocal image of hCB-EC heparan sulfate core protein, perlecan, (red), heparan sulfate (green), and nuclei (blue) to measure perlecan density for A) 22 PDL and B) 49 PDL; heparan sulfate density for C) 31 PDL and D) 62 PDL; E) Change in perlecan thickness with increasing cell age. #: $p<0.01$ compared to 27 PDL static control (n=3, N=15-27 cells); D) Change in perlecan intensity with increasing cell age. Dotted line represents intensity of isotype control (see Supplemental Figure 3). ^: $p<0.05$ compared to 22 PDL static control; ^^: $p<0.01$ compared to 22 PDL static control (n=3). Scale bar =50 μm.

We confirmed that these age-related changes in heparan sulfate fluorescence are

comparable to changes in glycocalyx thickness and abundance found with agents

known to enhance or reduce the glycocalyx. A 2 hour 15mU/mL heparinase treatment

prior to exposure of young hCB-ECs to exposed to 15 dyne/cm^2 for 48 hours led to a

significant 16% decrease in glycocalyx fluorescence intensity compared to untreated

controls (Table 4, $p<0.05$), but no change in the glycocalyx thickness (Table 4). This

agrees with previously reported results demonstrating that heparinase alters glycocalyx

density rather than thickness.[51] For aged hCB-ECs, a 30 minute treatment with

100ng/mL angiopoietin-1[149] prior to exposure to flow led to a 165% increase in

glycocalyx thickness (Table 4, $p<0.05$), which is consistent with previously reported

results for ECs.[149]

Table 4: Effect of treatments on glycocalyx density and thickness after 24 - 48 hour steady shear stress. *:p<0.05 compared to untreated control; #:p<0.01 compared to untreated control. n=3-4.

Treatment	Age (PDL)	Quantity Measured	Percent Change
Heparinase	< 31 PDL	Density	-16 ± 4*
Heparinase	< 31 PDL	Thickness	-11 ± 17
EX-527	< 31 PDL	Density	-47±13*
EX-527	< 31 PDL	Thickness	-55±5*
SIRT1 siRNA	< 31 PDL	Density	-54±6*
SIRT1 siRNA	< 31 PDL	Thickness	-86±8*
Angiopoietin-1	> 44 PDL	Density	9 ±32
Angiopoietin-1	> 44 PDL	Thickness	165 ± 27*
Brefeldin A	> 44 PDL	Density	-69 ± 15*
Brefeldin A	> 44 PDL	Thickness	-33 ± 9*
007	> 44 PDL	Density	-11 ± 27
007	> 44 PDL	Thickness	224 ± 110*
SRT1720	> 44 PDL	Density	30 ± 3#
SRT1720	> 44 PDL	Thickness	44 ± 30

Addition of glycosaminoglycans to the surface of ECs occurs through translocation of Golgi vesicles.[149, 181] To verify this and support that angiopoietin-1 acts upon the glycocalyx to regulate the response to shear stress, aged cells were treated with Golgi translocation inhibitor, Brefeldin A. Treatment with 100 μmol/L Brefeldin A for 30 minutes prior to the start of the flow experiment led to a significant decrease in both glycocalyx thickness and density in aged hCB-ECs (Table 4, $p<0.05$). While aged hCB-ECs treated with angiopoietin-1 had an increase in mean fluorescence after exposure to shear stress compared to untreated aged hCB-ECs (Figure 17, $p<0.05$), this angiopoietin-1 mediated response was inhibited when Brefeldin A was co-administered (Figure 17, $p<0.01$). These results show that angiopoietin-1 improves the response to shear stress in aged hCB-ECs by increased Golgi translocation of glycosaminoglycans to the cell surface.
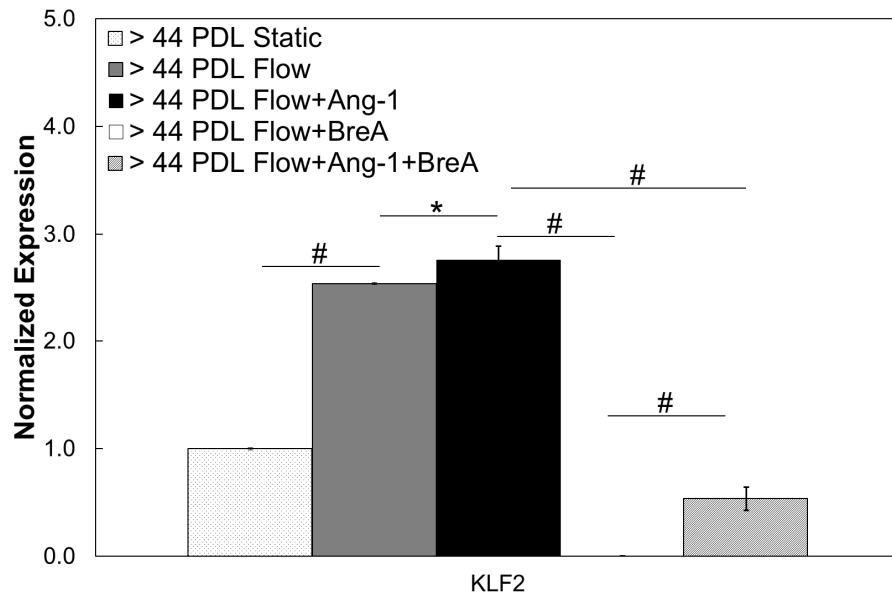
Figure 17: Inhibition of Golgi translocation with Brefeldin A reduces the effect of angiopoietin-1 on KLF2 levels in aged hCB-ECs. *:p<0.05; #:p<0.01 (n=3).

3.3.6 SIRT1 Regulates Glycocalyx Thickness and Density

Given the decrease in glycocalyx thickness and density with increasing cell age (Figure 16E and Figure 16F), we examined whether altering SIRT1 activity affects the hCB-EC glycocalyx. Untreated hCB-ECs exposed to 15 dyne/cm^2 for 48 hours were used as baseline references. Inhibition of SIRT1 in young hCB-ECs by treatment with 5 µmol/L EX-527 for 6 hours prior to the start of the flow experiment led to a 55±5% decrease in heparan sulfate thickness (Table 4, p<0.05) and a 47±13% decrease in heparan sulfate density (Table 4, p<0.05) compared to the untreated flow control. Knockdown of SIRT1 in young hCB-ECs with siRNA led to a 86±8% decrease in heparan sulfate thickness (Table 4, p<0.05) and a 54±6% decrease in heparan sulfate density (Table 4, p<0.05). Conversely, indirect activation of SIRT1 in aged hCB-ECs with 100µmol/L 007,

led to a 224±110% increase in heparan sulfate thickness (Table 4, p<0.05), but there was no significant effect on heparan sulfate density (Table 4). Direct activation of SIRT1 in aged hCB-ECs with 0.16µmol/L SRT1720 led to a 30±3% increase in heparan sulfate intensity (Table 4, p<0.01), but there was not a statistically significant effect on heparan sulfate thickness (Table 4). These results suggest that SIRT1 alters the heparan sulfate thickness and density.

3.3.7 Glycocalyx-Dependent Response of Aging hCB-ECs to Steady Shear Stress

To establish whether alteration of hCB-EC glycocalyx affected the response to shear stress in a similar manner to ECs undergoing cell senescence, we measured the response to shear stress after ECs were treated with agents that enhance or reduce the glycocalyx. Young and aged hCB-ECs were subjected to 15 dynes/cm^2 of shear stress for 48 hours. Some samples were treated with 15mU/mL heparinase for 2 hours prior to the flow experiment to ensure degradation of the glycocalyx, whereas other samples were treated with 100ng/mL angiopoietin-1 for 30 minutes prior to the flow experiment to increase glycocalyx thickness (Table 4). Untreated and static samples were used as controls. Heparinase-treated young hCB-ECs had significantly lower levels of KLF2 (Figure 18A) and eNOS (Figure 18B) mRNA than untreated cells for both static (Figure 5A and 5B, p<0.01) and flow (Figure 18A and Figure 18B, p<0.05) conditions. This result is consistent with the role of the glycocalyx in NO generation through eNOS[57] and establishes a role for the glycocalyx in regulating KLF2. Conversely, angiopoietin-1

treated aged hCB-ECs had significantly higher mRNA levels of KLF2 (Figure 18C) than untreated cells in both static (Figure 18C, p<0.05) and flow (Figure 18C, p<0.05) conditions. eNOS mRNA levels also increased in angiopoietin-1 treated hCB-ECs compared to untreated cells under both static (Figure 18B, p<0.01) and flow (Figure 18B, p<0.01) conditions. These results suggest that depletion of the glycocalyx alter the response to shear stress in a manner similar to age.
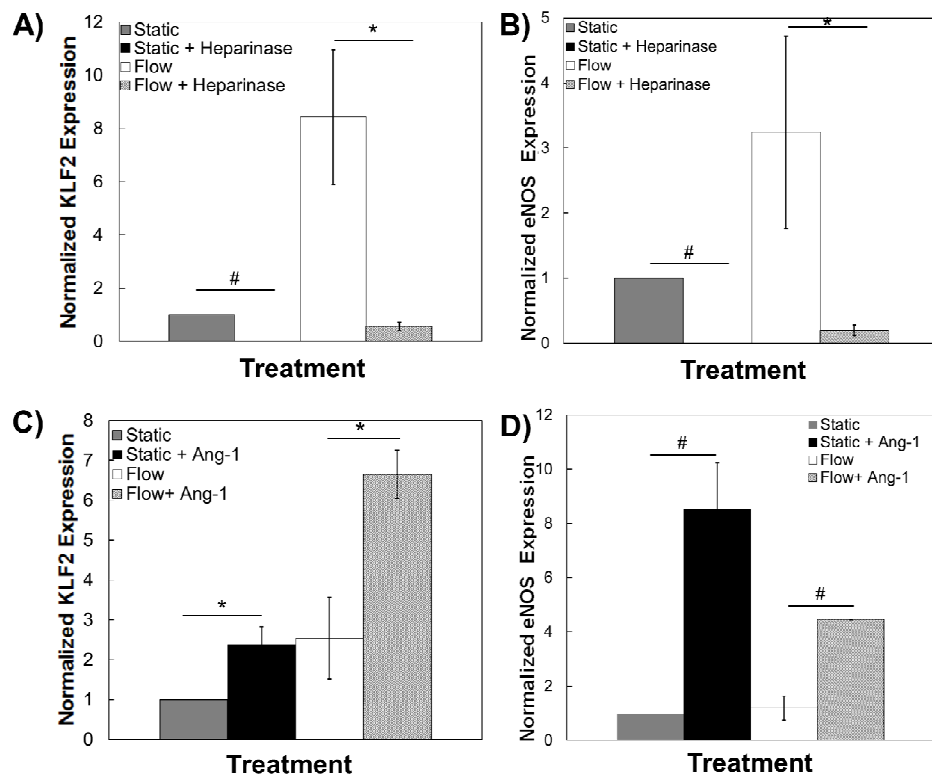
Figure 18: Effect of treatments to the glycocalyx upon KLF2 and eNOS levels following exposure to steady shear stress. A) Heparinase decreases KLF2 in young (< 31 PDL) hCB-ECs; B) Heparinase decreases eNOS in young hCB-ECs; C) Angiopoietin-1 increases KLF2 in aged (> 44 PDL) hCB-ECs; D) Angipoietin-1 increases eNOS in aged hCB-ECs *:p<0.05; #p<0.01 (n=3-4).

3.3.8 VE-cadherin Localization and Structure Under Shear Stress is Primarily Age-Dependent

High levels of trabecular VE-cadherin interact with PECAM to produce low EC permeability in areas of low actomyosin-mediated tension.[56] For 22 PDL hCB-ECs exposed to 15 dynes/cm^2 shear stress for 24 hours, VE-cadherin was localized to cell junctions (Figure 19) and 43%±1% of the junctional area was trabecular VE-cadherin. Glycocalyx disruption with heparinase in young hCB-ECs under flow conditions decreased trabecular VE-cadherin to 30%±2% compared to untreated flow control (p<0.01) and decreased localization at cell-cell junctions (Figure 19B). For 62 PDL hCB-ECs exposed to 15 dynes/cm^2 for 24 hours, VE-cadherin was diffuse within the cell, with only a small amount localized to cell junctions (Figure 19C). Only 7.9%±1% of the junctional area in the aged hCB-ECs was trabecular VE-cadherin. This was significantly less than that found with young hCB-ECs (p<0.01) and hCB-ECs treated with heparinase (p<0.01), indicating that cell age affects the trabecular structure and localization of VE-cadherin more than presence of the glycocalyx. Treatment of aged hCB-ECs with 007 to activate SIRT1 through Epac1 under flow conditions almost doubled the percentage of trabecular VE-cadherin to 13%±1% compared to the untreated ECs (n=3; p<0.01). Additionally, there was increased VE-cadherin localization to cell junctions after 007 treatment (Figure 19D).
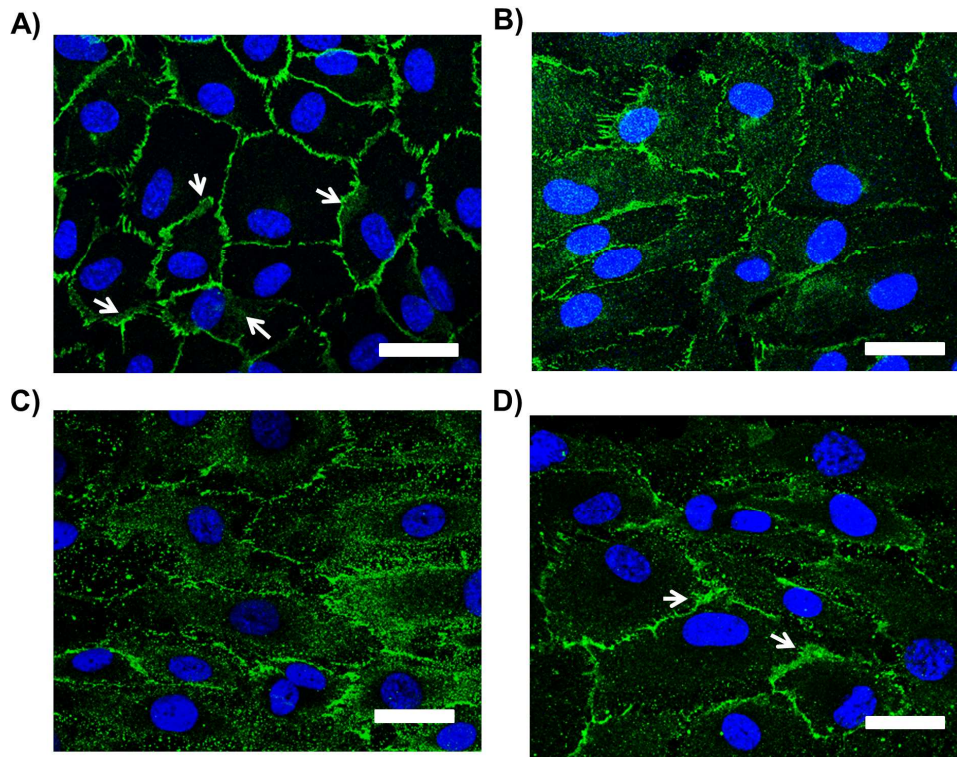
Figure 19: Trabecular VE-cadherin for hCB-ECs exposed for 24 hours to flow that produced a wall shear stress of 15 dyne/cm2. A) 22 PDL hCB-ECs; B) 22 PDL hCB-ECs treated with 15mU/mL heparinase; C) 62 PDL hCB-ECs; D) 62 PDL hCB-ECs treated with 100 µmol/L 8-pCPT-2'-O-Me-cAMP. White arrows indicate trabecular VE-cadherin. Scale bar = 50✳m (n=3).

Trabecular VE-cadherin was present in hCB-ECs of all population doublings under static conditions (Figure 20A-C, white arrows). hCB-ECs that underwent 27 PDL had significantly more trabecular VE-cadherin than 49 PDL hCB-ECs (Figure 20D, $p<0.01$). Treatment of aged hCB-ECs with 007 under static conditions had no effect on the amount of trabecular VE-cadherin (Figure 20E). While SIRT1 can influence the localization and organization of VE-cadherin after exposure of young and aged cells to

flow, trabecular VE-cadherin under static conditions is not significantly affected by

indirect activation of SIRT1.
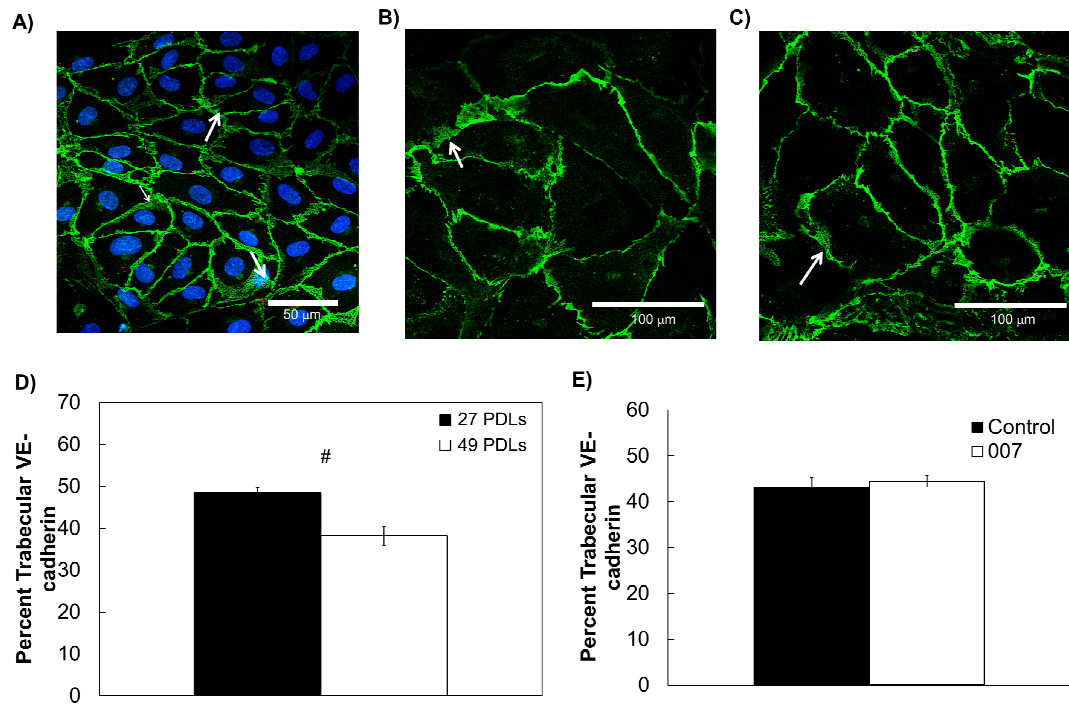
Figure 20: Decrease in trabecular VE-cadherin in aged hCB-ECs under static conditions. VE-cadherin (green) and Hoechst 33342 (blue). A) 27 PDL hCB-ECs; B) 49 PDL hCB-ECs; C) 49 PDL hCB-ECs treated with 100 μmol/L 8-pCPT-2'-O-Me-cAMP (007). D) Quantification of trabecular VE-cadherin for 27 and 49 PDL hCB-ECs. White arrows in panels A, B and C indicate trabecular VE-cadherin. #: p<0.01 (n=3, N=26-52 cells).

3.3.9 SIRT1 Mediates Phosphorylation of VE-cadherin at Tyr-658

Phosphorylation of VE-cadherin at Tyr-658 plays an important role in

mechanotransduction through inhibition of EC migration and increasing permeability

by uncoupling VE-cadherin from p120-catenin.[135] hCB-EC age led to a higher fraction

of Tyr-658 phosphorylation (Figure 21A and Figure 21B, p<0.05). Inhibition of SIRT1 with EX-527 in young hCB-ECs significantly increased the fraction of Tyr-658 phosphorylation (Figure 21, p<0.05). Knockdown of SIRT1 with siRNA also elevated the fraction of Tyr-658 expression (Figures 6E and 6F, p<0.05).
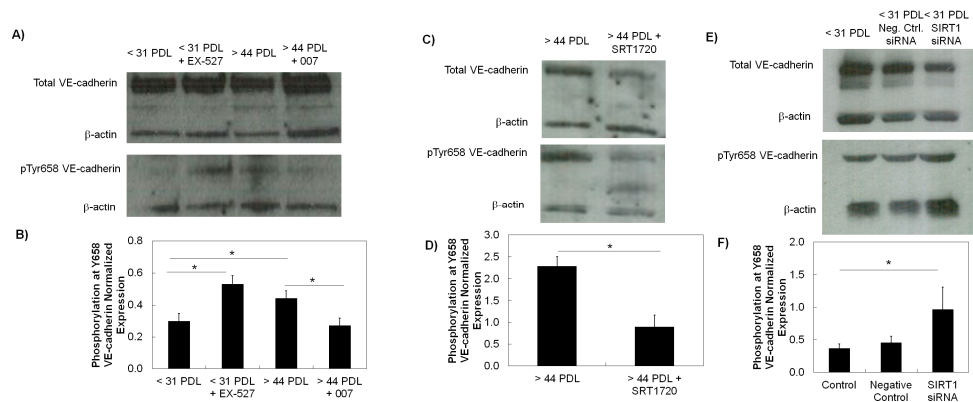
Figure 21: Phosphorylation of VE-cadherin at Tyr-658 is dependent on SIRT1 under static and flow conditions. A) Representative Western blot for treatment with EX-527 and 007 under flow conditions; B) Quantification of Tyr-658 phosphorylation for treatment with EX-527 and 007 under flow conditions; C) Representative Western blot for treatment with SRT1720 under flow conditions; D) Quantification of Tyr-658 phosphorylation with SRT1720 treatment under flow conditions; E) Representative Western blot for treatment with siRNA under static conditions with boiled sample; F) Quantification of Tyr-658 phosphorylation for SIRT1 siRNA treatment under static conditions with boiled sample *:p<0.05 (n=3-5).

Indirect activation of SIRT1 through Epac1 with 007 in aged hCB-ECs significantly decreased the fraction of Tyr-658 expression (Figure 21B, p<0.05). Direct activation of SIRT1 with SRT1720 significantly decreased the fraction of Tyr-658 expression in aged hCB-ECs compared to untreated aged hCB-ECs (Figure 21C and

Figure 21D, p<0.05). These results show that SIRT1 regulates tyrosine phosphorylation of

VE-cadherin at Tyr-658.

3.3.10 Glycocalyx Mediates Phosphorylation of VE-cadherin at Tyr-658

To determine whether the glycocalyx affects VE-cadherin phosphorylation, aged

hCB-ECs were treated with angiopoietin-1 and young hCB-ECs were treated with

heparinase and subjected to 48 hours shear stress at 15 dynes/cm^2. Untreated samples

exposed to the same shear stress served as controls.   Phosphorylation of VE-cadherin at

Tyr-658 increased in young hCB-ECs after heparinase treatment and in aged hCB-ECs

(Figure 22B and Figure 22C, p<0.05). Conversely, phosphorylation at Tyr-658 in aged

hCB-ECs decreased after angiopoietin-1 treatment (Figure 22A and Figure 22B, p<0.05).

These results indicate that phosphorylation of VE-cadherin at Tyr-658 depends on both

glycocalyx and age.

A)

< 31   < 31 + Hep   > 44   > 44 + Ang-1

Total VE-cadherin

β-actin

pTyr658 VE-cadherin

β-actin

B)
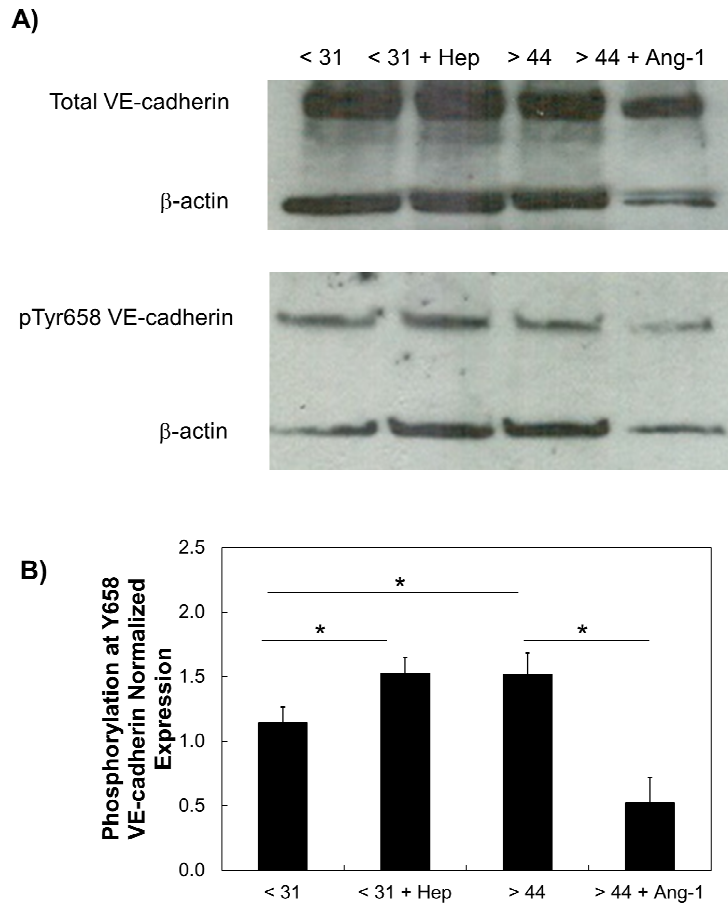
Figure 22: Tyrosine phosphorylation of VE-cadherin is glycocalyx-dependent under flow conditions. A) Representative Western blot; B) Quantification of Tyr-658 phosphorylation.*:p<0.05, #:p<0.01 (n=4-6).

3.3.11 Modulation of Glycocalyx Affects EC Permeability Under Static Conditions

We previously showed that hCB-EC permeability to albumin increases with

increasing cell age.[27] Since increasing age decreases both glycocalyx thickness and

density (Figure 16) and disrupts VE-cadherin phosphorylation (Figure 18 and Figure 21)

and localization (Figure 20), we sought to determine whether changes to the glycocalyx

affected EC permeability. Treatment of young ECs (< 31 PDL) with heparinase, which

reduces heparan sulfate density, led to an increase in EC permeability by $47\pm10\%$ ($p<0.05$). Treatment of aged ECs (>44 PDL) with angiopoietin-1, which increases the glycocalyx thickness, led to a $42\pm7\%$ decrease in EC permeability to albumin ($p<0.05$). Taken together with the results in Figure 21, these results suggest that the glycocalyx functions as both a physical barrier and as a mechanosensor acting together with phosphorylation of VE-cadherin.

3.3.12 Inhibition of NADPH Oxidase Increases Glycocalyx Thickness and Density in Aged ECs, but Is Not Sufficient to Improve Response to Shear Stress

Elevated levels of SIRT1 inhibit NADPH oxidase.[194] In atheroprone regions, aging is accelerated and the glycocalyx has been shown to be sensitive to oxidants.[168] After treatment of ECs with 200 μM H2O2 for 4.5 hours, young (< 31 PDL) ECs exhibited a $22\pm5\%$ decrease in heparan sulfate thickness ($p<0.05$) and $11\pm4\%$ decrease in intensity ($p<0.05$). Following H2O2 treatment, aged ECs did not exhibit any change in glycocalyx thickness or intensity relative to untreated ECs at the same age. To examine whether SIRT1 alters the glycocalyx through an NADPH oxidase-dependent mechanism, we treated aged hCB-ECs with NADPH oxidase inhibitor 5μM VAS2870 for 30 minutes prior to the start of the flow experiment. Inhibition of NADPH oxidase increased both glycocalyx thickness by $123\pm29\%$($p<0.01$) and density by $156\pm34\%$ ($p<0.05$) in aged ECs. When aged ECs under shear stress were treated with VAS2870, KLF2 levels were significantly upregulated (Figure 23, $p<0.01$). However, there was no significant effect

on KLF2 levels in static conditions and no significant effect on eNOS levels for static or

flow conditions. Therefore, restoration of the glycocalyx through inhibition of NADPH

oxidase was not sufficient to fully restore the response to shear stress.
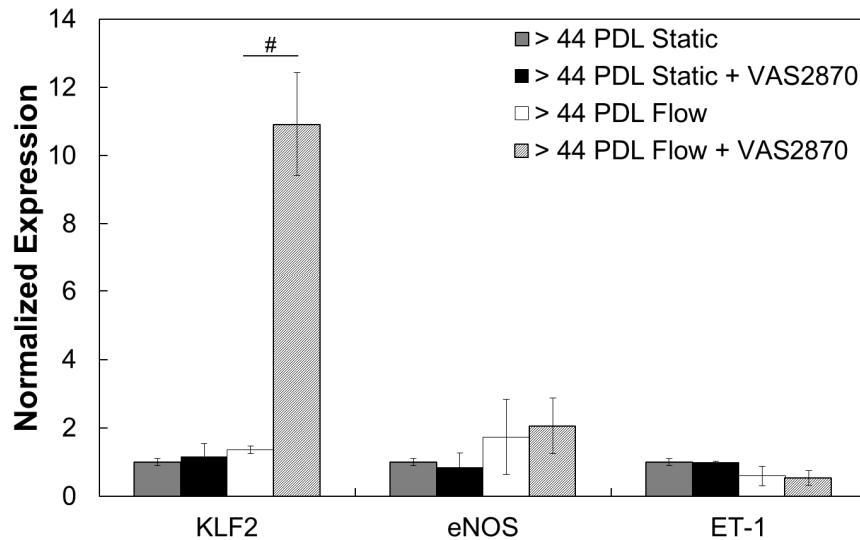
Figure 23: Inhibition of NADPH oxidase elevates KLF2 in aged ECs under flow conditions, but has no significant effect on eNOS. While inhibition of NADPH oxidase does enhance glycocalyx thickness (24%) and density (94%) in aged ECs, it is not sufficient to restore response to shear stress. #p<0.01 (n=3).

3.4 Discussion

In young ECs, increased levels and activity of SIRT1 in response to steady,

unidirectional flow provides a protective mechanism against oxidative stress

damage.[24, 182] SIRT1 activation under atheroprotective flow enhances deacetylation

of eNOS and increases bioavailability of NO.[24] Regions of disturbed flow accelerate

local replication and oxidative stress, leading to senescence of ECs, which promote

endothelial dysfunction. SIRT1 protects ECs from senescence induced by disturbed flow via p53.[182] The findings of the current study suggest that reduced SIRT1 levels, which occur during stress-induced and replicative senescence, result in reduced responsiveness to flow by reduction of the glycocalyx and phosphorylation of VE-cadherin. We demonstrate that as ECs age their responsiveness to steady shear stress declines, in part, due to the reduced effectiveness of the cell mechanotransducers, the glycocalyx and VE-cadherin. The decreased response to steady shear stress in aged hCB-ECs can be mitigated by indirect or direct activation of SIRT1. Increasing the level of SIRT1 in older ECs increases the thickness and density of heparan sulfate in aged cells and restores the expression of KLF2 and eNOS. Additionally, SIRT1 plays an important role in VE-cadherin mechanotransduction. Alteration of SIRT1 affects VE-cadherin localization, trabecular structure, and phosphorylation at site Tyr-658.

The glycocalyx is degraded in atheroprone regions of mice and even in regions away from branches in the apoE mouse.[168] Further, a pro-oxidant environment can reduce the thickness of the glycocalyx.[108] Elevated levels of SIRT1 inhibit NADPH oxidase and protect the cells from oxidative damage.[194] Reduced SIRT1 activity in older cells led to higher levels of NADPH oxidase, which produces oxygen radicals that damage the glycocalyx. We showed that inhibition of NADPH oxidase in aged ECs restored the thickness and density of the glycocalyx, suggesting that SIRT1 may influence the response to flow by limiting reactive oxygen species damage, leading to

increased glycocalyx. While elevated SIRT1 activity did increase KLF2 levels under flow, it was not sufficient to restore eNOS levels. Thus, SIRT1 regulation of the glycocalyx may differentially affect KLF2 and eNOS. In young ECs, inhibition of NADPH oxidase also substantially altered the glycocalyx density, but the change was smaller than in the aged ECs (unpublished observation). These results show that in aged ECs, oxidative damage alters mechanotransduction via the glycocalyx. Restoration of the function can be partly achieved by activating SIRT1 which then inhibits NADPH oxidase.

The heparan sulfate and perlecan thickness of the aged ECs measured in this study is comparable to the previously measured value of 1.38±0.07µm in bovine aortic ECs.[51] While perlecan is a core protein of the glycocalyx, there is evidence that it is secreted in the glycocalyx[72] and it has been used to measure glycocalyx thickness.[77] We also further supported these results by staining for heparan sulfate, and found that the results are consistent. There are several limitations to measuring the glycocalyx with confocal microscopy including low resolution and high background fluorescence.[51] An alternative way to visualize the glycocalyx is with cryo-TEM as this eliminates the need for aldehyde fixation or alcohol dehydration, which are associated with confocal microscopy or traditional TEM.[51] In this study, we only examined the heparan sulphate and perlecan components of the glycocalyx. However, transmembrane

syndecans also are important in mechanotransduction. They have been shown to be important in age-related maintenance of skeletal tissue[131] and skin tissue.[100]

After depletion with heparinase, the glycocalyx regrows in 20 hours under static and 12 hours under flow conditions.[64] This subsequently leads to a normal response to shear stress. However, the results from the study by Giantsos-Adams et al. were obtained after only a 10-minute pretreatment with heparinase,[64] which removed less glycocalyx than the 2-hour treatment used in this study. We have demonstrated that the heparan sulfate component of the glycocalyx is moderately depleted even 48 hours after treatment (Table 4) and that heparinase treatment lowers KLF2 and eNOS gene expression levels in aged hCB-ECs under flow compared to young hCB-ECs (Figure 16). Because of this, it is likely that the difference in results is due to the longer heparinase exposure time used in this study.

Although we used ECs derived from human umbilical cord blood, others and we have found that the hCB-ECs function very similarly to vascular ECs.[11, 20, 27, 88, 89] As noted, the changes to the glycocalyx induced by heparinase and angiopoietin1 are similar to those reported for vascular cells. A key difference and a reason for their choice in this study, is that hCB-ECs can undergo many more population doublings before senescence.

Other signaling pathways could affect the aging EC response to flow besides SIRT1-mediated mechanosensing. Epac1 can bind directly to VE-cadherin to stabilize

VE-cadherin on actin bundles via interactions with α-catenin and β-catenin.[121] Shear-mediated activation of PI3-kinase has been shown to lead to the activation of Nrf2[43] which influences KLF2 activation.[84] Flow-mediated signaling through PI3-kinase and Akt-dependent pathways may also be altered through aging.[163] In soleus muscle feed arteries, NO-mediated dilation of the vessel declines with increasing age.[163] This decline was attributed to reduced potential for PI3-kinase/Akt-dependent phosphorylation of eNOS on Ser1177.[163] These studies suggest a role for a PI3-kinase/Akt-dependent mechanism in regulating the aging EC response to shear stress. Application of aortic intraluminal pressure of 200 mmHg led to a significant increase in phosphorylation of focal adhesion kinase in young rat aortas, but not in aged rat aortas.[145]

During cell senescence, levels of SIRT1 are reduced which also reduces a number of anti-thrombotic and anti-inflammatory genes, including eNOS. [24, 108] In this study, we extend previous work and demonstrate that SIRT1 also impacts KLF2 gene expression (Figure 24). Furthermore, we show a novel role for SIRT1 in regulating mechanosensing through the glycocalyx and VE-cadherin, leading to the altered response to shear stress (Figure 24). Based on these results, it is likely that SIRT1 plays a central role in the regulation of aging EC response to fluid flow (Figure 24).

SIRT1

Phosphorylation of VE-cadherin

NADPH oxidase

at Tyr658   at Tyr731

free radicals

Unbinding of VE-cadherin from p120-catenin

Unbinding of VE-cadherin from β-catenin

glycocalyx

eNOS   KLF2

Leakiness of VE-cadherin

Permeability
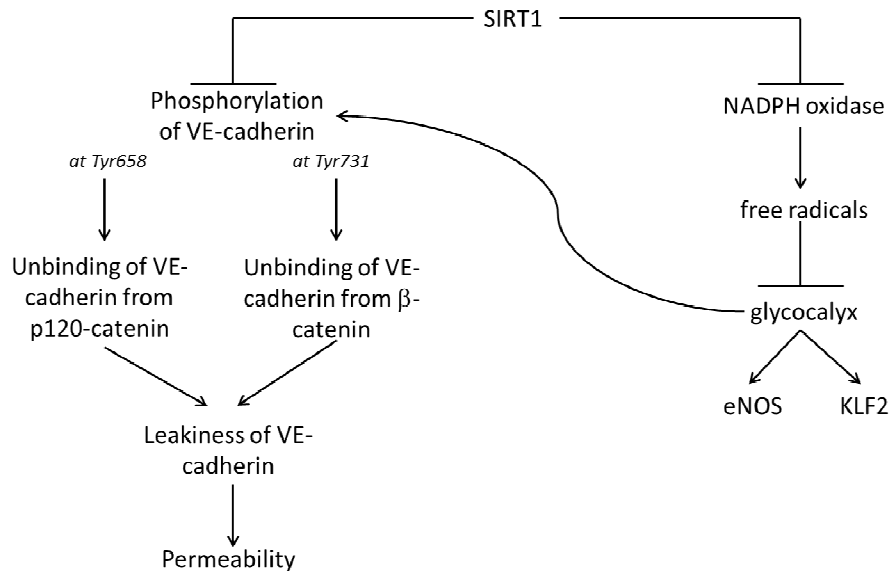
Figure 24: SIRT1 plays a central role in regulating the EC response to shear stress. Shear stress is sensed by the glycocalyx,[57] leading to alteration in KLF2 and eNOS levels. eNOS is in a positive feedback loop with SIRT1,[24] which can alter the glycocalyx thickness and density and lead to an altered response to shear stress. An external activator of membrane-bound cAMP to activate Epac1-Rap1 can lead to activation of SIRT1[129] and an improved response to flow. Furthermore, binding of membrane-bound cAMP to Epac1 to activate SIRT1 leads to increased junctional localization of VE-cadherin[42] in young cells. In aged hCB-ECs, phosphorylation of VE-cadherin at site 658 leads to uncoupling from p120 catenin.[135] The glycocalyx also regulates binding of VE-cadherin to both p120 catenin and β-catenin through tyrosine phosphorylation at 658 and 731, respectively.[135] SIRT1 inhibits NADPH oxidase,[194] leading to improved cell resistance to free radicals that can damage the glycocalyx.

3.5 Chapter Acknowledgements

I would like to acknowledge Justin Fu for his assistance with staining and

quantification of VE-cadherin and the glycocalyx. I gratefully acknowledge Dr. Brent

Hoffman and Dr. Ellie Tzima for their helpful feedback and suggestions related to the

study. The work was supported by an NSF Graduate Research Fellowship (T.M.C.), and

a McChesney Graduate Fellowship (T.M.C.).

Chapter 4. Endothelial Cell Senescence Increases Traction Forces due to Age-Associated Changes in the Glycocalyx and SIRT1

4.1 Introduction

Atherosclerosis is the primary pathology underlying cardiovascular disease and its development has been attributed to both changes in the local mechanical environment and endothelial cell (EC) aging. Changes in vessel composition and structure have been linked to the development and progression of atherosclerosis.[170] There is also evidence of accelerated aging in atheroprone regions, including the presence of giant cells,[13] elevated levels of β-galactosidase staining,[108] and telomere shortening.[123] Aging in atheroprone regions is likely due to high oxidative stress[54] which causes apoptosis. The resulting increase in cell turnover leads to an increase in EC replication. The increased oxidative stress and EC replication can lead to localized senescence. Further, aging endothelium has been shown to have increased permeability to macromolecules[29] and increased sensitivity to oxidative stress.[26] A localized increase in the permeability of the endothelial layer to proteins[79] is one of the earliest events in atherosclerosis development and influences the progression of atherosclerosis.[118, 158]

Traction forces in ECs play an important role in cell migration and adhesion, with forces being highest at the periphery of the cell.[140] Bovine aortic ECs on stiff substrates had increased cell traction forces and permeability compared to those seeded

on soft substrates.[87] This result correlated with increased actomyosin contractility for cells isolated from old mice. This increase in contractility, traction force, and permeability could be reversed through inhibition of the Rho-associated kinase (ROCK) pathway.[87]

Chemically, the environment surrounding the lesion tends to be highly oxidative. This is due to local variations in shear stress leading to the development of oscillatory and reversing flows that increase oxidative stress through NADPH-dependent oxidase,[153] and is exacerbated by elevated levels of lipids and cholesterol. Exposure of ECs to oxidative stress from H_2O_2 treatment elevated their permeability.[14, 26, 124]   Reactive oxygen species regulate the dynamics of the actin cytoskeleton[110] and cell traction forces.[94]   Oxidative stress can disrupt the glycocalyx – a thin layer of glycoproteins and proteoglycans on the surface of endothelial cells both *in vitro* and *in vivo*.[168][101]   Damage to the glycocalyx can increase endothelial permeability and impair shear-mediated NO production.[142, 150, 168]

SIRT1 is a deacetylase that regulates antioxidant activity and the cellular energy balance. Levels of SIRT1 are reduced during aging or due to exposure to oxidative stress and disturbed fluid flow in atheroprone regions.[24] Activation of SIRT1 reverses several age-associated phenotypes.[26, 29, 128, 199] In ApoE-knockout mice, overexpression of SIRT1 in ECs decreased atherosclerosis.[128] Furthermore, SIRT1 may regulate permeability through regulation of cell junction proteins, such as occludin.[29]

While changes in the mechanical environment and cell aging are known to impact atherosclerosis development, the relationship between the two remains unclear. In this study, we tested the hypothesis that age-associated changes in the EC glycocalyx or SIRT1 increase cell traction forces due to changes in actin localization and stress fiber thickness. To test this hypothesis, we used human cord blood-derived ECs (hCB-ECs) as a model for cell aging because of their low, physiological permeability at low population doublings,[29] high proliferative potential in subconfluent cultures,[29] and similarity to arterial ECs.[11] We examined traction forces of aging ECs and assessed their dependence on activators and inhibitors of SIRT1 and heparan sulfate. We also examined the effect of these agents on the actin cytoskeleton.

4.2 Methods

4.2.1 Cell Culture

Human umbilical cord blood derived endothelial cells (hCB-ECs) were isolated from blood as previously described by Ingram et al.[89] For isolation of hCB-ECs, umbilical cord blood was obtained from the Carolina Cord Blood Bank (n=3 donors). Prior to receipt, all patient identifiers were removed. The Duke University Health System IRB has determined that the following protocol meets the definition of research not involving human subjects as described in 45 CFR 46.102(f), 21 CFR 56.102(e) and 21 CFR 812.3(p) and satisfies the Privacy Rule as described in 45CFR164.514.

After collection, blood was diluted 1:1 with Hanks Balanced Salt Solution (HBSS, Invitrogen), placed onto Histopaque 1077 (Sigma), and centrifuged at 740xg for 30 minutes. Buffy coat mononuclear cells were collected and washed three times with "complete EC growth medium," comprising 8% (vol/vol) fetal bovine serum (FBS) added to Endothelial Basal Media-2 (Cambrex) supplemented with Endothelial Growth Media-2 SingleQuots (containing 2% FBS plus growth factors, Cambrex), and 1% antibiotic/antimycotic solution (Invitrogen). Mononuclear cells were plated on plastic 6 well 35 mm diameter plates coated with collagen I (rat tail, BD Biosciences) in complete EC growth medium. Medium was exchanged every 24 hours for the first week in culture, to remove non-adherent cells. Colonies of EPC-derived ECs appeared 7-10 days after the initial isolation. The colonies were trypsinized and 200 cells were plated onto a collagen-coated T25 and labeled passage 1.

The hCB-ECs were grown in T75 flasks using EBM2 basal media supplemented with penicillin/streptomycin, EGM2 Singlequots Kit, and 10% Fetal Bovine Serum (10% complete media). Media was changed every other day until the time of experiment. The hCB-ECs were passaged 1:10 into new T75 flasks upon reaching confluence. Cells were then subsequently split 1:10. The number of population doublings (PDLs) that occurred between each passage was adjusted based upon a 75% attachment rate and calculated according to the formula ln(10)/ln(2)*(4/3) = 4.43 as previously described.[169]

4.2.2 EC Characterization

hCB-ECs with fewer than 31 population doublings (PDL) have been extensively studied and function very similar to vascular ECs.[11, 20, 34, 88, 89] The hCB-ECs are positive for the endothelial-specific CD31 and CD34, and negative for CD14, CD45 and CD115 found on monocytes or hematopoietic cells.[29] We previously characterized hCB-ECs and found that they also expressed von Willebrand factor and VE-cadherin.[11] Following exposure to 15 dyne/cm^2 for 24 or 48 hours, hCB-ECs aligned with the direction of flow,[11, 20] increased nitric oxide production, and increased mRNA for endothelial cell specific genes sensitive to flow, KLF2, eNOS, cyclo-oxygenase 2, and thrombomodulin.[11] The level and organization of actin filaments are similar in hCB-ECs and human aortic ECs (HAECs) as are the associated values of cell stiffness. hCB-ECs with 31 or fewer PDL had high levels of telomerase and low levels of senescence-associated β-galactosidase staining, so we refer to them as "young" ECs.[29] hCB-ECs with 44 or more PDL had low levels of telomerase and high levels of senescence-associated β-galactosidase staining compared to hCB-ECs < 31 PDL, so we refer to them as "aged" ECs.[29]

4.2.3 Synthesis of Variably Compliant Polyacrylamide Gels

Coverslips were prepared as previously described.[139, 175, 180] *Briefly,* square glass coverslips (No. 2, 22 × 22 mm, VWR) were coated with 0.1 N NaOH (Sigma), and allowed to dry. The coverslips were coated with 3-aminopropyl-trimethoxysilane

(Sigma), washed in deionized water, and incubated with a coating of a 0.5% solution of glutaraldehyde (Sigma) in phosphate-buffered saline without calcium and magnesium ((PBS), Invitrogen) at room temperature for 30 min. The coverslips were washed with deionized water and allowed to dry.

Polyacrylamide gels with a Young's modulus of 15,000 Pascals were made with 12% acrylamide/0.13% bis-acrylamide ratio in the gel solution mixture.[193] The solutions were adjusted to pH 6.0 with 1N HCl (Sigma) and degassed for 30 min to remove oxygen that may inhibit polymerization. 0.5 μm diameter fluorescent beads (Invitrogen) were added to the gel for traction force experiments. Polymerization was initiated by the addition of a 0.1% ammonium persulfate (Bio-Rad) solution in water to the acrylamide mixture. A total of 20 μL of the mixture was pipetted onto an activated coverslip and a circular coverslip (No. 2, 18 mm diameter, VWR) was used to flatten the drop. Polymerization was allowed to occur for 30 min at room temperature. The circular coverslip was removed, and the gel was glutaraldehyde-immobilized[93] with 10 μg/mL of fibronectin (Sigma) for two hours at 4 °C. Gels were washed with DI water and stored in DI water in 35mm petri dishes at 4°C. Gels were used for experiments within two weeks.

4.2.4 Traction Force Microscopy

Traction force microscopy was performed as previously described.[81-83, 140] Briefly, low or high passage hCB-ECs were seeded at 100,000 cells on 15,000 Pascal

polyacrylamide gels embedded with 0.5-μm-diameter fluorescent beads. The cells were

allowed to adhere for 24 hours. Cells were imaged with differential interference contrast

microscopy and the fluorescent bead field beneath the cell was imaged immediately

after with a XD Spinning Disk Confocal Microscope (Andor). A second fluorescent

image of the bead field was taken after the cells were removed with 0.025%

trypsin/EDTA (Invitrogen). Removal of the cells with trypsin takes less than 5 minutes.

Bead displacements were used to compute cellular traction vectors, T, by using a

gradient-based digital image correlation technique to map the displacement fluorescent

beads in the gel.[83] The displacement map was converted to the stress distribution,

using a numerical algorithm based on the integral Boussinesq solution. The root mean

square of the force, $|F|$, was calculated using the individual components of the traction

vectors integrated over the cell area,

$$|F| = \iint \left(T_x^2(x,y) + T_y^2(x,y) \right)^{\frac{1}{2}} dxdy$$

(4)

where $\mathbf{T}(x,y) = [T_x(x,y), T_y(x,y)]$ is the continuous field of traction stress vectors

defined at any spatial position (x,y) within the cell.[139] Because the cells have

negligible acceleration, the sum of forces should equal zero in order to satisfy Newton's

first law of motion. In these studies, the sum of the force on the cell was about 0.01pN,

far below the reported root mean square force.

For each experiment, at least 5 cells were examined per condition. These traction forces were averaged together to obtain results for a single experiment.

4.2.5 Actin Immunofluorescence

For these experiments, each coverslip with a gel was attached to six-well plates with vacuum grease (Corning). ECs were plated on polyacrylamide for these experiments to maintain consistency with traction force measurements which were performed on gels. hCB-ECs were seeded at 100,000 cells/well on 6-well plates. At 24 hours post plating, cells were fixed with 3.7% formaldehyde for 30 minutes at room temperature and permeabilized with 1% Triton in PBS for 5 minutes at room temperature. The cells were then incubated with fluorescein phalloidin (1:40, Invitrogen) to stain for F-actin for 1 hour at room temperature. Hoechst 33342 (Invitrogen) was used to stain for cell nuclei (1:2000). The stains were visualized with a Zeiss 510 Upright Microscope.

4.2.6 Immunofluorescence

hCB-ECs were seeded at 100,000 cells on 15,000 Pa polyacrylamide gels for consistency with traction force measurements which were performed on gels. At 24 hours post plating, cells were fixed and permeabilized for 3 minutes with methanol or fixed with 2% formaldehyde. Samples were then blocked with PBS/0.02% Tween 20 (Biorad)/3% bovine serum albumin (Sigma) for 1 hour at room temperature. The samples were then incubated with mouse antibody against heparan sulfate

112

proteoglycan, perlecan (1:250 dilution, clone 7E12, Thermo Scientific) or with mouse

antibody against heparan sulfate (1:100 dilution, clone 10E4, US Biological) for 1-2 hours

at room temperature. This was followed by secondary antibody incubation with goat

anti-mouse Alexa Fluor 546 (1:250 dilution, Invitrogen) or goat anti-mouse Alexa Fluor

488 (1:250 dilution, Invitrogen) for 1 hour at room temperature. All antibodies were

diluted in PBS/1% BSA. The stains were visualized with a Zeiss 510 Upright

Microscope. To examine localization of the   antibodies, some samples were not

permeabilized.

4.2.7 Glycocalyx Thickness and Density Measurements

The heparan sulfate and perlecan core protein components of the glycocalyx and

the nucleus were stained as described above. To measure glycocalyx thickness, z-stack

images were taken on the Zeiss 510 Upright Confocal Microscope at 63x at 0.33μm

intervals. The results we obtained with this method are similar to other established

methods to measure the glycocalyx thickness in cultured ECs using fluorescence and

optical sectioning. [51, 159] The Zeiss LSM Image Browser was used for generation of z-

stack images, 3-D reconstructions, and cross-sectional images. With the cross-sectional

images, heparan sulfate or perlecan thickness was measured for each individual EC for

the region over the center of the cell nucleus. Only cells that were completely in the field

of view and whose surface glycocalyx was continuous were included in the data.[51]

For each condition, at least 2 fields of view are analyzed. Within each field of view, at least 5 cells are analyzed.

To measure the glycocalyx density, images were taken on the Zeiss 510 Upright Confocal Microscope at 63x. Fluorescence intensity of the samples was measured with ImageJ (NIH). An IgG isotype control was used to determine background fluorescence values. For each condition, at least 5 fields of view were analyzed. In each field of view, there are 4-5 cells.

4.2.8 Quantification of Actin Stress Fibers

Distribution of actin was determined by drawing a line perpendicular to the direction of actin fibers at random locations with ImageJ. This plot profile was saved as a text file and imported into a custom Matlab program to replot the data as a function of the percentage of distance across the cell in the direction perpendicular to the actin fibers. The fiber thickness was calculated by measuring the distance between line scan peaks at 1/3 of the maximum fluorescence intensity.

4.2.9 Modulation of SIRT1

Modulation of SIRT1 activity was performed using an inhibitor, EX-527 (5µmol/L, Sigma) for 6 hours prior to the start of the experiment, or with an activator SRT1720 (0.16µmol/L, Sigma) for 1 hour prior to the start of the experiment.

4.2.10 Modulation of Glycocalyx

Degradation of the glycocalyx was performed with *Flavobacterium heparinum* heparinase III (Sigma) at 15 mU/mL for 2 hours prior to the start of the experiment.[22, 64, 126, 192] Cells were incubated with Angiopoietin-1 (R&D Systems) at 100 ng/mL for 30 minutes prior to the start of the experiment to increase the thickness of the glycocalyx.[149]

4.2.11 Statistical Analysis

For Figure 25B and 25C, an ANOVA was performed to determine whether cell age significantly affected hCB-EC traction forces. This was followed by a post-hoc Tukey test to determine between the different ages examined. For Figure 27, a two-factor ANOVA was performed to determine the effect of treatment and age on glycocalyx and cell traction force, respectively. For Figure 29A, a 2-factor ANOVA was performed to determine the effect of treatment and age on cell traction force. For Figure 29B, a two-factor ANOVA was performed to determine the effect of treatment and age on junction tension. For Tables 5-7, a two-factor ANOVA for age and treatment was performed to determine the effect of both factors on stress fiber thickness or number of fibers per cell width. A post-hoc Tukey test was then performed to determine differences between treatment groups. All statistical analysis was performed in JMP. The value of n represents the number of experiments performed. All data is reported as mean ± S.E.

4.3 Results

4.3.1 Aged hCB-ECs from Multiple Isolations Exhibit Increased Traction Forces

To determine whether traction forces differed between young and old hCB-ECs, we measured the traction forces for isolated young (< 31 PDL) and aged (> 44 PDL) hCB-ECs from 3 separate isolations. For these experiments, hCB-ECs of all ages were seeded on 15 kPa gels. In our method, the resolution of the displacement is 0.1 pixel and the resolution of the traction stress is 10Pa. While the distribution pattern of traction stresses are similar for young and old hCB-ECs on 15kPa gels, (Figure 25A), aged hCB-ECs exhibited total traction forces that were about 50% higher than young hCB-ECs (Figure 25B, $p<0.05$). There was no statistically significant effect of EC donor on the traction forces.

A)

22 PDL   66 PDL

$|T|$(Pa)
500
400
300
200
100

B)

< 31 PDL hCB-ECs
> 44 PDL hCB-ECs

Force (µN)

*

C)

22 PDL
35 PDL
40 PDL
44 PDL

Force (µN)

*
*
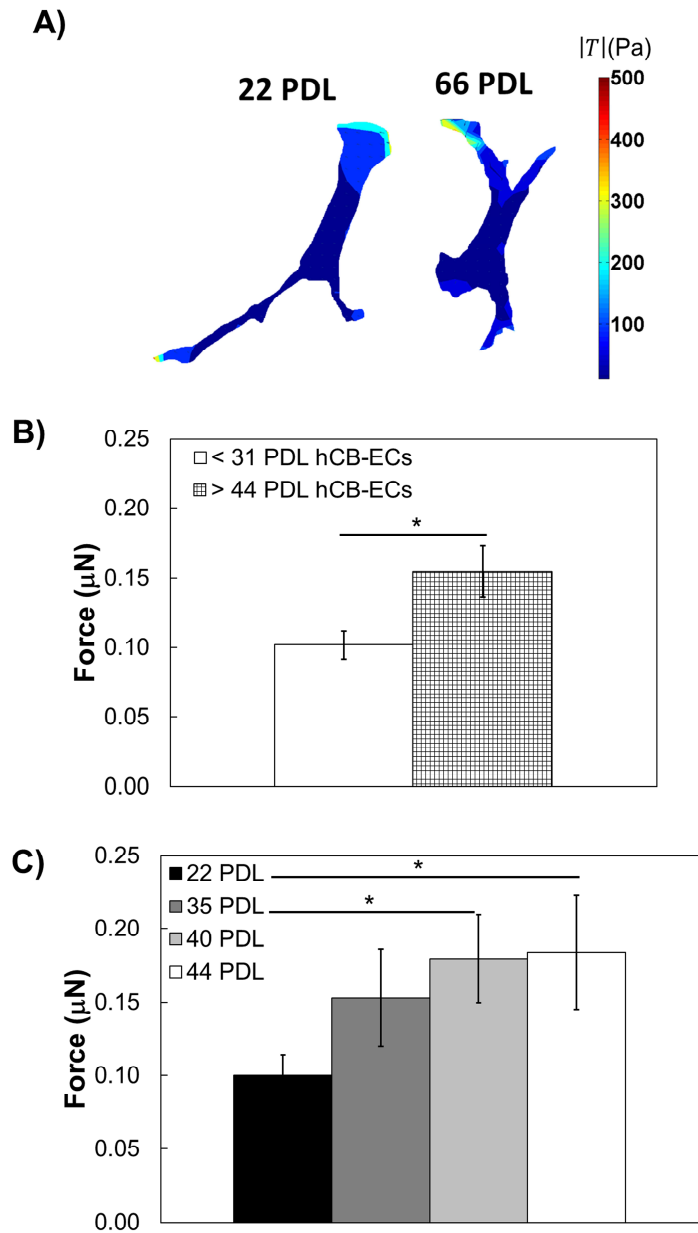
Figure 25: Aged hCB-ECs exhibit increased traction forces and altered actin localization. A) Representative contour plot of cell traction stresses; B) Aged (> 44 PDL) hCB-ECs have higher total traction force than young (< 31 PDL) hCB-ECs; n=4-5. *p<0.05. C) Traction forces increase with increasing cell age for cells from one isolation. n=4. *:p<0.05.

4.3.2 Traction Forces Increase with Increasing Cell Age for hCB-ECs from One Isolation

To eliminate any effect of the donor on the traction force results, we examined traction forces with increasing cell age for hCB-ECs from a single isolation and seeded on 15,000 Pa gels. The traction forces significantly increased with increasing cell age (Figure 25C, $p < 0.05$). Older hCB-ECs at 40 PDL and 44 PDL exhibited significantly higher forces than younger hCB-ECs at 22 PDL ($p < 0.05$). These results show that aging of hCB-ECs increases their traction forces for cells from a single isolation.

4.3.3 Modulation of Glycocalyx Alters hCB-EC Traction Forces

Because the glycocalyx plays an important role in regulation of endothelial mechanotransduction[168], we examined whether the glycocalyx differed between young and old cells and whether disruption of the glycocalyx in isolated cells led to elevated traction forces. To examine the glycocalyx, we quantified immunofluorescence for both a heparan sulfate core protein, perlecan, and heparan sulfate. Both of these proteins have been used to measure glycocalyx thickness and density and are secreted onto the endothelial cell surface.[51, 73, 77] The glycocalyx thickness was determined from confocal Z-sections. For young cells, a clear band was noticeable in the Z-sections for heparan sulfate (1.7 ± 0.2 μm, Figure 26A) and perlecan (2.0 ± 0.4 μm, Figure 26C). The difference in thickness of the two layers was not statistically significant. The perlecan band was located on the luminal surface and the location of the perlecan layer was not affected by permeabilization of the cells. Heparan sulfate was significantly

thicker (p<0.05) in young hCB-ECs (1.7 ± 0.2 μm, Figure 26A) compared to aged hCB-

ECs (1.2 ± 0.1 μm, Figure 26B). Immunofluorescence for the heparan sulfate core

protein, perlecan, was visible on the luminal surface of young cells (Figure 26C) and the

fluorescence intensity was greatly reduced for older cells (Figure 26D). For both young

and old cells, the fluorescence was above background isotype control values
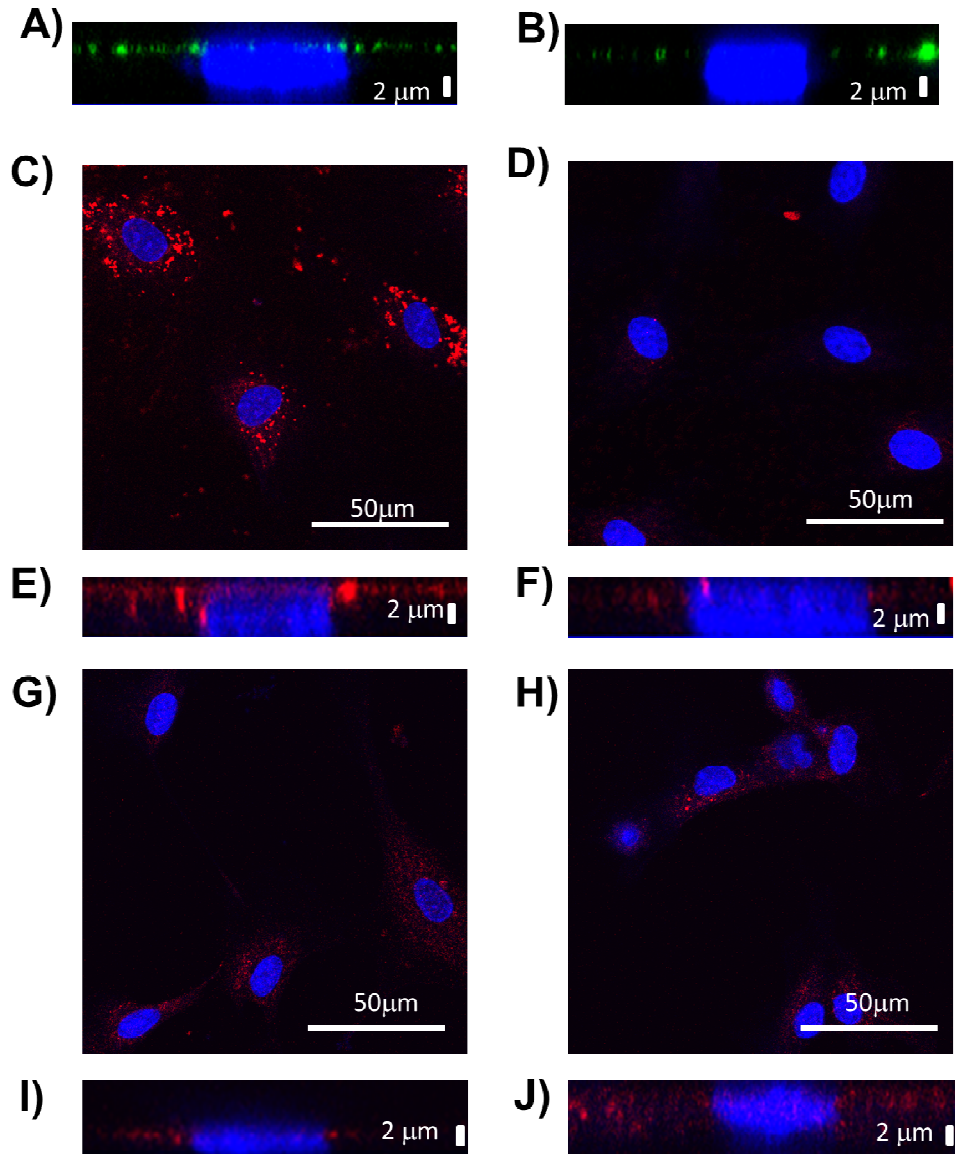
Figure 26: Representative images of Z-stack images of heparan sulfate layer thickness for A) young hCB-ECs and B) old hCB-ECs. Heparan sulfate core protein perlecan for C) young hCB-ECs and D) young hCB-ECs after treatment with heparinase. Z-stack images of perlecan layer thickness for E) young hCB-ECs and F) young hCB-ECs after treatment with heparinase. Representative images of heparan sulfate core protein perlecan for G) old hCB-ECs and H) old hCB-ECs after treatment with angiopoietin-1. Z-stack images of perlecan layer thickness for I) old hCB-ECs and J) old hCB-ECs after treatment with angiopietin-1.

In older cells, the perlecan thickness was 1.6 ± 0.2 μm (Figure 26I), which is a 20% decrease compared to young hCB-ECs (2.0 ± 0.4 μm, Figure 26E) (p<0.05). Perlecan density also decreased noticeably by 47% in aged hCB-ECs (Figure 26G) compared to young (Figure 26C). There was a significant effect of both age (p<0.05) and treatment (p<0.05) on perlecan immunofluorescence.

Heparinase treatment decreased the perlecan density of < 31 PDL hCB-ECs by $21\pm9\%$ compared to untreated controls (Figure 26A and Figure 26B, p<0.05). Heparinase did not significantly alter glycocalyx thickness which is consistent with previously reported results (Figure 26C and Figure 26D).[51] Angiopoietin-1 treatment enhanced the perlecan thickness in > 44 PDL hCB-ECs by $90\pm11\%$ compared to untreated controls (Figures 2G and 2H, p<0.05), but had no significant effect on perlecan density (Figure 26E and Figure 26F). Angiopoietin-1 has been shown to increase the perlecan thickness by increasing translocation of glycosaminoglycans from the Golgi.[149]

We then applied these treatments to the cells to determine the effect of the glycocalyx on traction forces. The heparinase treatment increased traction forces in < 31 PDL hCB-ECs by 48% (Figure 27A, p<0.05). Conversely, angiopoietin-1 decreased traction forces in > 44 PDL hCB-ECs by 51% (Figure 27A, p<0.05) compared to untreated controls. HAECs, which have telomerase activity similar to older hCB-ECs (45-71 doublings),[29] have substantially greater traction forces (Figure 27B). Treatment with angiopoietin-1 also decreased traction forces in HAECs by 71% (Figure 27B, p<0.05).

Taken together, these results show that traction forces are lower for cells with thicker and/or more abundant heparan sulfate or perlecan in the glycocalyx.
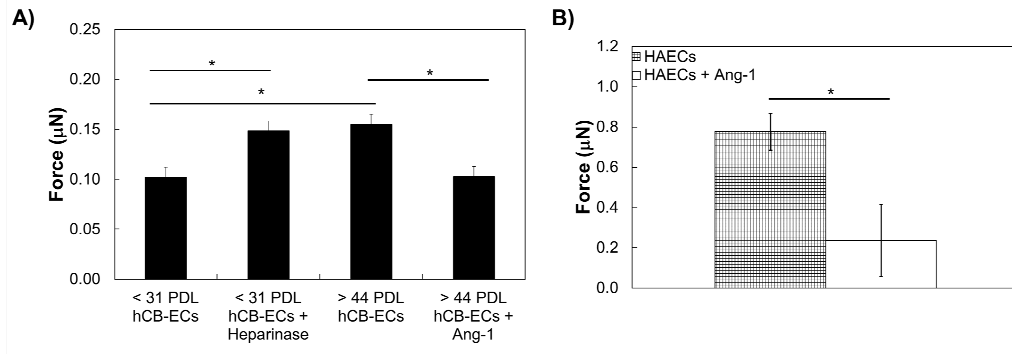
Figure 27: Traction forces are glycocalyx-dependent. A) Heparinase, which degrades the glycocalyx, significantly increases traction forces in < 31 PDL hCB-ECs. Angipoietin-1, which increases the glycocalyx thickness, significantly decreases traction forces in > 44 PDL hCB-ECs; B) Angiopoietin-1 significantly decreases traction forces in HAECs. n=3-5. *p<0.05.

4.3.4 Modulation of Glycocalyx Alters Actin Stress Fiber Formation

To determine whether altered traction forces due to disruption of the glycocalyx affect actin size and density, we examined actin stress fiber localization and thickness after treatment with agents known to alter the glycocalyx. In 27 PDL hCB-ECs, actin was localized at the periphery of the cells (Figure 28A). However, in 27 PDL hCB-ECs treated with heparinase to degrade the glycocalyx, there is some formation of actin stress fibers along the length of the cell (Figure 28B). In 49 PDL hCB-ECs, actin stress fibers were present throughout the length of the cell (Figure 28C). When these cells were treated with angiopoietin-1 to increases the thickness of the glycocalyx, actin stress

fibers appeared thinner and there was some increase in localization of actin to the

periphery of the cell (Figure 28D).
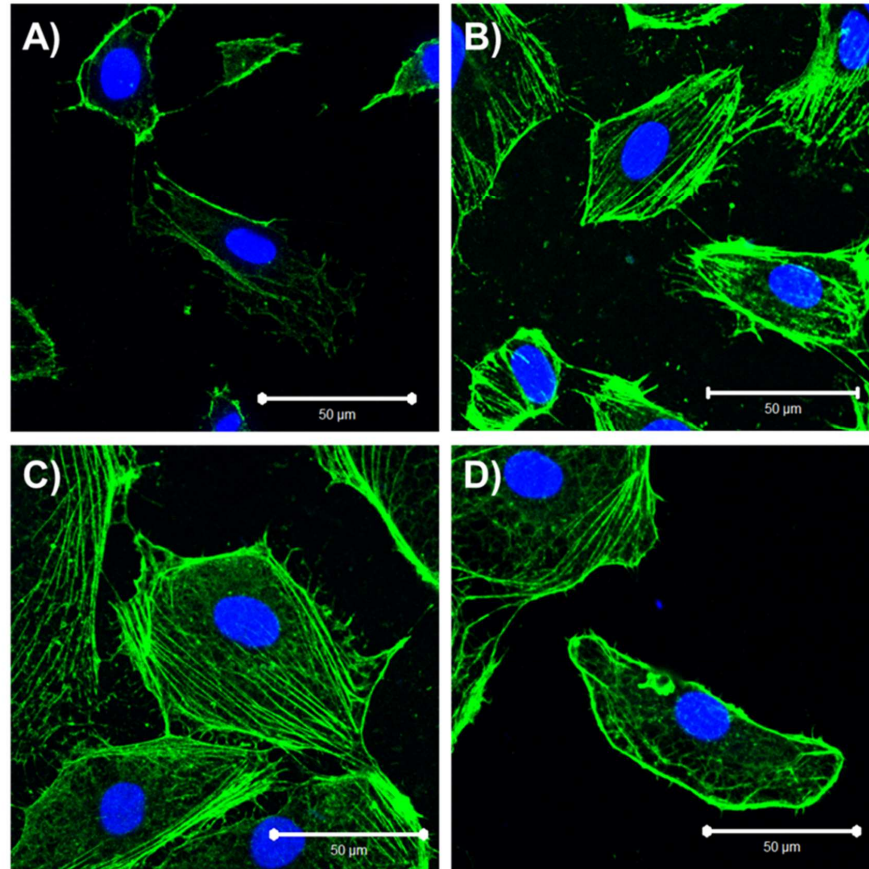
Figure 28: Actin localization is glycocalyx-dependent. Actin is localized to the cell periphery in A) 22 PDL hCB-ECs, while fibers form along the length of the cell in B) 22 PDL hCB-ECs with heparinase. Actin stress fibers are present throughout the cell in C) 49 PDL hCB-ECs, while fibers begin to localize to periphery in D) 49 PDL hCB-ECs with angiopioetin-1.

We also found that there was a significant effect of both age ($p<0.01$) and

treatment ($p<0.05$) on actin stress fiber thickness (Table 5). Heparinase led to an increase

in actin stress fiber thickness compared to untreated cells (Table 5, $p<0.05$). Actin fibers

123

in aged hCB-ECs were thicker than in 27 PDL hCB-ECs (Table 5, p<0.01), but became

thinner in aged hCB-ECs treated with angiopoietin-1 compared to the untreated control

(Table 5, p<0.05).

Table 5: Glycocalyx Alters Stress Fiber Thickness. *:p<0.05 compared to untreated control; #:p<0.01 compared to < 31 PDL. n=3.

Condition	Stress Fiber Thickness (μm)
< 31 PDL	1.1 ± 0.2
< 31 PDL + Heparinase	1.8 ± 0.1*
> 44 PDL	2.2 ± 0.2#
> 44 PDL + Angiopoietin-1	1.5 ± 0.1*

We also found that there was a significant effect of age (p<0.05) and treatment

(p<0.05) on the number of actin stress fibers per cell width (Table 6). Treatment of aged

hCB-ECs with angiopoietin-1 significantly reduced the number of actin stress fibers per

cell width (Table 6, p<0.05). Taken together, these results show that age-associated

changes in the glycocalyx can alter actin stress fiber localization and thickness.

Table 6: Effect of Agents that Affect SIRT1 or the Glycocalyx on Number of Actin Stress Fibers per Cell Width. *:p<0.05 compared to > 44 PDL; ^:p<0.05 compared to < 31 PDL. n=7-12.

Condition	Number of F-actin Fibers per Cell
< 31 PDL	10.8 ± 0.9
< 31 PDL + EX-527	9.7 ± 1.2
< 31 PDL + Heparinase	12.8 ± 0.9
> 44 PDL	15.7 ± 2.6^
> 44 PDL + SRT1720	10.4 ± 1.3
> 44 PDL + Angiopioetin-1	8.3 ± 0.9*

4.3.5 Effect of SIRT1 Treatments on Traction Forces

Because elevating SIRT1 plays an important role in reversal of senescence-associated phenotypes[26, 29, 42, 128, 199] and regulation of shear stress-induced eNOS,[24] we sought to determine whether modulation of SIRT1 altered cell traction forces. Isolated aged ECs (> 44 PDL) had significantly higher traction forces compared to the untreated young (< 31 PDL) hCB-EC control (Figure 29, p<0.05). Inhibition of SIRT1 in isolated young hCB-ECs with EX-527 had no significant effect on traction forces compared to the untreated young hCB-EC condition. However, activation of SIRT1 with SRT1720 in aged (> 44 PDL) hCB-ECs did significantly reduce traction forces compared to the untreated aged hCB-EC control (Figure 29, p<0.05).
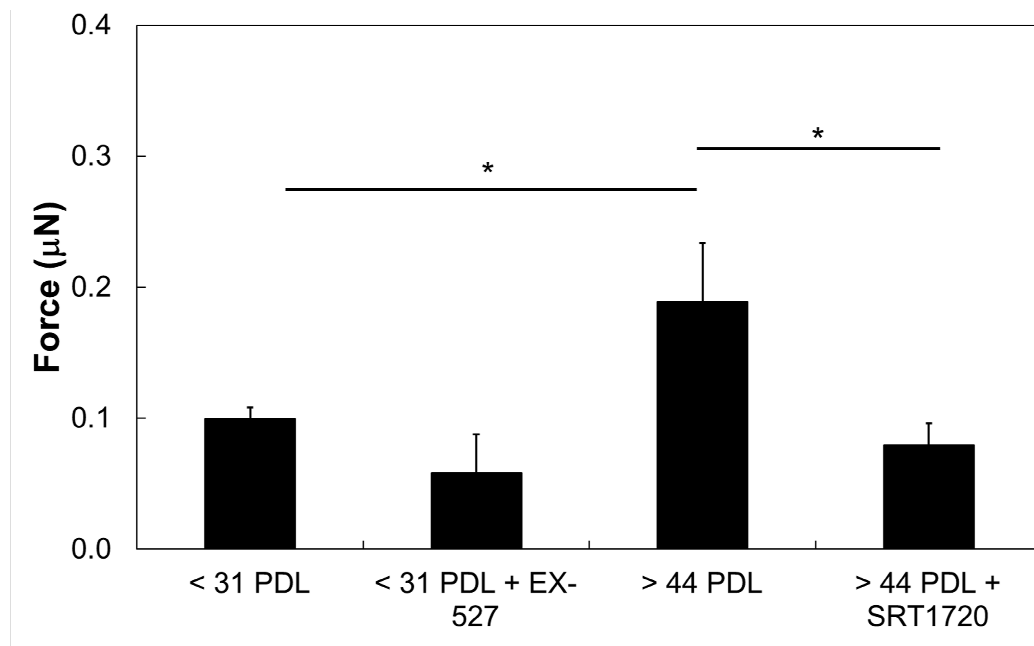
Figure 29: Effect of SIRT1 on traction forces. For isolated cells, inhibition of SIRT1 in young (< 31 PDL) with 5µM EX-527 has no significant effect on traction forces compared to untreated control. Elevation of SIRT1 in aged (> 44 PDL) with 0.16µM SRT1720 decreases traction forces compared to untreated control n=3-7. *:p<0.05.

4.3.6 Effect of SIRT1 Treatments on Actin Stress Fibers

Aged (> 44 PDL) hCB-ECs exhibited more actin stress fibers present throughout

the length of the cell (Figure 30C) compared to young (< 31 PDL) hCB-ECs (Figure 30A).

Stress fibers in aged hCB-ECs were also significantly thicker than those in young hCB-

ECs (Table 7, p<0.05). Treatment of young hCB-ECs with EX-527 to inhibit SIRT1

increased the number of stress fibers present in the cell (Figure 30B) compared to the

untreated condition (Figure 30A). There was no statistically significant change in stress

fiber thickness after treatment of young hCB-ECs with EX-527 (Table 7). Treatment of

aged hCB-ECs with SRT1720 to activate SIRT1 led to increased actin at the periphery of

the cells (Figure 30D) compared to the untreated aged hCB-ECs (Figure 30C). Treatment

with SRT1720 also significantly decreased actin stress fiber thickness compared to aged

hCB-ECs (Table 7, $p < 0.05$). There was a significant effect of age ($p < 0.05$) and treatment

($p < 0.05$) on the number of actin stress fibers per cell width (Table 6). These results

suggest that activating SIRT1 in older cells may affect actin stress fiber formation and

localization.

Table 7: Effect of SIRT1 on Actin Stress Fiber Thickness. *:p<0.05 compared to >44 PDL; ^:p<0.05 compared to < 31 PDL. n=3.

Condition	Stress Fiber Thickness (µm)
< 31 PDL	1.4 ± 0.1
< 31 PDL + EX-527	1.5 ± 0.1
> 44 PDL	1.7 ± 0.1[*]
> 44 PDL + SRT1720	1.4 ± 0.1*
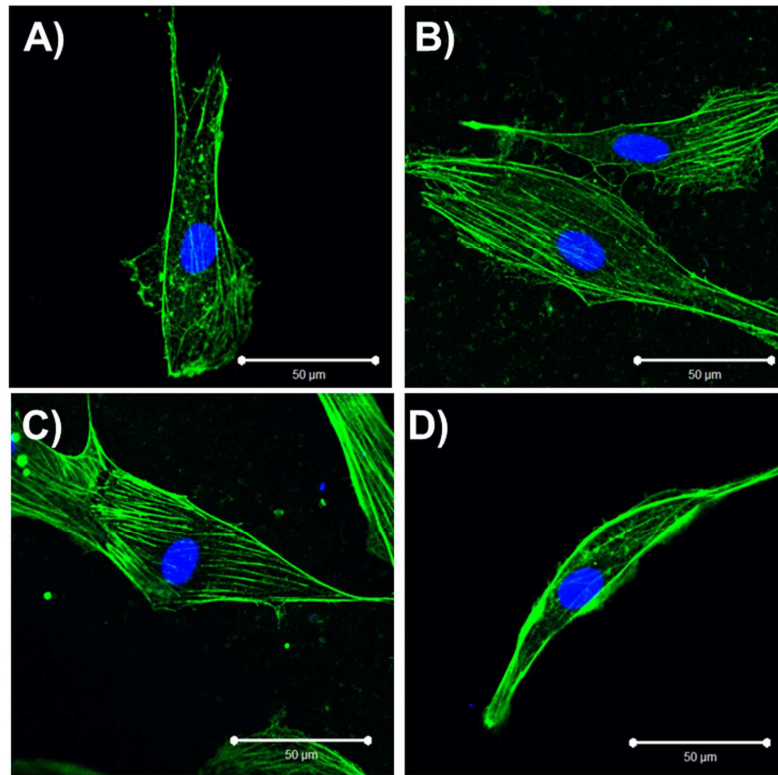
Figure 30: Effect of SIRT1 on actin stress fibers. A) Actin stress fibers localize to periphery in young hCB-ECs; B) Treatment of young hCB-ECs with 5μM EX-527 to inhibit SIRT1 leads to some formation of stress fibers throughout the length of the cell; C) Aged hCB-ECs have actin fibers present throughout the length of the cell; D) Aged hCB-ECs with 0.16μM SRT1720 have more actin localization at periphery of the cell.

4.4 Discussion

EC cell traction forces are affected by actin localization and actomyosin

contractility,[30, 87, 133] integrin levels,[151] focal adhesion formation,[34], [17] and Rho

activity.[87, 186] Actin binding to vinculin is necessary for cell traction force

generation.[160] Furthermore, elevated Rho or Rho-associated kinase activity can

stimulate cell contractility by modulating actomyosin contraction. In this study, we

demonstrated that senescent hCB-ECs exhibited increased traction forces and thicker

and more abundant stress fibers due to age-associated changes in the glycocalyx and

SIRT1. The traction force increase in senescent hCB-ECs correlated with decreased

glycocalyx intensity and thickness as well as increased actin fiber thickness. Altering

glycocalyx thickness and density affected actin stress fiber thickness and localization.

Likewise, activating SIRT1 in aged EC led to a decrease in actin stress fiber thickness,

although direct inhibition of SIRT1 with EX-527 for 6 hours prior to the start of the

experiment was not sufficient to elevate traction forces or altering actin fiber thickness in

young (< 31 PDL) hCB-ECs.

hCB-ECs were used in this study because of their low, physiological

permeability,[29] high proliferative potential,[29] and similarity to arterial ECs.[11]

Traction forces for both young and aged hCB-ECs were low compared to those

previously reported for BAECs.[16, 87]   For reference, we found that when attached to

polyacrylamide gels with an elastic modulus of 15 kPa, the traction force for human

aortic ECs were 0.78±0.09μN, which is close to previously reported values in BAECs.[87]

This traction force result correlates with the reduced permeability in hCB-ECs compared

to HAECs.[29] Both hCB-ECs and HAECs exhibited a decline in traction force after

exposure to angiopoietin-1.

There is increasing evidence that the method of fibronectin immobilization can

affect the interactions of fibronectin with integrins, which can modify cell adhesion to

polymer substrates. It has been shown that varying linker density can affect collagen protein tethering on polyacrylamide gels.[184] However, stiffness-induced stem cell differentiation was independent of changes to protein tethering or gel porosity.[184]

The glycocalyx thickness of the aged ECs measured in this study using antibodies to either heparan sulfate or perlecan is comparable to the previously measured value of 1.38±0.07μm in bovine aortic ECs.[51] Additionally, we stained for both a heparan sulfate core protein, perlecan, and heparan sulfate. We found that both stains yielded similar results and trends in the glycocalyx with age. Although perlecan is a core protein, it has been shown to be secreted to the glycocalyx[73] and has been used as to measure glycocalyx thickness.[77] Henderson-Toth et al show that treatment with heparinase does reduce the abundance of perlecan, which is consistent with our observations.[77] This suggests that the heparan sulfate does have a role in anchoring perlecan to the endothelial glycocalyx on the abluminal surface.

Z-stack sections of 0.33 μm were used to visualize the glycocalyx. The resolution of the confocal microscope section images was calculated to be 0.7 μm,[84] which is less than the values of the glycocalyx thickness that we measured in this study. Using antibodies to different components of the glycocalyx, we were able to resolve the glycocalyx (Figure 26) and determine changes in both thickness and density with age. An alternative way to visualize the glycocalyx is with cryo-TEM as this eliminates the need for aldehyde fixation or alcohol dehydration. The thickness of bovine aortic EC

glycocalyx measured by cryo-TEM was about 11 μm,[51] which is significantly thicker

than any estimate obtained from confocal imaging or from functional measurements.

Cryo-TEM would provide additional insight into the structure and appearance of the

glycocalyx, but the trends with age and treatments would remain the same.

There are several other factors that could contribute to elevated traction forces in

aging hCB-ECs, including integrin levels and changes in Rho activity. Integrin $\alpha_5\beta_1$

plays an important role in cell force generation through the RhoA-Rock pathway.[151]

Integrin β_4 has been shown to be elevated in a mouse model during aging and

atherosclerosis.[156] Knockdown of integrin β_4 in the mouse attenuated the decrease in

endothelial nitric oxide synthase associated with senescent ECs,[156] suggesting that the

integrins may play an important role in aging EC mechanotransduction.

Interaction between integrins and the extracellular matrix can lead to clustering

and the formation of focal adhesions.[3, 7, 61, 147] Focal adhesions mediate force

transmission between integrins and the actin cytoskeleton.[34, 60] Vinculin, a focal

adhesion protein, has been demonstrated to be important in regulating myosin

contractility dependent adhesions and traction forces.[49] Senescent human umbilical

vein ECs have inhibited migration due to an increased amount of focal adhesion

sites.[62] Therefore, it is possible that changes in the amount of focal adhesions in

senescent ECs play a role in altering cell traction forces.

131

Rho GTPases have also been shown to be important in mediating cell contractility and cell traction forces. In human umbilical vein ECs, inhibition of RhoA and Rac1 decreased permeability, cell contractility, and assembly of actin stress fibers.[186] Dominant-negative Cdc42 reduced stress fiber formation and contractility, but did not alter permeability.[186] In bovine aortic ECs, increases in traction force and permeability on stiff substrates was attributed to increased activation of RhoA.[87] When downstream effector Rho-dependent kinase was inhibited, there was a reduction in monolayer permeability and cell traction force.[87]

To fully understand the role of endothelial cell force generation in atherosclerosis development, the effect of shear stress and intracellular forces would have to be considered. After exposure to flow for 16 hours, the traction force for confluent ECs was slightly greater for cells exposed to steady shear stress than for cells under static conditions or cells exposed to recirculating flow.[161] Steady flow also caused the surface traction force vectors to align in the direction of flow and increased intracellular forces.[161] Static conditions or recirculating flow did not alter alignment of surface traction forces.[161] Interestingly, the tension induced by shear stress was significantly less than the intracellular tension,[161] suggesting that while changes to the intracellular tension are initiated by shear stress, the magnitude of the intracellular tension reflects both biochemical changes within the cell as well as cell-cell and cell-substrate interactions.

Under shear stress, the glycocalyx is necessary for rearrangement of the cytoskeleton and alignment in the direction of flow for ECs.[196] Our results for cells under static conditions on soft substrates also show a relationship between the cytoskeleton and glycocalyx. Modulation of the glycocalyx with heparinase or angiopoietin-1 altered both cell traction forces and actin localization and fiber thickness. There was also an age-related decline in glycocalyx thickness and density, suggesting that cell senescence can alter the mechanosensing ability of the actin cytoskeleton.

In summary, we showed that senescence of isolated hCB-ECs increases traction forces. Furthermore, traction forces can be modulated by altering the glycocalyx or SIRT1 in an age-associated manner. Changes in actin localization and stress fiber thickness also correlated with changes in aging hCB-EC traction forces.

4.5 Chapter Acknowledgements

Chapter 5. Elevated Traction Forces in Senescent Endothelial Cell Clusters Due to SIRT1-Dependent Changes in Junction Tension and Actin Localization

5.1 Introduction

Atherosclerosis is the primary pathology underlying cardiovascular disease. Development of the atherosclerosis is likely due to changes in both the local mechanical environment and endothelial cell (EC) aging. Changes in vessel composition and structure have also been linked to atherogenesis.[170] There is also evidence of accelerated aging in lesion-prone sites, including presence of giant cells,[13] elevated levels of senescence-associated β-galactosidase staining,[108] and telomere shortening.[123] In these sites, ECs are exposed to high oxidative stress leading to apoptosis.[54] This can result in increased EC turnover and replication, which can lead to localized senescence. Further, aging endothelium has been shown to have increased permeability to macromolecules,[29] which is one of the earliest events in atherosclerosis development, and increased sensitivity to oxidative stress.[26]

Traction forces in ECs play an important role in cell migration and adhesion. As cells migrate, changes in the distribution of traction stresses precede changes in the direction of migration.[115] Traction forces are not uniform on the cell substrate, with forces being highest at the periphery of the cell, likely due to redistribution of stresses at the leading edge of the cell as it migrates.[140] Bovine aortic ECs on compliant substrates had reduced cell traction forces and permeability compared to those seeded

on stiff substrates.[87] This result correlated with increased actomyosin contractility for cells isolated from old mice. These changes in cell contractility, traction force, and permeability could be reversed through inhibition of the Rho-associated kinase (ROCK) pathway.[87] While traction force measurements are typically done with isolated cells, traction force measurements have also been for pairs of cells[16] and confluent monolayers.[85] These results provide additional data into how cells behave when cell-cell junctions and cell-cell interactions are accounted for.

Sirtuin1 (SIRT1) is a deacetylase that regulates antioxidant activity. In atheroprone regions, levels of SIRT1 are reduced due to oxidative stress and disturbed fluid flow.[24] Activation of SIRT1 reverses several age-associated phenotypes,[26, 29, 128, 199] influences mechanosensing by regulating shear-induced endothelial nitric oxide synthase,[24] and regulates the structure and function of the glycocalyx. In ApoE-knockout mice, overexpression of SIRT1 in ECs decreased atherosclerosis.[128] Furthermore, SIRT1 regulates permeability through regulation of cell-cell junction proteins, such as occludin.[29]

While changes in the mechanical environment and cell senescence are known to impact atherosclerosis development, the relationship between the two remains unclear. In this study, we tested the hypothesis that age-associated changes in SIRT1 increases cell traction forces and the junction tension of endothelial cell clusters due to changes in actin localization and junction tension. To test this hypothesis, we used human cord

blood-derived ECs (hCB-ECs) as a model for cell aging because of their low,

physiological permeability at low population doublings,[29] high proliferative potential

in subconfluent cultures,[29] and similarity to arterial ECs.[11] We examined traction

forces of aging ECs in clusters or monolayers, and assessed their dependence on SIRT1

activity. We also examined the effect of these agents on the actin cytoskeleton and

junction tension.

5.2 Methods

5.2.1 Cell Culture

Human umbilical cord blood derived endothelial cells (hCB-ECs) were isolated

from blood as previously described by Ingram et al.[89] For isolation of hCB-ECs,

umbilical cord blood was obtained from the Carolina Cord Blood Bank (3 donors). Prior

to receipt, all patient identifiers were removed. The Duke University Health System IRB

has determined that the following protocol meets the definition of research not

involving human subjects as described in 45 CFR 46.102(f), 21 CFR 56.102(e) and 21 CFR

812.3(p) and satisfies the Privacy Rule as described in 45CFR164.514.

After collection, blood was diluted 1:1 with Hanks Balanced Salt Solution (HBSS,

Invitrogen), placed onto Histopaque 1077 (Sigma), and centrifuged at 740x*g* for 30

minutes. Buffy coat mononuclear cells were collected and washed three times with

"complete EC growth medium," comprising 8% (vol/vol) fetal bovine serum (FBS)

added to Endothelial Basal Media-2 (Cambrex) supplemented with Endothelial Growth

Media-2 SingleQuots (containing 2% FBS plus growth factors, Cambrex), and 1%

antibiotic/antimycotic solution (Invitrogen). Mononuclear cells were plated on plastic 6

well 35 mm diameter plates coated with collagen I (rat tail, BD Biosciences) in complete

EC growth medium. Medium was exchanged every 24 hours for the first week in

culture, to remove non-adherent cells. Colonies of EPC-derived ECs appeared 7-10 days

after the initial isolation. The colonies were trypsinized and 200 cells were plated onto a

collagen-coated T25 and labeled passage 1.

The hCB-ECs were grown in T75 flasks using EBM2 basal media supplemented

with penicillin/streptomycin, EGM2 Singlequots Kit, and 10% Fetal Bovine Serum (10%

complete media). Media was changed every other day until the time of experiment. The

hCB-ECs were passaged 1:10 into new T75 flasks upon reaching confluence. Cells were

then subsequently split 1:10. The number of population doublings (PDLs) that occurred

between each passage was adjusted based upon a 75% attachment rate and calculated

according to the formula $\ln(10)/\ln(2)*(4/3) = 4.43$ as previously described.[169]

5.2.2 EC Characterization

hCB-ECs with fewer than 31 population doublings (PDL) have been extensively

studied and function very similar to vascular ECs.[11, 20, 27, 88, 89] The hCB-ECs are

positive for the endothelial-specific CD31 and CD34, and negative for CD14, CD45 and

CD115 found on monocytes or hematopoietic cells.[27] We previously characterized

hCB-ECs and found that they also expressed von Willebrand factor and VE-

cadherin.[11] Following exposure to 15 dyne/cm^2 for 24 or 48 hours, hCB-ECs aligned

with the direction of flow,[11, 20] increased nitric oxide production, and increased

mRNA for endothelial cell specific genes sensitive to flow, KLF2, eNOS, cyclo-oxygenase

2, and thrombomodulin.[11] The level and organization of actin filaments are similar in

hCB-ECs and human aortic ECs (HAECs) as are the associated values of cell stiffness.

hCB-ECs < 31 PDL had high levels of telomerase and low levels of senescence-associated

β-galactosidase staining, so we refer to them as "young" ECs.[27] hCB-ECs > 44 PDL

had low levels of telomerase and high levels of senescence-associated β-galactosidase

staining compared to hCB-ECs < 31 PDL, so we refer to them as "aged" ECs.[27]

5.2.3 Synthesis of Variably Compliant Polyacrylamide Gels

Coverslips were prepared as previously described.[139, 176, 179] Briefly, square

glass coverslips (No. 2, 22 × 22 mm, VWR) were coated with 0.1 N NaOH (Sigma), and

allowed to dry. The coverslips were coated with 3-aminopropyl-trimethoxysilane

(Sigma), washed in deionized water, and incubated with a coating of a 0.5% solution of

glutaraldehyde (Sigma) in phosphate-buffered saline without calcium and magnesium

((PBS), Invitrogen) at room temperature for 30 min. The coverslips were washed with

deionized water and allowed to dry.

Polyacrylamide gels with a Young's modulus of 15,000 Pascals were made with

12% acrylamide/0.13% bis-acrylamide ratio in the gel solution mixture.[193] The

solutions were adjusted to pH 6.0 with 1N HCl (Sigma) and degassed for 30 min to

remove oxygen that may inhibit polymerization. 0.5 μm diameter fluorescent beads (Invitrogen) were added to the gel for traction force experiments. Polymerization was initiated by the addition of a 0.1% ammonium persulfate (Bio-Rad) solution in water to the acrylamide mixture. A total of 20 μL of the mixture was pipetted onto an activated coverslip and a circular coverslip (No. 2, 18 mm diameter, VWR) was used to flatten the drop. Polymerization was allowed to occur for 30 min at room temperature. The circular coverslip was removed, and the gel was immobilized with 10 μg/mL of fibronectin (Sigma) for two hours at 4 °C. Gels were washed with DI water and stored in DI water in 35mm petri dishes at 4°C. Gels were used for experiments within two weeks.

5.2.4 Traction Force Microscopy

Traction force microscopy was performed as previously described.[81-83, 140] Briefly, low or high passage hCB-ECs were seeded at 200,000 cells on 15,000 Pascal polyacrylamide gels embedded with 0.5-μm-diameter fluorescent beads. The cells were allowed to adhere for 24 hours and formed clusters. Clusters were imaged with differential interference contrast microscopy and the fluorescent bead field beneath the cell was imaged immediately after with a XD Spinning Disk Confocal Microscope (Andor). A second fluorescent image of the bead field was taken after the cells were removed with 0.025% trypsin/EDTA (Invitrogen). Removal of the cells with trypsin takes less than 5 minutes. For large clusters that appeared as confluent monolayers, stage positions were used to take 4 overlaying images. Bead displacements were used to

compute cellular traction vectors, T, by using a gradient-based digital image correlation technique to map the displacement fluorescent beads in the gel.[83] The displacement map was converted to the stress distribution, using a numerical algorithm based on the integral Boussinesq solution. The root mean square of the force, $|F|$, was calculated using the individual components of the traction vectors integrated over the cell area,

$$|F| = \iint \left(T_x^2(x,y) + T_y^2(x,y)\right)^{\frac{1}{2}} dxdy$$

(5)

where $\mathbf{T}(x,y) = [T_x(x,y), T_y(x,y)]$ is the continuous field of traction stress vectors defined at any spatial position (x,y) within the cell.[139] Because the cells have negligible acceleration, the sum of forces should equal zero in order to satisfy Newton's first law of motion. In these studies, the sum of the force on the cell was about 0.01pN, far below the reported root mean square force.

Because traction forces are balanced by intracellular tensions, we used Equation 6 to calculate intracellular tension as described by others.[85] For two cells in contact with each other, the junction tension of cell 1 is equal and opposite to the junction tension on the second cell. In general, for a cell in contact with several cells, as in a confluent monolayer, the traction and junction forces balance:

$$\int \sigma \, dA + \int T_j \, dl = 0 \quad \text{or} \quad \bar{T} = \int \sigma \, dA \big/ l_j$$

(6 a,b)

$\mathbf{T_j}$ is the junction tension between the cells (N m^{-1} or dyne cm^{-1}), σ is the stress between cell and substrate (N m^{-2} or dyne cm^{-2}), $\bar{T}$ is the traction vector (N or dyne), A

is the area of contact between the cell and the substratum, and l_j is the length of the EC

perimeter. The tension, which is the net force per unit length acting at the junctions,

equals the spatially averaged traction vector divided by the cell perimeter length.

5.2.5 Actin Immunofluorescence

For these experiments, each coverslip with a gel was attached to six-well plates

with vacuum grease (Corning). hCB-ECs were seeded at 200,000 cells/well on 6-well

plates. At 24 hours post plating, cells were fixed with 3.7% formaldehyde for 30 minutes

at room temperature and permeabilized with 1% Triton in PBS for 5 minutes at room

temperature. The cells were then incubated with fluorescein phalloidin (1:40,

Invitrogen) to stain for F-actin for 1 hour at room temperature. Hoechst 33342

(Invitrogen) was used to stain for cell nuclei (1:2000). The stains were visualized with a

Zeiss 510 Upright Microscope.

5.2.6 Modulation of SIRT1 Activity

Modulation of SIRT1 activity was performed using an inhibitor, EX-527

(5μmol/L, Sigma) for 6 hours prior to the start of the experiment, or with an activator

SRT1720 (0.16μmol/L, Sigma) for 1 hour prior to the start of the experiment. None of

these agents are present when the cells are exposed to flow.

5.2.7 Knockdown of SIRT1

Transient transfection was performed as previously described[24] with Lipofectamine RNAiMAX (Invitrogen). The hCB-ECs were grown to 70% confluency in T-75 flasks. Flasks were then transfected with either SIRT1 (Qiagen, SI00098434) or scramble (negative control) siRNA (Qiagen, 1022076) at 20nM in Opti-MEM (Gibco). Untransfected cells were used as a control. Four hours after transfection, the medium was changed back to fresh 10% complete medium. The cells were then cultured for 24 hours before the start of the experiment.

5.2.8 Western Blot

Western blots were performed to determine the expression of RhoA. Cells were seeded at a density of 50,000 cells/cm^2 on to 6 well plates and grown for 4 days. Cells were harvested with a cell scraper and subjected to a solution of CellLytic-M (Sigma) and Protease Inhibitor Cocktail (Sigma). Protein quantification was performed with the A280 Protein Quantification Method. 40 µg of protein was loaded into each well for the SDS-polyacrylamide gel electrophoresis (12% gel, Biorad). Afterwards, the protein bands were transferred to PVDF membranes. The membranes were blocked with a Tris-Buffered Saline with 0.1% Tween 20 (TBST) solution containing 1% BSA at room temperature for 1 hour. Primary antibodies for mouse-RhoA (1:250, 24kDa, Santa Cruz Biotechnology) and mouse-β-actin (1:2500 dilution, 42kDa, Santa Cruz Biotechnology) were diluted in a TBST and incubated with the membrane overnight at 4°C. Goat-anti-

mouse (1:5000 dilution, Invitrogen) secondary antibody was incubated with the membrane for 45 minutes at room temperature. After washing, immunoreactive bands were detected by luminography using Supersignal chemiluminescent substrate (Pierce). Integrated band density was determined by densitometry after scanning onto autoradiographic films (GE Healthcare) and evaluated by ImageJ (NIH). Protein expression was reported as a normalized intensity of the band of interest compared to the band of the housekeeping protein, β-actin. There was no significant effect of any of the conditions on the protein expression of loading control, β-actin.

5.2.9 Statistical Analysis

For Figure 31, an ANOVA was performed to determine the effect of cell age and cell grouping on traction forces. A post-hoc Tukey test was used to determine differences within factors. For Figure 32B, a paired t-test was used to determine the effect of age on RhoA activity. For Figure 33A, a 3-factor ANOVA was used to determine the effect of age, treatment, and cell grouping on traction forces. For Figure 33B, a 2-factor ANOVA was used to determine the effect of age and treatment on junction tension. This was followed by a post-hoc Tukey test. For Figure 34, an ANOVA was performed to determine the effect of treatment on traction forces or junction tension. All statistical analysis was performed in JMP. The value of n represents the number of clusters examined. All data is reported as mean ± S.E.

5.3 Results

5.3.1 Clusters Exhibit Higher Traction Forces Than Isolated ECs and Confluent EC Layers

Using the Integral Boussinesq method to calculate cell traction forces,[83] the resolution of the traction stresses is about 10Pa and the resolution of the displacement is about 0.1 pixel. The traction forces of endothelial cell clusters (groups of 2 or 3 cells) were about 3 times higher than for isolated cells for both young ($p < 0.05$) and aged ($p < 0.05$) hCB-ECs (Figure 31A). However, large clusters of cells which appeared as confluent layers (groups of 20-30 cells), had reduced levels of traction forces compared to clusters for both young ($p < 0.05$) and aged ($p < 0.05$) hCB-ECs (Figure 31A). This is likely due to increased junction tension in cell clusters compared to monolayers as was previously described.[86] There was also a significant effect of age on cell traction forces (Figure 31A, $p < 0.05$). Elevated traction forces in aged hCB-ECs correlated with altered actin localization. In young hCB-ECs, actin was localized primarily to the periphery of the cell (Figure 31B). In aged hCB-ECs, actin was present throughout the length of the cell (Figure 31C). These results show that aged hCB-ECs have elevated tractions and altered actin localization. Additionally, groups of 2 or 3 cells cause increased traction forces, while large groups of cells reduces traction forces.

144
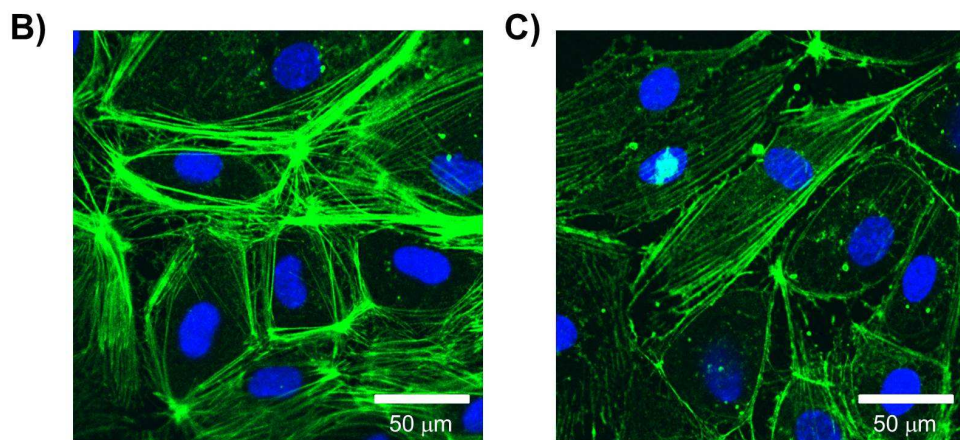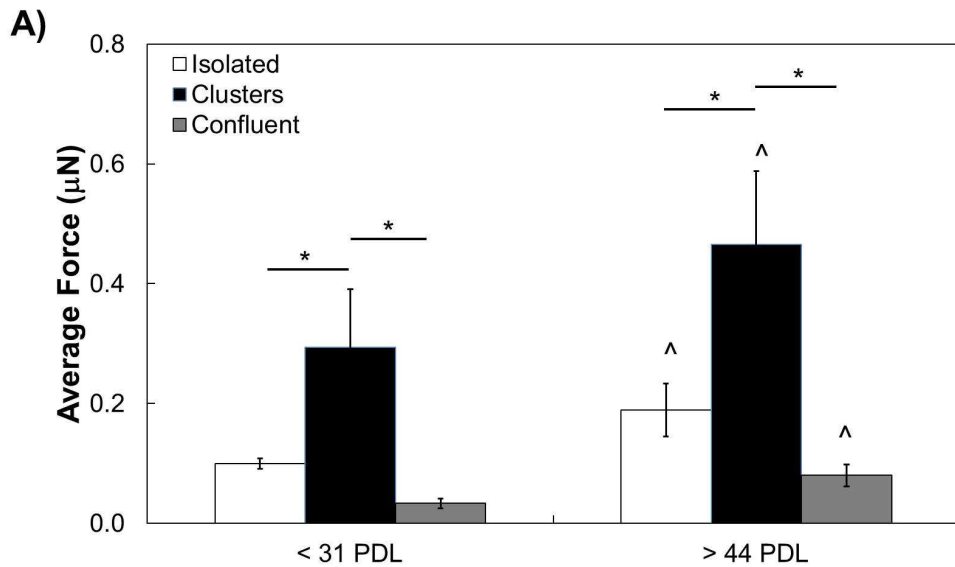
Figure 31: Aged hCB-ECs exhibit increased traction forces and altered actin localization regardless of cell number. A) Traction forces are elevated with increased cell age. Traction forces are highest for cells in clusters, but lower in monolayers. n= 20-25 cells, 6-12 clusters, 5-10 monolayers; *p<0.05, ^ p<0.05 compared to < 31 PDL condition; **B)** Representative image of F-actin for confluent 22 PDL hCB-ECs where actin is localized primarily at the periphery of the cell; **C)** Representative image of F-actin for confluent 58 PDL hCB-ECs where actin is localized throughout the length of the cell.

145

5.3.2 Increased RhoA Activity in Aged hCB-ECs

Because RhoA is important in cell contractility and mediation of cell traction forces, we examined RhoA activity in young and aged hCB-ECs. We found that RhoA activity was higher in aged hCB-ECs than young hCB-ECs (Figure 32). This result correlates with the elevated traction forces in aged hCB-ECs.
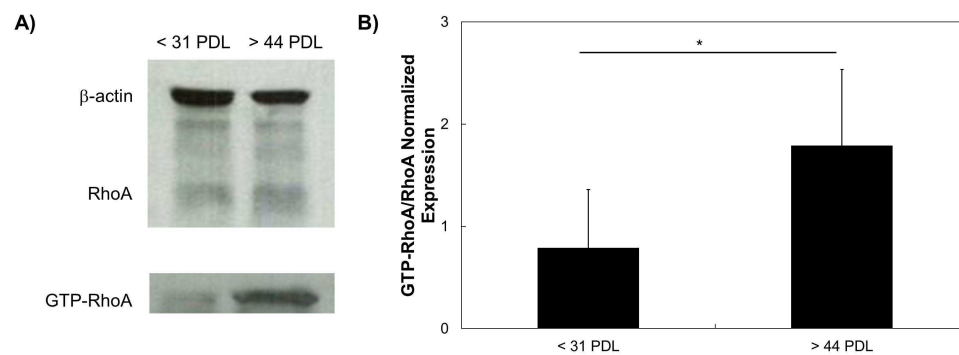
Figure 32: RhoA activity is higher in aged hCB-ECs. A) Representative Western blot of RhoA, GTP-RhoA, and loading control β-actin. There was no statistically significant effect of age on the loading control, β-actin. B) Quantification of Western blot. RhoA activity is higher in aged hCB-ECs compared to young hCB-ECs. (n=3) *: p<0.05

5.3.3 Effect of SIRT1 Treatments on Traction Forces for Isolated Cells and Clusters

Traction forces were elevated in cell clusters compared to isolated cells for all conditions (Figure 33A, p<0.05). For isolated young cells, inhibition of SIRT1 with EX-527 did not significantly alter traction forces compared to young hCB-ECs. For isolated aged hCB-ECs, activation of SIRT1 with SRT1720 reduced traction forces by 2.6X compared to the untreated control (Figure 33A, p<0.05). For young hCB-EC clusters, treatment with EX-527 increased traction forces by 100% in cell clusters compared to the

146

untreated condition (Figure 33A, p<0.05). Treatment with SRT1720 on aged hCB-EC

clusters reduced traction forces by 47% compared to the untreated control.

Because EX-527 was effective at increasing traction forces in cell clusters, but not

in isolated cells, it is likely that EX-527 may be acting on cell-cell junctions. To confirm

this, we calculated the junction tension using equation 6 in the Methods. Junction

tension in cell clusters was significantly elevated by inhibition of SIRT1 with EX-527

(Figure 33B, p<0.05) and with age (Figure 33B, p<0.05). Activation of SIRT1 with

SRT1720 reduced junction tension (Figure 33B, p<0.05). These results indicate that SIRT1

alters cell-cell junctions, which may be a cause for the differences in cell traction force.
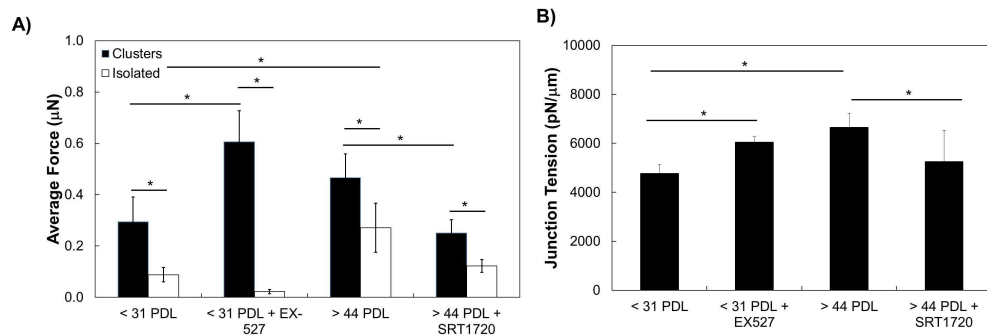
Figure 33: Traction forces are dependent on SIRT1 for ECs in clusters. A) Effect of SIRT1 on traction forces. For isolated cells, inhibition of SIRT1 in young (< 31 PDL) with 5µM EX-527 has no significant effect on traction forces compared to untreated control. However, EX-527 did significantly elevate traction forces for young hCB-EC clusters. Elevation of SIRT1 in aged (> 44 PDL) with 0.16µM SRT1720 decreases traction forces compared to untreated control for both isolated and clusters of cells. Traction forces are higher for clusters of cells than isolated cells for all conditions. n=10-28 clusters. *:p<0.05. B) Junction tension in cell clusters is altered by SIRT1. Inhibition of SIRT1 with EX-527 increases junction tension in < 31 PDL hCB-ECs compared to untreated control. Activation of SIRT1 with SRT1720 reduces junction tension in aged hCB-ECs compared to untreated control.

5.3.4 Knockdown of SIRT1 Elevates Traction Forces

To further confirm the role of SIRT1 on traction forces in young hCB-EC clusters, we used siRNA for SIRT1. The effect of the SIRT1 siRNA was confirmed with Western blotting (Figure 34A). The negative control (scrambled) siRNA did not significantly alter traction forces (Figure 34B). In contrast, knockdown of SIRT1 significantly elevated traction forces compared to the untreated control (Figure 4B, $p<0.05$) and compared to the negative control (Figure 34B, $p<0.01$). These responses corresponded with increased junction tension for SIRT1 siRNA treated hCB-ECs (Figure 4C, $p<0.05$). Increased traction forces in the SIRT1 siRNA could also be attributed to increased cell area in SIRT1 siRNA treated ECs.
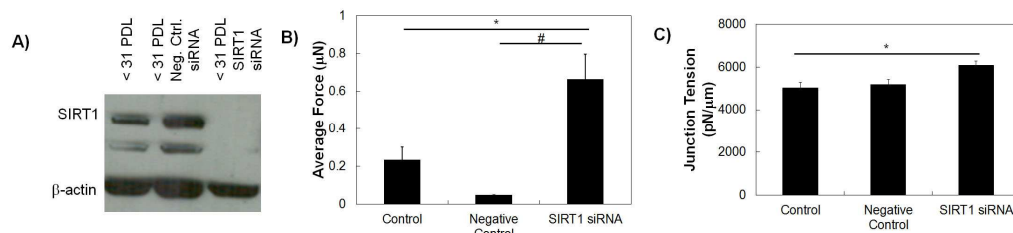
Figure 34: Traction forces are dependent on SIRT1 for ECs in clusters. A) Effect of SIRT1 on traction forces. For isolated cells, inhibition of SIRT1 in young (< 31 PDL) with 5μM EX-527 has no significant effect on traction forces compared to untreated control. However, EX-527 did significantly elevate traction forces for young hCB-EC clusters. Elevation of SIRT1 in aged (> 44 PDL) with 0.16μM SRT1720 decreases traction forces compared to untreated control for both isolated and clusters of cells. Traction forces are higher for clusters of cells than isolated cells for all conditions. n=10-28 clusters. *:p<0.05. B) Junction tension in cell clusters is altered by SIRT1. Inhibition of SIRT1 with EX-527 increases junction tension in < 31 PDL hCB-ECs compared to untreated control. Activation of SIRT1 with SRT1720 reduces junction tension in aged hCB-ECs compared to untreated control.

5.3.5 Knockdown of SIRT1 Alters Actin Localization

To determine whether changes in traction forces and junction tension in SIRT1 knockdown cells correlated with changes in F-actin, we examined actin localization. In young hCB-ECs, F-actin was localized primarily at the periphery of the cell (Figure 35A). Treatment of young hCB-ECs with the negative control (scrambled) siRNA had no effect and actin was localized to the periphery of the cell (Figure 35B). However, knockdown of SIRT1 altered actin localization and caused fibers to be present throughout the length of the cell (Figure 35C). These results show that SIRT1 affects actin localization, which correlates with the elevated traction forces and increased junction tension observed in SIRT1 siRNA-treated young hCB-ECs.
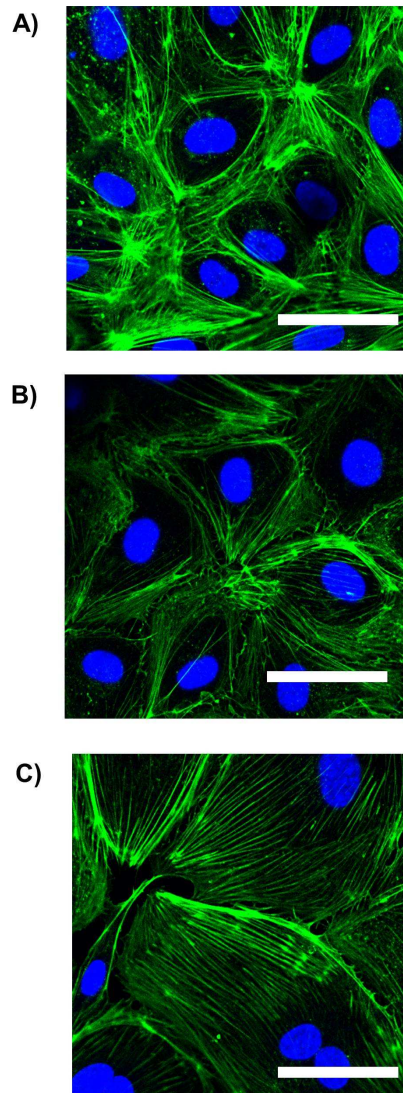
Figure 35: Effect of SIRT1 knockdown on F-actin. Representative images of A) F-actin localized to periphery in young hCB-ECs (< 31 PDL); B) Treatment of young hCB-ECs with negative control (scrambled) siRNA also has F-actin localized primarily to the periphery of the cell; C) Knockdown of SIRT1 with siRNA in young hCB-ECs causes F-actin formation throughout the length of the cell. Scale bar = 50 μm.

5.4 Discussion

There are several factors known to influence cell traction forces for isolated ECs

including changes in actin localization and actomyosin contractility,[30, 87, 133] integrin

levels,[151] focal adhesion formation,[12, 17] and Rho activity.[87, 186] There have also been some studies measuring cell traction forces for cell pairs[16] or confluent monolayers.[85] In this study, we demonstrated that senescent hCB-ECs exhibited elevated traction forces, increased junction tension, and more abundant F-actin fibers due to age-associated changes in SIRT1. We also show that traction forces are higher for hCB-ECs in clusters compared to isolated cells, which is consistent with previously reported results.[16] The traction force increase in senescent hCB-EC clusters correlated with increased junction tension, altered actin localization, and increased levels of RhoA. While inhibiting SIRT1 had no significant effect on traction forces for isolated, young hCB-ECs, inhibition of SIRT1 did elevate traction forces in clusters of young hCB-ECs. This also led to a corresponding increase in junction tension. Furthermore, siRNA knockdown of SIRT1 elevated traction forces, increased junction tension, and altered actin localization. Conversely, activation of SIRT1 reduced traction forces and junction tension in aged hCB-ECs. These results indicate an important role for SIRT1 in regulating aging EC traction forces.

hCB-ECs were used in this study because of their low, physiological permeability,[29] high proliferative potential in subconfluent cultures,[29] and similarity to arterial ECs.[11] Traction forces for both isolated young and aged hCB-ECs were low compared to those previously reported for BAECs.[16, 87]   When young and aged hCB-ECs formed cell clusters, their traction forces increased by about 3x, which is consistent

with results obtained by other groups.[16] We also found that junction tension in young

hCB-ECs was about 4800 pN/μm, which is close to values reported by others.[85] When

the ECs became senescent, the junction tension significantly increased. Because traction

forces are highest for cell clusters rather than cell monolayers, these results also suggest

that cell-substrate interactions are important for clusters of cells, but that cell-cell

interactions are more important for cells in monolayers. Hur et al demonstrate that

junction tension is elevated in cell pairs compared to cell monolayers,[85] which

demonstrates that cell-cell and cell-substrate interactions are dependent on cell number.

Our measurement of monolayer traction forces utilizes large clusters of cells (20-30

cells). We found no significant effect of cell number on traction forces for these large

clusters. To examine traction forces for a true monolayer, another method of measuring

traction forces would need to be used. Polio et al. have developed a technique that

addresses the limitations of the traction force microscopy technique used in this

study.[132] By patterning fluorescent dots in a regularized array, the need for

trypsinization of the cells is eliminated.[132]

Rho GTPases are important in mediating cell contractility and cell traction forces.

In cells on stiff polyacrylamide gels, permeability of ECs was elevated along with Rho

activity.[87] We found that elevated traction forces in aging hCB-ECs correlated with

increased levels of total RhoA in senescent cells. Similarly, others have found that in

human umbilical vein ECs, inhibition of RhoA and Rac1 decreased permeability, cell

contractility, and assembly of actin stress fibers.[186] In bovine aortic ECs, age-related

matrix stiffening caused an increase in permeability and traction forces due to RhoA

activity.[87]

In summary, we showed that senescence of hCB-ECs increases traction forces,

which correlates with changes in localization of actin and elevated levels of RhoA.

Traction forces are elevated for cell clusters, but reduced in monolayers. Additionally,

aged hCB-EC traction forces can be modulated by altering SIRT1. This led to

corresponding changes in junction tension and altered actin localization.

5.5 Chapter Acknowledgements

Chapter 6. Dissertation Summary & Future Work

6.1 Dissertation Summary

Overall, the results within this dissertation provide the novel results that (1) human cord blood-derived endothelial cells exhibit low, physiological permeability at low passages and this permeability increases with increasing cell senescence, (2) aging of endothelial cells decreases their response to steady shear stress by altering mechanotransduction through the glycocalyx and VE-cadherin, and (3) traction forces are increased in senescent cells due to changes in actin structure and localization. The results from this work demonstrate that SIRT1 regulates the glycocalyx and cell-cell junctions. SIRT1 treatments modulated permeability via cell junctions, altered the response to shear stress by affecting cell mechanotransduction of the glycocalyx and VE-cadherin, and affected cell traction forces through changes in junction tension and the actin cytoskeleton. These results also demonstrate the use of human cord blood-derived endothelial cells as model to study cell aging and age-associated diseases.

The global hypothesis that motivated this research was that senescence of ECs would alter permeability and mechanotransduction, key events in atherogenesis. The proposed research tested the following hypotheses: (1) hCB-EC permeability was low at low population doublings, but increases with increasing cell age due to changes in cell junctions, (2) aged hCB-ECs would have inhibited flow-induced levels of KLF2 and eNOS that can be reversed through activation of SIRT1 which affects the structure and

function of the glycocalyx and VE-cadherin, (3) traction forces in isolated aging hCB-ECs increases because of changes to actin, and (4) traction forces in clusters of aging hCB-ECs is elevated compared to isolated cells, and SIRT1 acts on cell junctions to alter tractions.

Chapter 2 results showed that hCB-EC permeability was about 3.1×10^{-7} cm/s, which is close to previously reported values for permeability of endothelium *in vivo*. The permeability of HAECs was about $1\text{-}2 \times 10^{-6}$ cm/s at low passages, indicating that this model is not as physiologically accurate as hCB-ECs. We verified that increased population doublings of hCB-ECs led to increased senescence by examining levels of senescence-associated β-galactosidase and telomerase. The permeability increased monotonically with increasing cell age. While tight junction protein expression was not significantly altered with age, we found that phosphorylation of occludin was increased in aged hCB-ECs. Occludin and ZO-2 were localized to the periphery in young cells, but were primarily cytosolic in aged cells. The percentage of cells in S-phase or M-phase also positive correlated with the increase in permeability in senescent ECs. We used several different indirect activators of SIRT1, including Resveratrol, 007 and Rolipram. Activation of SIRT1 decreased permeability and reduced phosphorylation of occludin, but did not significantly alter the amount of senescence. This result suggests that SIRT1 may be altering other biochemical pathways in the cell, rather than directly affecting the senescent state. The results from this chapter confirm our hypothesis that hCB-ECs have a low permeability that increases with increasing age due to changes in tight junctions.

However, phosphorylation of tight junctions, rather than total amount of junction

protein, was more directly related to permeability changes in senescent cells.

Results from **Chapter 3** show that young hCB-ECs align better in the direction of

fluid flow than aged hCB-ECs. Young hCB-ECs also had flow-induced increases in

KLF2 and eNOS. However, aged hCB-ECs do not have this increase in KLF2 and eNOS

gene expression, suggesting a decreased ability to sense shear stress. We then

investigated how cell senescence alters mechanotransducers, the glycocalyx and VE-

cadherin. We found that the decreased flow responsiveness of aged hCB-ECs correlated

with decreased glycocalyx and thickness and density, decreased trabecular VE-cadherin,

and increased phosphorylation of VE-cadherin. Furthermore, agents that affect the

glycocalyx also altered the response to shear stress and VE-cadherin. Our findings

suggest an important relationship between cell aging and mechanotransduction.

Because of our findings on SIRT1 in chapter 2, we then investigated how SIRT1

altered cell mechanotransduction and the response to shear stress. Inhibition or

knockdown of SIRT1 decreased flow-induced KLF2 and eNOS in young hCB-ECs. It

also reduced glycocalyx thickness and/or density and increased phosphorylation of VE-

cadherin. Conversely, activation of SIRT1 in aged cells elevated KLF2 and eNOS

compared to untreated conditions. SIRT1 activation also restored the glycocalyx

thickness and/or density and reduced phosphorylation of VE-cadherin. The results from

this chapter support our hypothesis that aging ECs are less sensitive to shear stress as

measured by changes in KLF2 and eNOS. Our findings show an important role for SIRT1 in regulating the senescent EC functional response to shear stress through changes to the glycocalyx and VE-cadherin.

Results from **Chapter 4** indicate that for isolated ECs, traction forces increase with increasing cell age. This increase correlated with an increase in actin stress fiber formation and altered actin localization. Reduction of the glycocalyx led to increased traction forces and increased actin fiber width and density.   Changes to the glycocalyx also significant altered EC monolayer permeability. This suggests that age-associated changes in the glycocalyx can alter cell contractility through actin, which affects cell tractions and permeability. We further showed a relationship between SIRT1 and cell tractions, whereby SIRT1 activation in aged hCB-ECs reduced traction forces and thickness of actin. However, inhibition of SIRT1 in young hCB-ECs did not have any significant effect on cell tractions or actin. Inhibition of SIRT1 though did significant elevate permeability in young hCB-ECs compared to the untreated condition. One reason for this discrepancy may be that permeability was measured for a confluent layer of cells, whereas the traction experiments were done for single, isolated cells. This result also suggests that EX-527, SIRT1 inhibitor, may be acting upon cell junctions. The results of this study support our hypothesis that increased cell age elevates traction forces due to changes in actin. We further demonstrate that age-associated changes in

the glycocalyx and SIRT1 may also play a role in elevated traction forces and permeability.

Results from **Chapter 5** show that traction forces are significantly higher for cell clusters than for individual, isolated cells. This result could be due to increased cell contractility for cells in contact. It has been shown that actin stress fiber organization occurs with cell-cell contacts [193]. Increased actin stress fiber organization could facilitate increased cell contractility for cell clusters, resulting in increased forces in cell clusters compared to individual cells. However, large cell clusters that behaved like monolayers, had reduced levels of cell tractions compared to isolated cells. The trend of elevated traction forces with increased senescence that we observed in Chapter 4 was also present for both cell clusters and monolayers. Furthermore, we also found a correlation between elevated traction forces in aged cell monolayers and altered actin fiber localization. These results indicate that the magnitude of the cell traction force changes depending on the number of cells, but that the trend of changes in traction force with increasing age remains the same. Because of the importance of SIRT1 in regulating permeability and shear-induced gene expression and mechanotransduction, we examined whether SIRT1 treatments affected cell clusters. While the SIRT1 inhibitor, EX-527, did not affect traction forces for isolated ECs (Chapter 4), it did increase traction forces when young ECs formed clusters. Activation of SIRT1 also reduced traction forces in older cells. These changes in traction force also correlated with changes in

junction tension. Both age and inhibition of SIRT1 increased junction tension, while

activation of SIRT1 reduced junction tension. These results suggest that SIRT1 may be

acting on cell-cell junctions to alter traction forces.   We confirmed these results by using

siRNA for SIRT1 and see similar trends for traction forces, actin, and junction tension.

Because RhoA plays an important role in cell contractility, we examined levels of RhoA

in aging hCB-ECs to determine whether senescent cells were more contractile, thus

leading to their elevated permeability. Western blots showed that RhoA was

significantly higher in aged hCB-ECs than young hCB-ECs, suggesting that differences

in the contractile state of the cell may be causing the elevated traction forces and altered

actin structure.

6.2 Strengths & Weaknesses of Work

In **Chapter 2**, we demonstrated that young hCB-ECs had a low permeability of

about 3.1×10^{-7} cm/s [28]. This was the first time that the permeability of cultured

endothelium has been shown to be close to those obtained *in vivo* for large arteries. We

also found that permeability of hCB-ECs increased with increasing cell age. This

increase could be mitigated by treatment with different SIRT1 activators. However, the

duration and concentration of the treatments was not fully optimized. Instead, we relied

on values from the literature for the treatments. It is possible that other treatment

conditions could have shown a greater effect of SIRT1 on permeability. However, we

found that high doses of Resveratrol were toxic to the cells, suggesting that additional

activation of SIRT1 may not be efficacious. To address the limitation of using pharmacological agents to alter SIRT1, we examined the effect of several different activators of SIRT1. In Chapter 5, we also use SIRT1 knockdown to show a stronger relationship between SIRT1 and permeability.

Our findings demonstrate that elevated permeability in senescent hCB-ECs is due to altered tight junction protein expression and occludin phosphorylation, but we did not examine phosphorylation of tight junction proteins other than occludin. It is possible that the age-associated changes in permeability also involve other tight junction proteins or adherens junction proteins like VE-cadherin. In Chapter 3, we show that VE-cadherin phosphorylation is altered with age. This result indicates that changes in VE-cadherin function with increasing cell age are likely a cause of elevated permeability in senescent ECs. VE-cadherin phosphorylation at Tyr 658 regulates its binding to p120-catenin, which can alter cell junction tension through changes to cytoskeletal actin. This could lead to alteration in actin filaments and traction forces that we observed in Chapters 4 and 5. To further test the impact of cell age on VE-cadherin or occludin phosphorylation, we could mutate phosphorylation sites to block binding and then measure changes in permeability with age. This would allow us to determine whether age-associated increases in permeability are dependent on junction protein phosphorylation.

While the study examined senescence in aging cells, we did not determine how cell apoptosis changes with increased age. Increased amounts of apoptotic cells could also lead to increased permeability and disruption of cell-cell junctions.[19] To address this, I would visualize the number and location of apoptotic cells in hCB-ECs of different ages. I would then see if the location of the apoptotic cells were localized in regions of elevated permeability. Insights into whether regions of elevated permeability are due to presence of apoptotic or senescent cells would provide additional information into how aging affects monolayer permeability.

Another limitation of the study is the use of hCB-ECs as a model to study cell aging. Replicative senescence *in vitro* is done by passaging of cells. However, this is not necessarily representative of the *in vivo* cell turnover and oxidative stress experienced by cells in atherosclerotic regions. Additionally, the age and behavior of hCB-ECs is donor-dependent and also depends on the original number of cells isolated. The number of population doublings from isolation to passage 1 varies and could lead to variability in hCB-EC permeability results. Using cells isolated from aging animals would provide a different perspective on how cell behavior changes with increased chronological age. A limitation of this approach would be that cells from aging animals may not be representative of accelerated aging of ECs observed in atheroprone areas. However, our model does provide better insights into aging at the cellular level, which is not necessarily related to aging of the organism as a whole.

161

In spite of these limitations, the work was consistent with findings in the literature. The permeability values of HAECs were about 1-2 x 10^{-6} cm/s, which is similar to what has been reported *in vitro* for bovine aortic ECs. Additionally, the relationship that we demonstrate between permeability and tight junction protein phosphorylation is also well-established in the literature. While we saw changes in cell turnover, this did not seem to be a major factor in the altered permeability, which agrees with what others have reported. Therefore, our studies built upon previous findings in the literature and led to new important information, demonstrating that hCB-ECs have very low permeability values that can increase with increasing cell age due to changes in cell junctions.

In **Chapter 3**, key findings are that SIRT1 regulates the aging EC response to shear stress through alteration of cell mechanotransducers, the glycocalyx and VE-cadherin. We show a strong relationship between SIRT1, gene expression, and the abundance of heparan sulfate component of the glycocalyx. However, there are several other components of the glycocalyx, such as syndecan-1, that may be important in mechanotransduction and the response to shear stress. Because syndecan-1 is a transmembrane protein that is linked to the cell cytoskeleton,[50] and the cytoskeleton is important in mechanosensing during exposure to shear stress, it is possible that syndecan-1 may be important in aging EC mechanotransduction. To address this question, we could knockdown syndecan-1 in young hCB-ECs and examine how this

alters the flow-induced levels of KLF2 and eNOS. Furthermore, we could examine

whether there is a relationship between syndecan-1 and SIRT1.

Another limitation of this study is in our visualization of the glycocalyx. We

used immunofluorescence to stain and visualize the heparan sulfate component of the

glycocalyx. While this is one established way to view the glycocalyx, the preparation of

samples for immunofluorescence requires aldehyde fixation which can cause

dehydration of the sample. However, in our studies, we were interested in seeing

whether age or SIRT1 would cause relative changes to the glycocalyx, so the

immunofluorescence technique was sufficient. If we were to determine the absolute

thickness of the glycocalyx, we could use cryo-TEM as this does not require aldehyde

fixation or graded-ethanol dehydration of samples. This technique would give us more

insights into the structure and components of the glycocalyx and how they change with

samples from cells of increasing age. However, this method is time consuming and

requires specialized skill. While several conclusions are based upon our use of

pharmacological agents that affect SIRT1, we used several different activators and

inhibitors to strengthen the argument. Additionally, we used SIRT1 siRNA to

knockdown SIRT1 in young cells as a way to more specifically investigate the effects of

SIRT1 on the response to shear stress.

Other important aspects of this chapter are the novel finding that SIRT1 regulates

the aging EC response to shear stress. Our finding that flow-induced KLF2 and eNOS is

elevated in young hCB-ECs are consistent with the previously literature. We also show that the glycocalyx is decreased in thickness and density with increasing age, which is similar to what is seen in atheroprone regions of the blood vessel. The heparan sulfate thickness that we measured was also similar to what has been reported for bovine aortic ECs *in vitro*. The results show a strong relationship between SIRT1 activity and eNOS levels are also consistent with findings published by other groups. We also found that by using agents known to enhance or reduce the glycocalyx, we are able to alter KLF2 and eNOS expression levels. This agrees with previous research demonstrating that the glycocalyx is an important mechanosensor and that its degradation can impair shear-mediated increases in KLF2 and eNOS.

In this study, we exposed hCB-ECs to steady shear stress of 15 dynes/cm². In atheroprone regions of the blood vessel, which are curved or branched, there is disruption in the local fluid flow patterns. Further studies investigating the effects of oscillatory or reversing flows could provide additional insights into how aging EC mechanotransduction is altered in response to disturbed flow.

In **Chapter 4**, we demonstrate that cell traction forces increase with increasing population doublings due to age-associated changes in the glycocalyx and SIRT1. For this study, we used isolated cells on 15kPa polyacrylamide gels to measure cell traction forces. We found that young hCB-ECs on 10kPa gels did not exhibit any traction forces, so the stiffness of the gel was increased to 15kPa. A limitation of the study is that we did

not optimize protein type. In these experiments, we used 10µg/mL of fibronectin. Immobilizing with a different protein, such as collagen, or a different protein concentration could have led to different results. Additionally, immobilizing with a different covalent linker, such as N6 or sulfo-SANPAH could also alter results by altering how cells adhere to the substrate. While polyacrylamide is highly tunable for Young's modulus, cells do not readily adhere to the surface, which is why protein immobilization is required.[165] A different material surface that would deform, but that allows for cell adhesion without protein deposition, could allow for better measurement of cell traction forces because of changes in the cell's affinity for receptors.

While SIRT1 inhibitor, EX-527, had no significant effect on traction forces or actin for individual cells, we believe that the inhibitor works primarily on cell junctions. In Chapter 5, we explored the effect of SIRT1 on clusters of hCB-ECs to account for the presence of cell junctions.

The traction forces we measured for HAECs was about 0.78 µN, which is significantly higher than that of hCB-ECs. However, it is very close to traction forces for bovine aortic ECs measured by others [16, 87]. Additionally, we see a strong correlation between increases in traction forces and changes in the actin cytoskeleton, which is consistent with results reported by others.[74, 87] Age associated-changes in the glycocalyx thickness and density are also consistent with what we have previously reported in Chapter 3 and what is shown in atheroprone regions *in vivo*.

In **Chapter 5**, we found that cell aging increased traction forces for hCB-EC

clusters and monolayers. Strengths of the work include consistency with previously

reported data in the literature. We show that tractions are almost 3 times higher for cell

clusters compared to individual cells, which agrees with results from others [16].

Because traction forces are highest for cell clusters rather than cell monolayers, these

results also suggest that cell-substrate interactions are important for clusters of cells, but

that cell-cell interactions are more important for cells in monolayers. Further

experiments would need to be done to investigate the role of cell-substrate interactions

to determine which factors are important for traction forces of different cell groups.

While we did examine the effect of SIRT1 on cell junctions by measuring junction, we

did not examine specific junction proteins. However, we did try to address this question

by measuring cell junction tension. Besides using SIRT1 activators and inhibitors, we

performed experiments with SIRT1 siRNA to more specifically inhibit SIRT1 and

provide more conclusive evidence of the role of SIRT1 on traction forces. Additional

work examining adherens junctions, like VE-cadherin, which connect to the actin

cytoskeleton, could provide additional insights into the mechanism of action of SIRT1.

In Chapter 3, we show that phosphorylation and localization of VE-cadherin is altered in

aging cells in a SIRT1-dependent manner.

Another limitation of the work is that we examined large clusters of cells that

appeared as monolayers. The current traction force method requires areas in the field of

166

view which do not have any bead displacement and trypsinization of the cells since the polymerization of the gel cause the beads to be randomly dispersed. The development of a traction force microscopy which uses fiduciary markers, similar to one used by Polio et al [132], would eliminate the need for trypsinization and would include markers that are not displaced. This would allow us to further study traction forces for confluent monolayers. The development of a surrogate measure of cell traction forces would also allow us to determine whether cell tractions are altered *in vivo*. If changes in cell shape could be related to changes in traction forces, then it could potentially be used to detect areas of elevated cell traction in blood vessels. One could then determine whether areas of high cell traction are also areas of elevated EC permeability.

6.3 Implications for Treatment of Atherosclerosis

Overall, the results from this study present novel insights into endothelial cell aging. We demonstrate that hCB-ECs are a suitable model for studying cell aging because of their high proliferative potential in subconfluent cultures and their low, physiological permeability [28]. Permeability of hCB-EC monolayers increases with increasing population doublings due to changes in tight junction protein phosphorylation and localization. Because ECs in atheroprone regions exhibit accelerated aging and elevated permeability, these results further support the use of hCB-ECs as a model to study age-associated pathologies. To reverse the elevated permeability at high population doublings, we used several different agents known to

modulate SIRT1. By activating SIRT1, we saw a decrease in permeability in aged hCB-ECs. This result implicates a possibility for using SIRT1 activators in treatment of atherosclerosis. Furthermore, the results demonstrate that SIRT1 alters permeability by acting upon cell-cell junctions to alter localization and phosphorylation.

We further implicate SIRT1 by describing its role in regulating mechanotransduction through the glycocalyx and VE-cadherin. We demonstrate that aged hCB-ECs have a decreased response to shear stress, a thinner glycocalyx, and elevated VE-cadherin phosphorylation. Activation of SIRT1 alters all of these responses. Conversely, inhibition or knockdown of SIRT1 in younger hCB-ECs caused them to behave like older hCB-ECs. The results from this study show that SIRT1 can directly modulate the response to fluid flow in aging ECs. We further demonstrate that SIRT1 can directly affect mechanotransduction of ECs. Changes in mechanotransduction can be attributed to the effect of SIRT1 on phosphorylation and localization of adherens junction protein, VE-cadherin. SIRT1 may be a viable target for treatments for atherosclerosis because of its ability to restore mechanosensitive properties in senescent cells.

Furthermore, SIRT1 plays an important role in cell traction forces and the actin cytoskeleton. Elevated traction forces in aged hCB-ECs correlated with increased permeability and increased actin fiber thickness. While inhibition of SIRT1 did not have a significant effect on young hCB-ECs, activation of SIRT1 did restore function in aged

hCB-ECs. The relationship between the glycocalyx and SIRT1 in mediating cell traction

forces is consistent with our finding that the glycocalyx and SIRT1 can both mediate the

hCB-EC response to shear stress. Extending our results for isolated EC traction forces,

we examined traction forces for cells in clusters or confluent monolayers to account for

the presence of cell junctions. Here, SIRT1 is able to alter the traction forces, junction

tension, the actin cytoskeleton, and levels of cell contractility protein RhoA. SIRT1 plays

an important role in mediating integrity cell-cell junctions. Through changes in

phosphorylation of occludin and VE-cadherin, SIRT1 alters actin structure, leading to

corresponding changes in cell traction forces and permeability.

As a whole the results from this dissertation implicate an important role for

SIRT1 in regulating aging EC function (Figure 36). We used several different

approaches to demonstrate how SIRT1 regulates permeability, cell-cell junctions, and the

glycocalyx. Treatments that target SIRT1 may be a suitable option for preventing the

permeability increases that are associated with early stages of atherosclerosis. Further

studies would need to be done to fully characterize the role of SIRT1. Extensive *in vivo*

testing of different SIRT1 activators and inhibitors would also be needed to determine its

efficacy on reducing or preventing atherosclerosis.
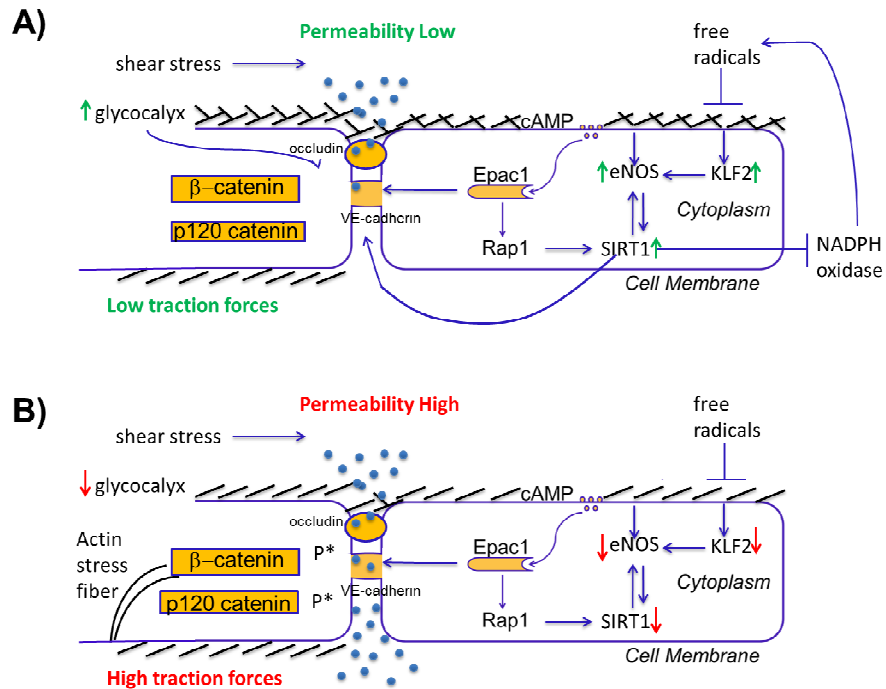
Figure 36: SIRT1 levels alter permeability and mechanotransduction in aging hCB-ECs. A) Young hCB-ECs have high levels of SIRT1, which inhibits NADPH oxidase and protects the glycocalyx from damage from free radicals. An intact glycocalyx and high SIRT1 levels increase levels of atheroprotective genes, eNOS and KLF2 when cells are exposed to shear stress. Furthermore, SIRT1 and glycocalyx help maintain the endothelial barrier by preserving cell-cell junctions. This also results in lower traction forces. B) Aged hCB-ECs have low levels of SIRT1, which does not allow for protection of the glycocalyx from free radicals. The damaged glycocalyx and low levels of SIRT1 causes aged hCB-ECs to not be as responsive to shear stress, thus, having lower levels of KLF2 and eNOS. Additionally, low levels of SIRT1 and the glycocalyx cause cell junctions to be phosphorylated, leading to degradation of the EC barrier. This elevates permeability, causes an increase in traction forces and leads to the formation of actin stress fibers.

Appendix A: EC Media

<u>**Materials**</u>
- EBM-2
- EGM2 Singlequots
- 5mL of AB/AM
- FBS (if needed)

<u>**Procedure**</u>
1. Add EGM2 singlequots, and AB/AM to bottle of EBM-2.
2. Remove 50mL of media mixture.
3. Add 50mL of FBS (10mL from singlequots and 40mL from freezer aliquots)
4. Write name, date, and label on the bottle.

Note: AB/AM and FBS (all frozen) are always aliquoted for use. EGM2 and EBM2 must be purchased from CCF.

Appendix B: EC Passage and Seeding

<u>Materials</u>
- Media
- Sterile PBS without Calcium/Magnesium
- Trypsin (0.025%)
- T75 flask
- 50mL tube labeled "cell suspension"
- 15mL tubes labeled with experimental conditions
- 5mL pipettes
- 10mL pipettes
- Hemacytometer
- Micropipettes

<u>Procedure</u>
1. Put all materials in hood
2. Label a T75 with cell line, passage number (n+1), date, name
3. Add 10mL of media to T75 and put aside
4. Remove cells from incubator and suck out media
5. Wash cells twice with PBS (5-10mL)
6. Add 2mL of trypsin
    - Wait for cells to detach (5 minutes at 37C), rap gently; use scope to check
7. Add 8mL of media for a final volume of 10mL
8. Pipette up and down gently but mix thoroughly
9. Add 1mL of suspension to fresh T75 (pass 1:10)
    - Put this flask in the incubator
    - Rock back and forth gently

10. Remove remaining cell suspension and place in 50mL tube labeled "cell suspension"
11. Mix thoroughly, and seed a hemacytometer with 15uL per side
12. Count cells with the scope (count individual squares, average, multiply by 10,000 to get cells/mL)
13. Calculate total cells needed by multiplying the number of wells by the number of cells you want per well
14. Mix suspension thoroughly and remove amount of cells needed to put in 50mL tube(s) labeled experimental conditions
15. Mix thoroughly, and seed each plate/well

Appendix C: Generating Calibration Curve for Plate Reader for Transwell Permeability Assay

Materials:

FITC-BSA (A9771-100MG from Sigma, ordered through CCF)
EC Serum Free Media
1 50mL conical labeled FITC 1 mg/mL
1 50mL conical labeled 1mg/mL unlabeled BSA
1 15mL conical labeled 3 ug/mL
5 Small Eppendorf tubes labeled 0, 0.2, 0.5, 0.6, 1.0
Micropipettes (2-20, 20-200, and 100-1000)
Pipettes (1 25mL, 3 5mL)
1 96 well plate
Foil

Procedures:

1. Make stock solution (1 mg/mL) of FITC-BSA in EC serum-free media.
    a. Weigh out about 6 mg (if using 12 wells of Transwell plate) of FITC-BSA onto a 50mL conical tube cover. Keep covered with foil to prevent bleaching.
    b. Add 6 mL of EC media to make a final concentration of 1 mg/mL.
    c. Mix well!
2. Make stock solution (1 mg/mL) of unlabeled BSA in EC serum-free media.
    a. Weigh out about 18 mg (if using 12 wells of Transwell plate) of BSA onto a 50mL conical tube cover. Keep covered with foil to prevent bleaching.
    b. Add 18 mL of EC media to make a final concentration of 1 mg/mL.
    c. Mix well!
3. Dilute stock FITC-BSA solution to 3ug/mL to make lower calibration concentrations.
    a. Add 15uL of stock into 5mL of EC media in a 15mL conical tube. Keep covered with foil to prevent bleaching.
    b. Mix well!
4. Use the table below to dilute to the desired concentrations.

Desired Conc (ug/mL)	Vol of stock (3ug/mL) in uL	Vol of media in uL

0.2	10	140
0.5	25	125
0.6	30	120
1.0	50	100

5. Add above volumes to small eppendorf tubes. Each eppendorf tube will have 150 uL of solution. Note: add media first, then the stock volumes.
6. Mix solution in eppendorf tubes well. Then, add 50uL each concentration to the prepared 96-well plate. Cover with foil to prevent bleaching.

Appendix D: EC Permeability Plating and Experiment Protocol

Day 1 Supplies
- Media
- PBS (-, -) for passaging
- Trypsin (5mL)
- TNS (5mL)
- 50mL sterile centrifuge tube labeled "Cell Suspension"
- 15mL tube labeled 8 x 10^5 cells (8 wells times number of cells per well), 4mL (8 wells times 0.5mL sol'n per well)
- Hemocytometer
- 1 Transwell Plate 12-well (VWR: 29442-078)
- T-75 flask
- Marker
- Pipettes and Pipette Aids
- Micropipettes
- Sterile Tweezer

Day 2 Supplies (once cells are confluent on the Transwell plate)
- 1 Regular 96-well Plate for sampling and calibration
- 1 15mL conical tube labeled "waste"
- FITC-BSA when starting experiment and other materials for "Generating Calibration Curve" Protocol
- Serum-Free Media
- Micropipettes
- Timer
- Foil

Day 1
1. Grow Cells in T-75 to Confluence
2. Passage and Seed Cells for Experiment
3. During passaging, centrifuge cells at 1000rpm for 5 minutes after the TNS step.
4. Plate Cells in Transwell Permeable Support Plates (12 well)
   a. Add Total Volume for Plate Well **(abluminal) = 1.5mL** [from Transwell booklet]
   b. Count cells with hemocytometer
      i. Hemocytometer gives cells/1 mL (= cells/cm³)
   c. Seed at density of 10^5 cell/mL [from Ji dissertation] for each well (luminal)

i. Set up ratio

$$\frac{h\ cells}{1mL} = \frac{10^5\ cells}{x\ mL}$$

Where h=number of cells counted from hemocytometer

x=amount of cell solution to add to each well in a 12-well plate

ii. Total volume for Transwell Insert (luminal) = 0.5mL

$$y = 0.5mL - x\ mL$$

Where y=amount of media that needs to be added per well

x= from step i.

iii. Set up 15mL tube labeled 8 x 10^5 cells (8 wells times number of cells per well), 4mL (8 wells times 0.5mL sol'n per well)

d. Seed 8 wells (see below) with 0.5mL sol'n each
e. Cells C1-C3 will be used for membrane permeability (if needed for the experiment)
f. C4 will be a control with media only.

Transswell Plate

	1	2	3	4
	EC 1-1	EC1-2	EC1-3	EC1-4
	EC1-5	EC1-6	EC1-7	EC1-8
	Membrane	Membrane	Membrane	Control

Day 2

5. Aspirate the media from each well using a 100-1000uL micropipette. Add the discarded media to the 15mL conical labeled "waste." Be sure to aspirate from the side of the well and not from directly on top of the cells.

176

6. Add 0.5mL of serum-free media to each well. Let this incubate for **1 hour**.
7. Add 0.5mL of prepared 1 mg/mL FITC-BSA solution to top well. Add 1.5mL of prepared 1 mg/mL unlabeled BSA solution bottom well (see "Generating Calibration Curve Protocol". This is the start of the experiment.
8. Take 10 ul samples from abluminal (bottom) chamber at 0, 20, 40, 60, 80, 100, 120 minutes. Dilute the samples with 40ul media.
   a. The samples will only contain media that has FITC-BSA, so this should be placed into a normal 96 well plate.
   b. Notation: ECX-Y X = experiment number; Y=sample number
9. The samples for the calibration curve will be in row H of the plate (see "Generating Calibration Curve Protocol")

Appendix E: EdU Assay for 8 wells of a Transwell Plate

<u>Materials</u>
- One Click-IT Alexa Fluor Imaging Kit containing components A-G.
- PBS +/+
- Small eppendorf tubes
- Deionized water
- 100% Methanol (in freezer)
- Transwell plate with cells
- 1 15mL conical labeled "media"
- 1 15mL conical labeled "media + Component A"
- 1 dark 50mL conical labeled "reaction cocktail"
- 1 dark 50mL conical labeled "1:2000 Component G"
- Vectashield
- 8 glass slides
- 8 22x22mm coverslips
- Forceps
- Scalpel
- 2 large petri dishes
- 1 filter paper

<u>Procedure</u>
Pre-plating Steps (do in dark)
1. Need to prepare four stock solutions. Use solutions immediately or store as designated.
2. 10mM EdU solution: add 2 mL of DMSO (Component C) to the EdU vial. Mix well with vortex. Store at *-20 degrees Celsius/-4 degrees F*.
3. Azide solution: add 70ul of DMSO (Component C) to the azide vial. Mix well with vortex. Store at *-20 degrees Celsius/-4 degrees F*.
4. 1X buffer: Transfer all of component D into a falcon tube filled with 36mL of deionized water. Mix well with vortex.
5. 10x buffer: add 2mL of deionized water
6. Make 50uL aliquots of components A and F. Store these aliquots in small eppendorf tubes.

Labeling Cells with EdU (in dark, in cell-culture hood)
7. Prepare a 2X working solution of EdU by diluting the 10mM stock solution using cell culture media to obtain a concentration of 10uM.
    i. For the 12-well Transwell inserts, this is 250uL of media/well and 250 uL of solution/well.

        ii.   Two 15mL conicals
             1.   Media: 2mL
             2.   Stock: 2mL Media, 4uL component A

8. Incubate at 37C for **2 hours**.

Fixing and Permeabilizing Cells

9. Aspirate media and rinse 3x with PBS +/+.
10. Add 100% methanol to the wells (add just enough to cover the bottom of the well).
11. Incubate for 2-3 minutes.

Detecting EdU-Reaction (in dark)

12. Prepare the 1X click-iT EdU buffer by diluting 10x solution, 1:10 in deionized water (90uL DI water, 10uL component F).
13. Prepare reaction cocktail (1000uL total) in the following order 50mL conical in the following volumes:
    i. Component D (1X Click-iT reaction buffer prepared): 860uL
    ii. Component E ($CuSo_4$): 40uL
    iii. Component B (Alexa Fluor Azide): 2.4uL
    iv. Reaction buffer additive (prepared in step 12).
    v. Note: This must be used within 15 minutes of preparation.
14. Remove methanol and rinse 3x with PBS +/+.
15. Add 125uL of reaction cocktail to each well. Rock plate and incubate for 30 minutes, protected from light at room temperature.
16. Remove the reaction cocktail and wash each well 3x with PBS.

DNA Staining (in dark)

17. Dilute component G 1:2000 to obtain 1X Hoeshst 33342 solution a 1X Hoechst 33342 solution (concentration of 5 ug/mL).
    i. 2uL component G
    ii. 3998uL PBS +/+
18. Add 0.5 mL/well of diluted Hoechst 33342 solution. Incubate for 30 minutes at room temperature, covered from light.
19. Wash each well 3x with 1 mL/well of PBS. Remove the wash.

Mounting Slides (in dark)

20. Remove well from Transwell Plate and place on filter paper on top of Petri dish to dry the excess liquid.
21. Aspirate PBS wash from Transwell insert.

22. Cut out membrane with scalpel (do on top of petri dish). I find that is best to rotate the insert and leave the scalpel in place.
23. Transfer the membrane to a glass slide with forceps.
24. Add a drop of vectashield to the membrane.
25. Cover with a 22x22mm glass coverslip and repeat for other wells.

Imaging and Analysis
26. Use excitation/emission of 495/519nm for Alexa Fluor 488 and 350/461 for Hoechst. For the Reichert scope this is the FITC and DAPIn filters.
27. % proliferation = #EdU-stained cells/#Hoechst-stained cells * 100%

Cleaning Slides
28. To clean slides, remove coverslip and membrane with kim wipe. Discard membrane.
29. Spray ethanol on kim wipe and wipe coverslips and slides. Dry coverslips and slides with kim wipes and then store for later use.

Appendix F: Senescence β−Galactosidase Staining for 6 wells of a 24 well plate

Materials
1 β-Galactosidase Staining Kit (Cell Signaling)
DMF
PBS+/+
3 eppendorf (labeled "X-gal/DMF", "Fixative Soln", and "Staining Soln")
15mL conical (labeled "Staining Mix")
Micropipettes (1mL, 200μL, 20μL)
24 well plate with cells
Deionized water

Preplating Steps (lasts over three plates)
1. Dissolve 20mg X-gal in 1mL DMF to prepare 20X stock solution in eppendorf. Mix very well. Store excess solution in a light resistant container at -20°C up to one month.

Setup
2. Prepare 1X dilution of 10X Staining Solution with distilled water.
    a. 300μL 10X Staining solution, 2700μL distilled water
3. Prepare 1X dilution of 10X Fixative Solution with distilled water.
    a. 150μL 10X Fixative solution, 1350μL distilled water

Procedure
1. Remove media from wells (top and bottom) and wash plate once with PBS.
2. Fix cells with 250μL/well 1X Fixative solution for 10-15 minutes at room temperature.
3. While plate is in Fixative Solution, prepare the Staining Solution in 15mL conical:
    a. 2790μL 1X Staining Solution
    b. 30μL Staining Supplement A
    c. 30μL Staining Supplement B
    d. 150μL 20mg/ml X-gal in DMF
4. pH solution to 6.0.
5. Wash the wells twice with PBS.
6. Add 500μL of Staining Solution mix to each well in the plate
7. Incubate plate overnight in dry incubator at 37°C.
8. Image with color camera using "Auto White" and medium contrast.

Appendix G: qRT-PCR Protocol

Making fresh 5µM primer stock solutions (NOTE: There are stock 100µM solutions of the primers in the -20°C that are stable for around 24 months or so. These stocks should be unthawed rarely. There are also 5µM solutions of the primers in the 4°C that are stable for around 1-2 months.

1) Place the 100µM stock solution in an ice bucket to unthaw.
2) Add 475µL of nuclear-free water to a 2.0mL colored tube.
3) Add 25 µL of the 100µM stock solution to the 2.0mL colored tube.
4) Place the 100µM stock primer solution in the -20°C immediately.
5) Place the 5µM solution in the 4°C.

Measuring RNA Concentration using the Nanodrop (NOTE: Avoid free-rethaw cycles as RNA degrades really quickly. Also the RNA should ALWAYS be kept on ice.)

1) Wipe down the bench, pipettes, and your gloves thoroughly with RNAse Zap.
2) Place the RNA samples, nuclease-free water, P2 pipette, small tips, and RNAse Zap in a bucket of ice.
3) Go upstairs to the nanodrop (username: microarray, password: extraction).
4) Select the correct program.
5) Wipe the stage down with RNase zap using the small spray bottle (only use enough to barely moisten a Kimwipe).
6) Next wash the stage with nuclease-free water.
7) Add 1.5uL of nuclear-free water to the stage.
8) Select "Blank"
9) Remove the water using only a Kimwipe.
10) Change DNA-### to RNA-### using the pull-down menu in the upper-right corner.
11) Add 1.5uL of nuclear-free water to the stage.
12) Select blank again.
13) Remove the water using only a Kimwipe.
14) Add 1.5uL of the first RNA sample to the stage.
15) Select measure.
16) Remove the sample using a Kimwipe, wipe the stage with a Kimwipe that is barely moistened by RNAse Zap, wipe the stage with a Kimwipe that is wet with nuclease-free water, and dry the stage with a dry Kimwipe.
17) Repeat steps 14) through 16) for each RNA sample
18) Select the "Print Report" button on the top right of the screen.
19) Turn 90°C to the left (facing the computer screen) and walk to the end of the hall and pick up the report from the printer.
20) Log-out when you are finished.

Making cDNA (NOTE: You need to do this step on the same day)
1) Add 5x iScript Reaction Mix (blue tube) and iScript Reverse Transcriptase (yellow tube) to the ice bucket.
2) Calculate the number of μL of RNA required to add 250 ng of RNA by dividing 250ng by "ng/ μL."
3) Calculate the number of μL of nuclear-free water required such that the total amount of nuclear-free water + RNA is 18 μL.
4) Add the nuclease-free water to the small microcentrifuge tubes (one for each RNA sample) first.
5) Add the calculated μLs of RNA next.
6) Add 5μL of the 5x iScript Reaction Mix (blue tube) to each microcentrifuge tube.
7) Add 1.25μL of the iScript Reverse Transcriptase (yellow tube) to each tube (NOTE: This is the polymerase that initiates the reaction, so you should add this last).
8) Pipette gently up and down (NOTE: Do not vortex as RNA is unstable).
9) Add the microcentrifuge tubes to the Thermocycler. Select "Run" as the thermocycler is already preset for use with the BioRad iScript cDNA Synthesis Kit. The cycle takes exactly 40 minutes. (NOTE: After 40 minutes, the thermocycler will attempt to "hold" the cDNA at 4°C. You should ideally remove the samples after the 40 minute period and continue with the next step or else store them in the -20°C).

NOTE: You can take a break here if you need to, but it is best to just get everything over with. If you decide to take a break, store the cDNA in -20°C.

RT-PCR protocol (NOTE: Keep everything on ice during this process).
1) Wipe down the bench, pipettes, and your gloves thoroughly with RNAse Zap.
2) Take a freezer box from the -20°C and place a 96-well plate in the freezer box. (NOTE: Make sure that you do not touch the bottom of the 96-well plate, set it on the counter, etc.).
3) Place the iQ SYBR Green Supermix (orange tube) and primers (both 5' and 3' primers) in an ice bucket.
4) Let X be the number of genes of interest (2 in the case of smMHC and β2). Label a 600mL colored microcentrifuge tube with the name of the gene for each gene of interest.
5) Let Y be the number of conditions (6 in the case of SMC(mono), SMC(HAEC), SMC(EPC), MSC(mono), MSC(HAEC), and MSC(EPC)). Then combine the following reagents in each 600mL microcentrifuge tube
$$6.6*(3.5*Y+3) \text{ μL nuclease-free water}$$

$$1.2*(3.5*Y+3) \ \mu L \ 3' \ primer \ (5\mu M)$$
$$1.2*(3.5*Y+3) \ \mu L \ 5' \ primer \ (5\mu M)$$
$$10*(3.5*Y+3) \ \mu L \ IQ \ SYBR \ Green \ Supermix$$

6) Mix the solutions by pipetting up and down.
7) Next label X 600mL microcentrifuge tubes with the gene of interest. (NOTE: All of the microcentrifuge tubes should be the same color).
8) Repeat step 6) for each of the Y treatments and using a different color for each treatment. (NOTE: You should have X*Y tubes total clearly labeled with the gene name). (i.e. If you were running SMC(mono) and MSC(mono) for smMHC and $\beta 2$ only, you would have 1 red and 1 blue tube labeled "smMHC" and 1 red tube and 1 blue tube labeled "$\beta 2$" where the red tubes correspond to SMC(mono) and the blue tubes correspond to MSC(mono).
9) Add 66.5μL of the solutions prepared in step 5) to each of the corresponding, labeled 600mL microcentrifuge tubes. (NOTE: At this point, you should have X*Y labeled microcentrifuge tubes containing 66.5μL of the corresponding primer solution).
10) Resuspend the cDNA samples using 20μL of nuclear-free water.
11) Add 3.5μL of the cDNA sample to each 600mL microcentrifuge tube of a single color.
12) Mix the cDNA solution by pipetting up and down or gentle vortexing.
13) Add 20μL of the mixed solution to each of 3 wells of the 96-well plate. (NOTE: Add the mixed solution to the side of the well and let it drip down. Make sure to avoid making air bubbles even though this a lot with the new tips). Repeat for the other microcentrifuge tubes.
14) Repeat steps 11-13) for each treatment.
15) Cut a piece of optical tape to fit precisely over all 96 wells of the plate.
16) Move the air bubbles to the top by centrifuging 3 times for 30 seconds each. Hold the forward arrow down for 30 seconds rather than specifying a specific speed or duration. (NOTE: Again, try to not touch the bottom of the 96-well plate)
17) Place the 96-well plate in the RT-PCR machine.
18) Open the MyiQ Software and select the protocol "2stepmelt4ebd.tmo."
19) Select "View Plate Setup" and then select "Edit This Plate Setup."
20) Label each triplicate set with a unique number (NOTE: Do not label the blank wells as "Blank," just leave them unlabeled.)
21) Save the plate setup and select "Run with Selected Protocol."
22) Change the sample size to "20μL" and select "Begin Run."
   (NOTE: If you receive an error message, then the baseline iQ SYBR fluorescence was not detected in at least one of the wells. You may have mislabeled the wells

using the MyiQ software, or you may have forgotten to load the iQ SYBR reagent into one of the wells.)

Appendix H: RNA Isolation

for use with Aurum Total RNA Mini Kit from Bio-Rad
created by C.Cheng 05.25.2011
modified by C.Cheng 06.15.2011

1. RNase Zap bench surface and wipe down all micropipettors and the aspirator tip. RNase Zap your hands and get 3 capped 1.5-ml tubes, 1 capless tube + filter for each sample. Place 90ul of elution *per sample* into **one** capped 1.5- or 2-ml tube and place into heat block set to 70°C.

2. Bring sample over to RNA station and place on ice. Aspirate all media.

3. Gently add 1ml of DPBS to each sample, making sure not to add directly on top of the cells. Aspirate DPBS.

4. Add 250ul of DPBS directly to the cells. Use a cell scraper and carefully scrape off cells.

5. Use a micropipetter to transfer DPBS + cell mixture from all wells into one 1.5-ml capped microcentrifuge tube. Place tube (with a balance) into microcentrifuge and spin down for 5 min at speed 10. While the cells are spinning down, place used plate and cell scrapers in biohazard trash and scraper wrappers in the normal trash.

6. After spinning down, carefully aspirate all supernatant and add 350ul of lysis solution to the cell pellet. Vortex tube for 1min to lyse cells.

7. Add 350ul of 70% Ethanol to tube and vortex 1min.

8. Transfer solution into filter (aka "RNA binding column"). Centrifuge for 30sec at speed 10. After centrifugation, hold filter while aspirating filtered liquid. Place filter back into tube

9. Add 700ul of low stringency wash solution to filter. Centrifuge 30sec at speed 10; aspirate filtered liquid

10. For **each** sample, mix 5ul of reconstituted DNase I (in -20 freezer) with 75ul DNase dilution solution in a 1.5-ml capped tube. Add 80ul of mixture directly to the membrane of each filter. Incubate at room temperature for 15min.

11. After 15min incubation, centrifuge for 30sec at speed 10. Aspirate liquid

12. Add 700ul of high stringency wash solution to filter; centrifuge for 30sec at speed 10; aspirate

13. Add 700ul of low stringency wash solution to filter; centrifuge for 1min at speed 10; aspirate

14. Centrifuge for 2min to remove residual wash solution. Check that heat block for elution solution has reached 70°C.
15. Transfer filter to a new 1.5-ml capped centrifuge tube and pipet 90ul of warmed elution solution onto membrane in the filter. Let sit for 1min to allow solution to saturate membrane. Centrifuge uncapped for 2min at speed 10 to elute the RNA from the filter.
16. Store in -80.

Appendix I: Western Blot Protocol

Modified from CR and SW Protocols

Materials
- Lysis Buffer: CellLytic-M (Sigma C2978)+Protease inhibitor cocktail (Sigma P8340)
- Mini Ready Gel
- Laemmli's Sample Buffer (Biorad #161-0737)
- Beta-Mercaptoethanol (Biorad 161-0710)
- TBST: Dilute 10x Tris-Buffered Saline (Biorad #170-6435) to 1X with DI water and add 0.1 % Tween 20 (Biorad 170-6531) (i.e. 50mL TBS, 450mL DI water, 0.5mL Tween 20)
- Transfer Buffer: 100 mL 10x Tris Glycine Buffer (Biorad #161-0771), 700mL distilled water, 200mL methanol (if using PVDF membrane, otherwise 900mL distilled water)
- Running Buffer: 100mL 10x Tris/Glycine/SDS Buffer (Biorad #161-0772), 900mL distilled water
- PVDF membrane
- Fiber pads
- Filter paper
- Kaleidoscope Ladder (Biorad 161-0375)
- SuperSignal West Pico Stable Peroxide Solution
- SuperSignal West Pico Luminal/Enhancer Solution
- RESTORE Stripping Solution (21059)
- Pierce BCA Assay Kit (Pierce 23227)
- Film
- Non-Fat Dry Milk Powder
- Primary and Secondary Antibodies
- Methanol
- PBS -/-
- Eppendorf tubes
- Micropipettes
- Pipettes
- 96-well plate for BSA
- 50mL and 15mL conical tubes

DAY 1
Buffer Preparation

1. Mix ingredients together for Transfer and Running Buffers and put into labeled 1L jars. These can be stored in the fridge overnight.
2. Mix ingredients together for TBST. Tween 20 is very viscous. Store in fridge overnight.

DAY 2
Protein Harvest (Can be done as cells are ready and stored in -20C)
1. Prepare Lysis Buffer (KEEP ON ICE)
   - Cell-lytic M (Add 0.5mL protease/phosphatase inhibitor cocktail to every 5mL Cell-lytic M used)
2. Carefully aspirate media from cells. The whole process should be done on ice.
3. Wash once with cold DPBS -/-
4. Add DPBS to each flask or well (~400uL/well).
5. Scrape cells with cell scraper. Keep plate tilted at all times in order to keep all the cellular debris in the PBS. Pipette out all liquid and cells. Add suspension to 2.0mL eppendorf tube.
6. Spin down tubes with microcentrifuge at speed 3 for 5 minutse.
7. Remove supernant and resuspend cells in ~70uL of of lysis buffer.
8. Shake for 30 minutes at 4C with lab quake.
9. Spin down tubes at max speed for 15 minutes at 4C (place microcentrifuge in fridge).
10. Remove supernatant (this is the protein soluble fraction) and place each into sterile vials. Store in -20C.

BSA Protein Concentration Determination Protocol
1. Prepare BSA Standards as described in the manual that comes with the BSA kit, EXCEPT dilute in lysis buffer rather than PBS. (Note: The standards can be prepared ahead of the time and aliquoted and stored at -20C.)
2. Prepare BCA indicator solution (# samples + # of samples) * (number of replicates) * (volume of indicator solution per sample) = total volume of indicator solution needed. Make the solution with 50 parts Reagent A with 1 part Reagent B (example: 2500uL Reagent A, 50uL Reagent B).
3. Add 100uL of BCA solution to each well of a 96-well plate.
4. Add 2uL of each BSA standard to the wells (do in duplicate in rows A and B of plate).
5. Add 2uL of each unknown sample to wells (do in duplicate, rows C and D).
6. Shake for 30s on plate shaker.
7. Incubate at 37C for 35 minutes.
8. Read using plate reader in Yuan lab (ABS 590) or Bursac Lab (Mina_BSA).

Prepare Proteins
1. Use Excel spreadsheet and BSA results to calculate volume of lysate needed to get desired amount of protein (usually, 10ug-30ug).
2. In 1.5mL eppendorf tubes, add amount of DI water calculated on spreadsheet, then add protein lysate (amount specified on spreadsheet).
3. Make Loading Buffer in a separate 1.5mL tube; solution should be 19 parts Laemmli's Sample Buffer, 1 part BME (calculation on spreadsheet). This should be added 1:1 with the rest of your protein solution (protein+water made in step 2), see spreadsheet for calculation. ADD AND STORE BME in fume hood.
4. Put samples on heat block set at 100C for 5 minutes. Squirt DI H2O on set to help seal space between tube and set. Make sure tubes are sealed and use forceps to poke holes in top of tube so that the pressure does not build up. DO NOT BOIL STANDARD.

Run Gel
1. During 5 minutes-Add gel to box
   a. Cut bottom film from ready gel (leave no black from cut line).
   b. Add gel to box with comb facing inward (push all the way down and lock). The shorter plate faces the inside.
   c. Carefully remove comb.
   d. Add running buffer and then add to box (fill to top in inner and near top to outer).
2. Add protein samples and ladder (15uL for ladder, usually 30uL for protein samples depending on gel lane size).
3. Run the gel at 150 volts, max current and power for ~30-45 min (until visible bands reach bottom of gel, near wire).

Transfer
1. While the gel is running, soak the PVDF membrane in 100% methanol.
2. Soak PVDF membrane, 2 fiber pads, 2 pieces of thin transfer/filter paper in transfer buffer right before the gel is done.
3. Take the gel out of the cassette and gently break it open in transfer buffer. Pour out Running Buffer, but DO NOT wash gel box (need a small amount of SDS in transfer buffer).
4. Cut off top and bottom parts of gel with green blade.
5. Open up the cassette (black and clear parts) and lay the black part down.
6. Put items in following order on the black part: fiber pad, filter paper, gel, PVDF membrane, filter paper, fiber pad. Roll out air bubbles with pipette after you add membrane, paper, and pad.

7. Cut one corner of the membrane so that you remember which side of the membrane is in contact with the gel.
8. Close and clamp cassette.
9. Place the holder into the trans-blot, BLACK FACING BLACK.
10. Put box in bin (like the small autoclave bin) on stir plate with magnetic stirrer set at a 9, add transblot, and BioIce (in freezer).
11. Fill box to the top with transfer buffer.
12. Add ice to the bin to surround the box. This is to keep the transfer cold.
13. Set transfer for 200V, 500mA, 40W current for 3 hours for proteins above 175kDa, 2.5 hours for proteins 100-175kDa, 1.5 hours for 45-100kDa, and 1 hour for less than 45kDa (RT) and stir at Fast setting.

Probe with Antibodies
14. While transferring, make 5% milk (1g non-fat milk with 20ml TBST) in 50mL conical tube and 1% milk (1g non-fat milk with 100mL TBST) in flask. Add stir bar to flask and stir to mix.
15. Take apart trans-blot and remove the membrane and put into a tray with 5% milk, rock at RT for 1 hour (this can be extended if there is a lot of background).
16. Rinse membrane quickly with 1% milk in TBST.
17. Place the membrane in 1% milk and add the primary antibody (usually about 5mL milk needed) at the proper dilution.
18. Incubate overnight in the cold room using gentle tilting.

DAY 3
19. Rinse once quickly, then 3X for 10 minutes each in TBST using gentle tilting.
20. Add secondary antibody to the membrane in 1% nonfat dry milk (usually about 1:5000 dilution).
21. Incubate for 45 minutes at RT using gentle tilting.
22. Rinse 3X, 10 minutes each in TBST using gentle tilting.

Expose Membrane to Film
1. In foil-wrapped 15mL conical tube, mix together 2.5mL of SuperSignal West Pico Stable Peroxide Solution and 2.5mL of SuperSignal West Pico Luminal/Enhancer Solution (1:1 ratio) (ECL Solution).
2. Lay the membrane on Plastic Wrap and put ECL solution on the membrane (~5mL/membrane).
3. Turn off the lights and let the solution sit on the membrane for 5 minutes.
4. Transfer membrane with forceps over to new Plastic Wrap which is laid on top of a book or the film box.

5. Add a new piece of Plastic Wrap over the top of the membrane and seal. Roll out any air bubbles with pipette.
6. Cut Plastic Wrap around membrane.
7. Place and tape membrane into the cassette.
8. Take cassette, film, scissors, pen, and timer to the dark room (2nd floor C wing of LSRC).
9. Remove film and cut corner to match the cut corner on the membrane. Place film on membrane, and close cassette. The film can be cut in half if only one membrane is being used.
10. Set timer for exposure time (3 minutes is a good place to start).
11. Remove film from cassette at end of exposure time, flip over, and add to developing machine.
12. Repeat film exposure with other pieces of film and adjust exposure time as necessary.
13. Analyze films using densitometry (see protocol below).

Strip Membrane (Only necessary if reprobing)
1. Submerge membrane in RESTORE Stripping Solution (Pierce) and incubate at RT for 15 minutes with occasional agitation.
2. Wash with TBST 3X for 5 minutes each. Repeat steps 1 and 2 of this section.
3. Re-block in 5% milk for 1 hour at RT, then can probe for a different primary antibody.

Data Analysis – Densitometry Protocol (Using ImageJ Software)
1. Scan films with scanner.
2. Open ImageJ Software. Go to File>Open and open the scanned image of your membrane.
3. Select the rectangle tool and draw a box around your first lane. Make sure that you do not overlap an y other lanes.
4. Once first lane is selected, go to Analyze>Gels>Select First Lane, or type ctrl+1.
5. Drag box onto the next land and go to Analyze>Gels>Select Next Lane, or type ctrl+2. The box for each lane must be the same size. Make sure that each box encloses only the desired lane and does not overlap with other bands … this will create error in your data.
6. Repeat this until all lanes on your gel have been selected.
7. Go to Analyze>Gels>Plot Lanes, or type ctrl+3.
8. Select the line drawing tool and draw a horizontal line even with the baseline (no signal) part of the graph for each line. Make sure that the curve corresponding to your band is completely closed in by this line (draw vertical lines if necessary to

create a closed shape. NOTE: Your procedure for this part isn't as important as making sure you are consistent with what you do for all bands.

9. Select the wand tool (to the left of the text tool). Click inside each closed curve. Another box will appear, containing the area of the enclosed area (arbitrary units).

10. If you are using a loading control or standard (such as B-actin), divide the numbers you get by the corresponding number for that control for the same lane.

11. Plot your results using excel.

Appendix J: JMP Statistical Package for ANOVA and post-hoc Tukey Test

2-factor ANOVA
1. Copy and paste data into JMP.
2. Name the columns by double clicking on the column header.
3. If necessary, stack columns. Go to **Tables->Stack Columns**. Stack your numerical data. The data type is shown by an icon next to the column name at the left hand side of the window.
4. Rename the "label" column to reflect the condition.
5. Go to **Analyze -> Fit Model**
6. Under **Y**, add the "data" column.
7. Under **Construct Model Effects** add your factors (i.e. "days post plating", "cell type"). You should have two factors for a 2-factor ANOVA. If you only have one factor, you are doing a one-way ANOVA. This is also known as a t-test.
8. After you have added your factors, hit **Run**.
9. In the results window, look under effect tests for the p-values.

Tukey Test
1. Copy and paste data into JMP.
2. Name the columns by double clicking on the column header.
3. If necessary, stack columns. Go to **Tables->Stack Columns**. Stack your numerical data. The data type is shown by an icon next to the column name at the left hand side of the window.
4. Rename the "label" column to reflect the condition.
5. Go to **Analyze -> Fit Y by X**.
6. Add the "data" column, to "Y, response" by clicking on the **"Y, response"** button.
7. Add any factors to "X, factor" by clicking on the **"X, factor"** button.
8. Click **ok**.
9. In the results window, click the little red arrow next to the graph.
10. Select **Compare Means -> All Pairs, Tukey HSD**.
11. If necessary, click the little red arrow next to the newly generated graph.
12. Select **Connecting Letters Report**.

References

1. Ahmann KA, Johnson SL, Hebbel RP, Tranquillo RT. Shear Stress Responses Of Adult Blood Outgrowth Endothelial Cells Seeded On Bioartifical Tissue. Tissue Eng. 2011.

2. Albelda SM, Sampson PM, Haselton FR, McNiff JM, Mueller SN, Williams SK et al. Permeability characteristics of cultured endothelial cell monolayers. Journal of Applied Physiology. 1988;64(1):308-22.

3. Balaban NQ, Schwarz US, Riveline D, Goichberg P, Tzur G, Sabanay I et al. Force and focal adhesion assembly: a close relationship studied using elastic micropatterned substrates. Nat Cell Biol. 2001;3(5):466-72.

4. Balda MS, Gonzalez-Mariscal L, Matter K, Cereijido M, Anderson JM. Assembly of the tight junction: the role of diacylglycerol. Journal of Cell Biology. 1993;123(2):293-302.

5. Beatch M, Jesaitis LA, Gallin WJ, Goodenough DA, Stevenson BR. The Tight Junction Protein ZO-2 Contains Three PDZ (PSD-95/Discs-Large/ZO-1) Domains and an Alternatively Spliced Region. Journal of Biological Chemistry. 1996;271(42):25723-6.

6. Bell FP, Adamson IL, Schwartz CJ. Aortic endothelial permeability to albumin: Focal and regional patterns of uptake and transmural distribution of 131I-albumin in the young pig. Experimental and Molecular Pathology. 1974;20(1):57-68.

7. Beningo KA, Dembo M, Kaverina I, Small JV, Wang Y-l. Nascent Focal Adhesions Are Responsible for the Generation of Strong Propulsive Forces in Migrating Fibroblasts. The Journal of Cell Biology. 2001;153(4):881-8.

8. Boon R, Leyen T, Fontijn R, Fledderus J, Baggen J, Volger O et al. KLF2-induced actin shear fibers control both alignment to flow and JNK signaling in vascular endothelium. Blood. 2010;115:2533-42.

9. Braidy N, Guillemin GJ, Mansour H, Chan-Ling T, Poljak A, Grant R. Age Related Changes in NAD+ Metabolism Oxidative Stress and Sirt1 Activity in Wistar Rats. PLoS ONE. 2011;6(4):e19194.

10. Bratzler R, Chisolm G, Colton C, Smith K, Zilversmit D, Lees R. The distribution of labeled albumin across the rabbit thoracic aorta in vivo. Circulation Research. 1977;40(2):182-90.

11. Brown MA, Wallace CS, Angelos M, Truskey GA. Characterization of Umbilical Cord Blood-Derived Late Outgrowth Endothelial Progenitor Cells Exposed to Laminar Shear Stress. Tissue Engineering Part A. 2009;15(11):3575-87.

12. Brown MA, Zhang L, Levering VW, Wu JH, Satterwhite LL, Brian L et al. Human Umbilical Cord Blood-Derived Endothelial Cells Reendothelialize Vein Grafts and Prevent Thrombosis. Arteriosclerosis, Thrombosis, and Vascular Biology. 2010.

13. Burrig K. The endothelium of advanced arteriosclerotic plaques in humans. Arteriosclerosis, Thrombosis, and Vascular Biology. 1991;11(6):1678-89.

14. Cai H. Hydrogen peroxide regulation of endothelial function: Origins, mechanisms, and consequences. Cardiovascular Research. 2005;68(1):26-36.

15. Cai H, Harrison DG. Endothelial Dysfunction in Cardiovascular Diseases: The Role of Oxidant Stress. Circulation Research. 2000;87(10):840-4.

16. Califano J, Reinhart-King C. Substrate Stiffness and Cell Area Predict Cellular Traction Stresses in Single Cells and Cells in Contact. Cel Mol Bioeng. 2010;3(1):68-75.

17. Campisi J. Replicative Senescence: An Old Lives' Tale? Cell. 1996;84(4):497-500.

18. Cancel LM, Fitting A, Tarbell JM. In vitro study of LDL transport under pressurized (convective) conditions. American Journal of Physiology. 2007;293(1):H126-H32.

19. Cancel LM, Tarbell JM. The role of apoptosis in LDL transport through cultured endothelial cell monolayers. Atherosclerosis. 2010;208(2):335-41.

20. Cao L, Wu A, Truskey GA. Biomechanical effects of flow and coculture on human aortic and cord blood-derived endothelial cells. Journal of Biomechanics. 2011;44(11):2150-7.

21. Chang YS, Munn LL, Hillsley MV, Dull RO, Yuan J, Lakshminarayanan S et al. Effect of vascular endothelial growth factor on cultured endothelial cell monolayer rransport properties. Microvasc Res. 2000;59(2):265-77.

22. Chappell D, Jacob M, Rehm M, Stoeckelhuber M, Welsch U, Conzen P et al. Heparinase selectively sheds heparan sulfate from the endothelial glycocalyx. Biological Chemistry. 2007;389(1):79-82.

23. Chen Z, Peng I-C, Cui X, Li Y-S, Chien S, Shyy J-J. Shear stress, SIRT1, and vascular homeostasis. Proc Natl Acad Sci. 2010;107:10268–73

24. Chen Z, Peng I-C, Cui X, Li Y-S, Chien S, Shyy JY-J. Shear stress, SIRT1, and vascular homeostasis. Proceedings of the National Academy of Sciences. 2010;107(22):10268-73.

25. Chen Z, Peng I-C, Cuia X, Li Y-S, Chien S, Shyy JY-J. Shear stress, SIRT1, and vascular homeostasis. Proc Natl Acad Sci. 2010;107:10268–73.

26. Cheung T, Ganatra M, Fu J, Truskey G. The Effect of Stress-Induced Senescence on Aging Human Cord Blood-Derived Endothelial Cells. Cardiovasc Eng Tech. 2013;4(2):220-30.

27. Cheung TM, Ganatra MP, Peters EB, Truskey GA. Effect of cellular senescence on the albumin permeability of blood-derived endothelial cells. American Journal of Physiology - Heart and Circulatory Physiology. 2012;303(11):H1374-H83.

28. Cheung TM, Ganatra MP, Peters EB, Truskey GA. Effect of cellular senescence on the albumin permeability of blood-derived endothelial cells. vol 11. 2012.

29. Cheung TM, Ganatra MP, Peters EB, Truskey GA. The Effect of Cellular Senescence on the Albumin Permeability of Blood-Derived Endothelial Cells. American Journal of Physiology - Heart and Circulatory Physiology. 2012;303(11):H1374 - H83.

30. Chi Q, Yin T, Gregersen H, Deng X, Fan Y, Zhao J et al. Rear actomyosin contractility-driven directional cell migration in three-dimensional matrices: a mechano-chemical coupling mechanism. Journal of The Royal Society Interface. 2014;11(95).

31. Chien S. Effects of Disturbed Flow on Endothelial Cells. Annals of biomedical engineering. 2008;36(4):554-62.

32. Chiu J-J, Chien S. Effects of Disturbed Flow on Vascular Endothelium: Pathophysiological Basis and Clinical Perspectives. Physiological Reviews. 2011;91(1):327-87.

33. Chiu JJ, Chien S. Effects of Disturbed Flow on Vascular Endothelium: Pathophysiological Basis and Clinical Perspectives. Physiol Rev. 2011;91:327-87.

34. Choquet D, Felsenfeld DP, Sheetz MP. Extracellular Matrix Rigidity Causes Strengthening of Integrin–Cytoskeleton Linkages. Cell. 1997;88(1):39-48.

197

35. Chu T, Peters D. Serial analysis of the vascular endothelial transcriptome under static and shear stress conditions. Physiol Genom. 2008;34:185-92.

36. Cines DB, Pollak ES, Buck CA, Loscalzo J, Zimmerman GA, McEver RP et al. Endothelial cells in physiology and in the pathophysiology of vascular disorders. Blood. 1998;91:3527-61.

37. Colgan OC, Ferguson G, Collins NT, Murphy RP, Meade G, Cahill PA et al. Regulation of bovine brain microvascular endothelial tight junction assembly and barrier function by laminar shear stress. American Journal of Physiology. 2007;292(6):H3190-H7.

38. Collins C, Tzima E. Hemodynamic forces in endothelial dysfunction and vascular aging. Experimental Gerontology. 2011;46(2–3):185-8.

39. Collins NT, Cummins PM, Colgan OC, Ferguson G, Birney YA, Murphy RP et al. Cyclic Strain–Mediated Regulation of Vascular Endothelial Occludin and ZO-1. Arteriosclerosis, Thrombosis, and Vascular Biology. 2006;26(1):62-8.

40. Conway Daniel E, Breckenridge Mark T, Hinde E, Gratton E, Chen Christopher S, Schwartz Martin A. Fluid Shear Stress on Endothelial Cells Modulates Mechanical Tension across VE-Cadherin and PECAM-1. Current Biology. 2013;23(11):1024-30.

41. Csiszar A, Labinskyy N, Pinto JT, Ballabh P, Zhang H, Losonczy G et al. Resveratrol induces mitochondrial biogenesis in endothelial cells. American Journal of Physiology. 2009;297(1):H13-H20.

42. Cullere X, Shaw SK, Andersson L, Hirahashi J, Luscinskas FW, Mayadas TN. Regulation of vascular endothelial barrier function by Epac, a cAMP-activated exchange factor for Rap GTPase. Blood. 2005;105(5):1950-5.

43. Dai G, Vaughn S, Zhang Y, Wang ET, Garcia-Cardena G, Gimbrone MA. Biomechanical Forces in Atherosclerosis-Resistant Vascular Regions Regulate Endothelial Redox Balance via Phosphoinositol 3-Kinase/Akt-Dependent Activation of Nrf2. Circulation Research. 2007;101(7):723-33.

44. Davies PF. Flow-mediated endothelial mechanotransduction. Physiol Rev. 1995;75:519–60.

45. Davies PF. Hemodynamic shear stress and the endothelium in cardiovascular pathophysiology Nature Clin Pract Cardiovasc med. 2009;6:16-26.

46. Dekker R, van Soest S, Fontijn R, Salamanca S, de Groot P, VanBavel E et al. Prolonged fluid shear stress induces a distinct set of endothelial cell genes, most specifically lung Kruppel-like factor (KLF2). Blood. 2002;100:1689-98.

47. DeMaio L, Chang YS, Gardner TW, Tarbell JM, Antonetti DA. Shear stress regulates occludin content and phosphorylation. American Journal of Physiology. 2001;281(1):H105-H13.

48. Dewey CF. Effects of fluid flow on living vascular cells. Journal of Biomechanical Engineering. 1984;106:31-5.

49. Dumbauld DW, Lee TT, Singh A, Scrimgeour J, Gersbach CA, Zamir EA et al. How vinculin regulates force transmission. Proceedings of the National Academy of Sciences. 2013;110(24):9788-93.

50. Ebong EE, Lopez-Quintero SV, Rizzo V, Spray DC, Tarbell JM. Shear-induced endothelial NOS activation and remodeling via heparan sulfate, glypican-1, and syndecan-1. Integrative Biology. 2014;6(3):338-47.

51. Ebong EE, Macaluso FP, Spray DC, Tarbell JM. Imaging the Endothelial Glycocalyx In Vitro by Rapid Freezing/Freeze Substitution Transmission Electron Microscopy. Arteriosclerosis, Thrombosis, and Vascular Biology. 2011;31(8):1908-15.

52. Elias BC, Suzuki T, Seth A, Giorgianni F, Kale G, Shen L et al. Phosphorylation of Y398 and Y402 in occludin prevents its interaction with ZO-1 and destabilizes its assembly at the tight junctions. J Biol Chem. 2008:M804783200.

53. Erusalimsky JD, Skene C. Mechanisms of endothelial senescence. Exptl Physiol. 2009;94(3):299-304.

54. Erusalimsky JD, Skene C. Mechanisms of endothelial senescence. Experimental Physiology. 2009;94(3):299-304.

55. Farrall AJ, Wardlaw JM. Blood–brain barrier: Ageing and microvascular disease – systematic review and meta-analysis. Neurobiology of Aging. 2009;30(3):337-52.

56. Fernández-Martín L, Marcos-Ramiro B, Bigarella CL, Graupera M, Cain RJ, Reglero-Real N et al. Crosstalk Between Reticular Adherens Junctions and Platelet Endothelial Cell Adhesion Molecule-1 Regulates Endothelial Barrier Function. Arteriosclerosis, Thrombosis, and Vascular Biology. 2012;32(8):e90-e102.

57. Florian JA, Kosky JR, Ainslie K, Pang Z, Dull RO, Tarbell JM. Heparan Sulfate Proteoglycan Is a Mechanosensor on Endothelial Cells. Circulation Research. 2003;93(10):e136-e42.

58. Franke R-P, Gräfe M, Schnittler H, Seiffge D, Mittermayer C, Drenckhahn D. Induction of human vascular endothelial stress fibres by fluid shear stress. Nature. 1984;307:648-9.

59. Fukuhara S, Sakurai A, Sano H, Yamagishi A, Somekawa S, Takakura N et al. Cyclic AMP potentiates vascular endothelial cadherin-mediated cell-cell contact to enhance endothelial barrier function through an Epac-Rap1 signaling pathway. Mol Cell Biol. 2005;25(1):136-46.

60. Galbraith CG, Yamada KM, Sheetz MP. The relationship between force and focal complex development. The Journal of Cell Biology. 2002;159(4):695-705.

61. Gallant ND, Michael KE, García AJ. Cell Adhesion Strengthening: Contributions of Adhesive Area, Integrin Binding, and Focal Adhesion Assembly. Molecular Biology of the Cell. 2005;16(9):4329-40.

62. Garfinkel S, Hu X, Prudovsky IA, McMahon GA, Kapnik EM, McDowell SD et al. FGF-1-dependent proliferative and migratory responses are impaired in senescent human umbilical vein endothelial cells and correlate with the inability to signal tyrosine phosphorylation of fibroblast growth factor receptor-1 substrates. The Journal of Cell Biology. 1996;134(3):783-91.

63. Gertz M, Fischer F, Nguyen GTT, Lakshminarasimhan M, Schutkowski M, Weyand M et al. Ex-527 inhibits Sirtuins by exploiting their unique NAD+-dependent deacetylation mechanism. Proceedings of the National Academy of Sciences. 2013;110(30):E2772-E81.

64. Giantsos-Adams K, Koo A-A, Song S, Sakai J, Sankaran J, Shin J et al. Heparan Sulfate Regrowth Profiles Under Laminar Shear Flow Following Enzymatic Degradation. Cel Mol Bioeng. 2013;6(2):160-74.

65. Gracia-Sancho J, Villarreal Jr. G, Zhang Y, Garcıa-Cardena G. Activation of SIRT1 by resveratrol induces KLF2 expression conferring an endothelial vasoprotective phenotype. Cardiovasc Res. 2010;85:514-9.

66. Gu J, Wang C, Fan H, Ding H, Xie X, Xu Y et al. Effects of Resveratrol on Endothelial Progenitor Cells and Their Contributions to Reendothelialization in Intima-injured Rats. Journal of Cardiovascular Pharmacology. 2006;47(5):711-21.

67. Hagensen MK, Shim J, Thim T, Falk E, Bentzon JF. Circulating Endothelial Progenitor Cells Do Not Contribute to Plaque Endothelium in Murine Atherosclerosis. Circulation. 2010;121(7):898-905.

68. Hahn C, Orr AW, Sanders JM, Jhaveri KA, Schwartz MA. The Subendothelial Extracellular Matrix Modulates JNK Activation by Flow. Circ Res. 2009;104:995-1003.

69. Hahn C, Schwartz MA. Mechanotransduction in vascular physiology and atherogenesis. Nat Rev Mol Cell Biol. 2009;10(1):53-62.

70. Hahn C, Wang C, Orr AW, Coon BG, Schwartz MA. JNK2 Promotes Endothelial Cell Alignment under Flow. PLoS ONE. 2011;6(8):e24338.

71. Halcox J, Schenke W, Zalos G, Mincemoyer R, Prasad A, Waclawiw M et al. Prognostic value of coronary vascular endothelial dysfunction. Circulation. 2002;106:653-8.

72. Haraldsson B, Nyström J, Deen WM. Properties of the Glomerular Barrier and Mechanisms of Proteinuria. vol 2. 2008.

73. Haraldsson B, Nyström J, Deen WM. Properties of the Glomerular Barrier and Mechanisms of Proteinuria. Physiol Rev. 2008;88(2):451-87.

74. Harris AK, Wild P, Stopak D. Silicone Rubber Substrata: A New Wrinkle in the Study of Cell Locomotion. Science. 1980;208(4440):177-9.

75. Harrison DG, Widder J, Grumbach I, Chen W, Weber M, Searles C. Endothelial mechanotransduction, nitric oxide and vascular inflammation. Journal of Internal Medicine. 2006;259(4):351-63.

76. Hartmannsgruber V, Heyken W-T, Kacik M, Kaistha A, Grgic I, Harteneck C et al. Arterial Response to Shear Stress Critically Depends on Endothelial TRPV4 Expresssion. PLoS ONE. 2007;2(9):e827.

77. Henderson-Toth CE, Jahnsen ED, Jamarani R, Al-Roubaie S, Jones EAV. The glycocalyx is present as soon as blood flow is initiated and is required for normal vascular development. Developmental Biology. 2012;369(2):330-9.

78. Henry CBS, Duling BR. TNF-α increases entry of macromolecules into luminal endothelial cell glycocalyx. American Journal of Physiology - Heart and Circulatory Physiology. 2000;279(6):H2815-H23.

79. Herrmann RA, Malinauskas RA, Truskey GA. Characterization of sites of elevated low density lipoprotein at the intercostal, celiac, and iliac branches of the rabbit aorta. Arteriosclerosis, Thrombosis, and Vascular Biology. 1994;14(313–323).

80. Hirschi KK, Ingram DA, Yoder MC. Assessing identity, phenotype, and fate of endothelial progenitor cells. Arteriosclerosis, Thrombosis, and Vascular Biology. 2008;28(9):1584-95.

81. Huang J, Deng H, Peng X, Li S, Xiong C, Fang J. Cellular Traction Force Reconstruction Based on a Self-adaptive Filtering Scheme. Cel Mol Bioeng. 2012;5(2):205-16.

82. Huang J, Peng X, Qin L, Zhu T, Xiong C, Zhang Y et al. Determination of Cellular Tractions on Elastic Substrate Based on an Integral Boussinesq Solution. Journal of Biomechanical Engineering. 2009;131(6):061009-.

83. Huang J, Zhu T, Pan X, Qin L, Peng X, Xiong C et al. A high-efficiency digital image correlation method based on a fast recursive scheme. Meas Sci Technol. 2010;21:025101.

84. Huddleson JP, Ahmad N, Srinivasan S, Lingrel JB. Induction of KLF2 by Fluid Shear Stress Requires a Novel Promoter Element Activated by a Phosphatidylinositol 3-Kinase-dependent Chromatin-remodeling Pathway. Journal of Biological Chemistry. 2005;280(24):23371-9.

85. Hur SS, del Álamo JC, Park JS, Li Y-S, Nguyen HA, Teng D et al. Roles of cell confluency and fluid shear in 3-dimensional intracellular forces in endothelial cells. Proceedings of the National Academy of Sciences. 2012;109(28):11110-5.

86. Hur SS, del Alamo JC, Park JS, Li YS, Nguyen HA, Teng D et al. Roles of cell confluency and fluid shear in 3-dimensional intracellular forces in endothelial cells Proc Natl Acad Sc. 2012;109:11110-5.

87. Huynh J, Nishimura N, Rana K, Peloquin JM, Califano JP, Montague CR et al. Age-Related Intimal Stiffening Enhances Endothelial Permeability and Leukocyte Transmigration. Science Translational Medicine. 2011;3(112):112ra22.

88. Ingram DA, Mead LE, Moore DB, Woodard W, Fenoglio A, Yoder MC. Vessel wall-derived endothelial cells rapidly proliferate because they contain a complete hierarchy of endothelial progenitor cells. Blood. 2005;105(7):2783-6.

89. Ingram DA, Mead LE, Tanaka H, Meade V, Fenoglio A, Mortell K et al. Identification of a novel hierarchy of endothelial progenitor cells using human peripheral and umbilical cord blood. Blood. 2004;104(9):2752-60.

90. Jickling G, Salam A, Mohammad A, Hussain MS, Scozzafava J, Nasser AM et al. Circulating Endothelial Progenitor Cells and Age-Related White Matter Changes. Stroke. 2009;40(10):3191-6.

91. Karino T, Goldsmith HL, Motomiya M, Mabuchi S, Sohara Y. Flow Patterns in Vessels of Simple and Complex Geometriesa. Annals of the New York Academy of Sciences. 1987;516(1):422-41.

92. Ku D, Giddens D, Zarins C, Glasgov S. Pulsatile flow and atherosclerosis in the human carotid bifurcation: positive correlation between plaque location and low and oscillating shear stress. Arteriosclerosis. 1985;5:293-302.

93. Kuddannaya S, Chuah YJ, Lee MHA, Menon NV, Kang Y, Zhang Y. Surface Chemical Modification of Poly(dimethylsiloxane) for the Enhanced Adhesion and Proliferation of Mesenchymal Stem Cells. ACS Applied Materials & Interfaces. 2013;5(19):9777-84.

94. Lam CRI, Tan C, Teo Z, Tay CY, Phua T, Wu YL et al. Loss of TAK1 increases cell traction force in a ROS-dependent manner to drive epithelial-mesenchymal transition of cancer cells. Cell Death Dis. 2013;4:e848.

95. Lan F, Cacicedo JM, Ruderman N, Ido Y. SIRT1 Modulation of the Acetylation Status, Cytosolic Localization, and Activity of LKB1: POSSIBLE ROLE IN AMP-ACTIVATED

PROTEIN KINASE ACTIVATION. Journal of Biological Chemistry. 2008;283(41):27628-35.

96. Levsque M, Nerem R. The elongation and orientation of cultured endothelial cells in response to shear stress. Journal of Biomechanical Engineering. 1985;107(4):341-7.

97. Lin S-J, Jan K-M, Schuessler G, Weinbaum S, Chien S. Enhanced macromolecular permeability of aortic endothelial cells in association with mitosis. Atherosclerosis. 1988;73(2-3):223-32.

98. Livak KJ, Schmittgen TD. Analysis of Relative Gene Expression Data Using Real-Time Quantitative PCR and the 2−ΔΔCT Method. Methods. 2001;25(4):402-8.

99. Mammone T, Gan D, Foyouzi-Youssefi R. Apoptotic cell death increases with senescence in normal human dermal fibroblast cultures. Cell Biology International. 2006;30(11):903-9.

100. Maquart F-X, Brézillon S, Wegrowski Y. Proteoglycans in Skin Aging. In: Farage M, Miller K, Maibach H, editors. Textbook of Aging Skin. Springer Berlin Heidelberg; 2010. p. 109-20.

101. Marechal X, Favory R, Joulin O, Montaigne D, Hassoun S, Decoster B et al. Endothelial Glycocalyx Damage During Endotoxemia Coincides With Microcirculatory Dysfunction and Vascular Oxidative Stress. Shock. 2008;29(5):572-6 10.1097/SHK.0b013e318157e926.

102. Matsushita H, Chang E, Glassford AJ, Cooke JP, Chiu C-P, Tsao PS. eNOS Activity Is Reduced in Senescent Human Endothelial Cells. Circulation Research. 2001;89(9):793-8.

103. Mattagajasingh I, Kim C-S, Naqvi A, Yamamori T, Hoffman TA, Jung S-B et al. SIRT1 promotes endothelium-dependent vascular relaxation by activating endothelial nitric oxide synthase. Proceedings of the National Academy of Sciences. 2007;104(37):14855-60.

104. Megens RTA, Reitsma S, Schiffers PHM, Hilgers RHP, De Mey JGR, Slaaf DW et al. Two-Photon Microscopy of Vital Murine Elastic and Muscular Arteries. Journal of Vascular Research. 2007;44(2):87-98.

105. Mehta D, Malik AB. Signaling mechanisms regulating endothelial permeability Physiol Rev. 2006;86:279-367.

106. Meyer G, Merval R, Tedgui A. Effects of Pressure-Induced Stretch and Convection on Low-Density Lipoprotein and Albumin Uptake in the Rabbit Aortic Wall. Circulation Research. 1996;79(3):532-40.

107. Milne JC, Lambert PD, Schenk S, Carney DP, Smith JJ, Gagne DJ et al. Small molecule activators of SIRT1 as therapeutics for the treatment of type 2 diabetes. Nature. 2007;450(7170):712-6.

108. Minamino T, Miyauchi H, Yoshida T, Ishida Y, Yoshida H, Komuro I. Endothelial Cell Senescence in Human Atherosclerosis. Circulation. 2002;105:1541-4.

109. Minamino T, Miyauchi H, Yoshida T, Ishida Y, Yoshida H, Komuro I. Endothelial Cell Senescence in Human Atherosclerosis. Circulation. 2002;105(13):1541-4.

110. Moldovan L, Mythreye K, Goldschmidt-Clermont PJ, Satterwhite LL. Reactive oxygen species in vascular endothelial cell motility. Roles of NAD(P)H oxidase and Rac1. Cardiovascular Research. 2006;71(2):236-46.

111. Moon JJ, Matsumoto M, Patel S, Lee L, Guan J-L, Li S. Role of cell surface heparan sulfate proteoglycans in endothelial cell migration and mechanotransduction. Journal of Cellular Physiology. 2005;203(1):166-76.

112. Mun GI, Boo YC. Identification of CD44 as a senescence-induced cell adhesion gene responsible for the enhanced monocyte recruitment to senescent endothelial cells. Am J Physiol. 2010;298:H2102-H11.

113. Mun GI, Kim IS, Lee BH, Boo YC. Endothelial Argininosuccinate Synthetase 1 Regulates Nitric Oxide Production and Monocyte Adhesion under Static and Laminar Shear Stress Conditions. J Biol Chem. 2011;286:2536–42.

114. Mun GI, Lee SJ, An SM, Kim IK, Boo YC. Differential gene expression in young and senescent endothelial cells under static and
laminar shear stress conditions. Free Rad Biol Med. 2009;47:291–9.

115. Munevar S, Wang Y-l, Dembo M. Traction Force Microscopy of Migrating Normal and H-ras Transformed 3T3 Fibroblasts. Biophysical Journal. 2001;80(4):1744-57.

116. Murakami T, Felinski EA, Antonetti DA. Occludin Phosphorylation and Ubiquitination Regulate Tight Junction Trafficking and Vascular Endothelial Growth Factor-induced Permeability. Journal of Biological Chemistry. 2009;284(31):21036-46.

117. Nerem RM. Atherogenesis: hemodynamics, vascular geometry, and the endothelium. Biorheology. 1984;21(4):565-9.

118. Nielsen LB, Nordestgaard BG, Stender S, Kjeldsen K. Aortic permeability to LDL as a predictor of aortic cholesterol accumulation in cholesterol-fed rabbits. Arteriosclerosis, Thrombosis, and Vascular Biology. 1992;12:1402–9.

119. Nigro P, Abe J, Berk B. Flow Shear Stress and Atherosclerosis: A Matter of Site Specificity. Antiox Redox Sig. 2011;15:1405-14.

120. Nisoli E, Tonello C, Cardile A, Cozzi V, Bracale R, Tedesco L et al. Calorie Restriction Promotes Mitochondrial Biogenesis by Inducing the Expression of eNOS. Science. 2005;310(5746):314-7.

121. Noda K, Zhang J, Fukuhara S, Kunimoto S, Yoshimura M, Mochizuki N. Vascular Endothelial-Cadherin Stabilizes at Cell–Cell Junctions by Anchoring to Circumferential Actin Bundles through α- and β-Catenins in Cyclic AMP-Epac-Rap1 Signal-activated Endothelial Cells. Molecular Biology of the Cell. 2010;21(4):584-96.

122. Ogami M, Ikura Y, Ohsawa M, Matsuo T, Kayo S, Yoshimi N et al. Endothelial Cell Senescence in Human Atherosclerosis. Arterioscler Thromb Vasc Biol. 2004;24:546-50.

123. Ogami M, Ikura Y, Ohsawa M, Matsuo T, Kayo S, Yoshimi N et al. Telomere shortening in human coronary artery diseases. Arterioscler Thromb Vasc Biol. 2004;24:546-50.

124. Okayama N, Kevil CG, Correia L, Jourd'Heuil D, Itoh M, Grisham MB et al. Nitric oxide enhances hydrogen peroxide-mediated endothelial permeability in vitro. Am J Physiol-Cell Ph. 1997;273(5):C1581-C7.

125. Ota H, Eto M, Kano MR, Ogawa S, Iijima K, Akishita M et al. Cilostazol Inhibits Oxidative Stress–Induced Premature Senescence Via Upregulation of Sirt1 in Human Endothelial Cells. Arteriosclerosis, Thrombosis, and Vascular Biology. 2008;28(9):1634-9.

126. Pahakis MY, Kosky JR, Dull RO, Tarbell JM. The role of endothelial glycocalyx components in mechanotransduction of fluid shear stress. Biochemical and Biophysical Research Communications. 2007;355(1):228-33.

127. Palmer RMJ, Ferrige AG, Moncada S. Nitric oxide release accounts for the biological activity of endothelium-derived relaxing factor. Nature. 1987;327(6122):524-6.

128. Park S-J, Ahmad F, Philp A, Baar K, Williams T, Luo H et al. Resveratrol Ameliorates Aging-Related Metabolic Phenotypes by Inhibiting cAMP Phosphodiesterases. Cell. 2012;148(3):421-33.

129. Park SJ, Ahmad F, Philp A, Baar K, Williams T, Luo H et al. Resveratrol ameliorates aging-related metabolic phenotypes by inhibiting cAMP phosphodiesterases. Cell. 2012;148(3):421-33.

130. Parmar K, Larman H, Dai G, Zhang Y, Wang E, Moorthy S et al. Integration of flow-dependent endothelial phenotypes by Kruppel-like factor 2. J Clin Invest. 2006;116:49-58.

131. Pisconti A, Bernet J, Olwin B. Syndecans in skeletal muscle development, regeneration and homeostasis. Muscle, Ligaments and Tendons Journal. 2012;2(1):1-9.
132. Polio SR, Rothenberg KE, Stamenović D, Smith ML. A micropatterning and image processing approach to simplify measurement of cellular traction forces. Acta Biomaterialia. 2012;8(1):82-8.

133. Pollard T, Earnshaw W, Lippincott-Schwartz J. Cell Biology. Philadelphia, PA, USA: Elsevier, Inc.; 2008.

134. Potente M, Dimmeler S. NO Targets SIRT1: A Novel Signaling Network in Endothelial Senescence. Arteriosclerosis, Thrombosis, and Vascular Biology. 2008;28(9):1577-9.

135. Potter MD, Barbero S, Cheresh DA. Tyrosine Phosphorylation of VE-cadherin Prevents Binding of p120- and β-Catenin and Maintains the Cellular Mesenchymal State. Journal of Biological Chemistry. 2005;280(36):31906-12.

136. Quintas A, de Solís AJ, Díez-Guerra FJ, Carrascosa JM, Bogónez E. Age-associated decrease of SIRT1 expression in rat hippocampus: Prevention by late onset caloric restriction. Experimental Gerontology. 2012;47(2):198-201.

137. Rampersad SN, Ovens JD, Huston E, Umana MB, Wilson LS, Netherton SJ et al. Cyclic AMP phosphodiesterase 4D (PDE4D) Tethers EPAC1 in a vascular endothelial cadherin (VE-Cad)-based signaling complex and controls cAMP-mediated vascular permeability. J Biol Chem. 2010;285(44):33614-22.

138. Rauscher FM, Goldschmidt-Clermont PJ, Davis BH, Wang T, Gregg D, Ramaswami P et al. Aging, Progenitor Cell Exhaustion, and Atherosclerosis. Circulation. 2003;108(4):457-63.

139. Reinhart-King CA, Dembo M, Hammer DA. The Dynamics and Mechanics of Endothelial Cell Spreading. Biophysical Journal. 2005;89(1):676-89.

140. Reinhart-King CA, Dembo M, Hammer DA. Endothelial Cell Traction Forces on RGD-Derivatized Polyacrylamide Substrata. Langmuir. 2002;19(5):1573-9.

141. Reinhart-King CA, Dembo M, Hammer DA. Endothelial Cell Traction Forces on RGD-Derivatized Polyacrylamide Substrata†. Langmuir. 2002;19(5):1573-9.

142. Reitsma S, Slaaf D, Vink H, van Zandvoort MMJ, oude Egbrink MA. The endothelial glycocalyx: composition, functions, and visualization. Pflugers Arch - Eur J Physiol. 2007;454(3):345-59.

143. Reitsma S, Slaaf DW, Vink H, van Zandvoort MAMJ, oude Egbrink MGA. The endothelial glycocalyx: composition, functions, and visualization. Pflugers Archiv. 2007;454(3):345-59.

144. Remuzzi A, Dewey C, Davies P, Gimbrone M. Orientation of endothelial cells in shear fields in vitro. Biorheology. 1984;21:617-30.

145. Rice KM, Desai DH, Kinnard RS, Harris R, Wright GL, Blough ER. Load-induced focal adhesion mechanotransduction is altered with aging in the Fischer 344/NNiaHSd × Brown Norway/BiNia rat aorta. Biogerontology. 2007;8(3):257-67.

146. Rilla K, Siiskonen H, Spicer AP, Hyttinen JMT, Tammi MI, Tammi RH. Plasma Membrane Residence of Hyaluronan Synthase Is Coupled to Its Enzymatic Activity. J Biol Chem. 2005;280(36):31890-7.

147. Riveline D, Zamir E, Balaban NQ, Schwarz US, Ishizaki T, Narumiya S et al. Focal Contacts as Mechanosensors: Externally Applied Local Mechanical Force Induces

Growth of Focal Contacts by an Mdia1-Dependent and Rock-Independent Mechanism. The Journal of Cell Biology. 2001;153(6):1175-86.

148. Roger VL, Go AS, Lloyd-Jones DM, Benjamin EJ, Berry JD, Borden WB et al. Executive Summary: Heart Disease and Stroke Statistics—2012 Update. Circulation. 2012;125(1):188-97.

149. Salmon AHJ, Neal CR, Sage LM, Glass CA, Harper SJ, Bates DO. Angiopoietin-1 alters microvascular permeability coefficients in vivo via modification of endothelial glycocalyx. Cardiovascular Research. 2009;83(1):24-33.

150. Salmon AHJ, Satchell SC. Endothelial glycocalyx dysfunction in disease: albuminuria and increased microvascular permeability. The Journal of Pathology. 2012;226(4):562-74.

151. Schiller HB, Hermann M-R, Polleux J, Vignaud T, Zanivan S, Friedel CC et al. β1- and αv-class integrins cooperate to regulate myosin II during rigidity sensing of fibronectin-based microenvironments. Nat Cell Biol. 2013;15(6):625-36.

152. SenBanerjee S, Lin Z, Atkins G, Greif D, Rao R, Kumar A et al. KLF2 Is a novel transcriptional regulator of endothelial proinflammatory activation. J Exp Med. 2004;199:1305-15.

153. Silacci P, Desgeorges A, Mazzolai L, Chambaz C, Hayoz D. Flow Pulsatility Is a Critical Determinant of Oxidative Stress in Endothelial Cells. Hypertension. 2001;38(5):1162-6.

154. Sniadecki NJ, Chen CS. Microfabricated Silicone Elastomeric Post Arrays for Measuring Traction Forces of Adherent Cells. In: Yu-Li W, Dennis ED, editors. Methods in Cell Biology. Academic Press; 2007. p. 313-28.

155. Solomon JM, Pasupuleti R, Xu L, McDonagh T, Curtis R, DiStefano PS et al. Inhibition of SIRT1 Catalytic Activity Increases p53 Acetylation but Does Not Alter Cell Survival following DNA Damage. Molecular and Cellular Biology. 2006;26(1):28-38.

156. Sun C, Liu X, Qi L, Xu J, Zhao J, Zhang Y et al. Modulation of vascular endothelial cell senescence by integrin β4. Journal of Cellular Physiology. 2010;225(3):673-81.

157. Tarbell JM. Shear stress and the endothelial transport barrier. Cardiovascular Research. 2010.

158. Tarbell JM. Shear stress and the endothelial transport barrier. Cardiovasc Res. 2010;87(2):320-30.

159. Thi MM, Tarbell JM, Weinbaum S, Spray DC. The role of the glycocalyx in reorganization of the actin cytoskeleton under fluid shear stress: A "bumper-car" model. Proc Natl Acad Sc. 2004;101(47):16483-8.

160. Thompson Peter M, Tolbert Caitlin E, Shen K, Kota P, Palmer Sean M, Plevock Karen M et al. Identification of an Actin Binding Surface on Vinculin that Mediates Mechanical Cell and Focal Adhesion Properties. Structure. 2014;22(5):697-706.

161. Ting L, Jessica R. Jahn J, Jung J, Shuman B, Feghhi S, Han S et al. Flow mechanotransduction regulates traction forces, intercellular forces, and adherens junctions. Am J Physiol. 2012;302:H2220-H9.

162. Topakian R, Barrick TR, Howe FA, Markus HS. Blood–brain barrier permeability is increased in normal-appearing white matter in patients with lacunar stroke and leucoaraiosis. Journal of Neurology, Neurosurgery & Psychiatry. 2010;81(2):192-7.

163. Trott D, Luttrell M, Seawright J, Woodman C. Aging impairs PI3K/Akt signagling and NO-mediated dilation in soleus muscle feed arteries. European Journal of Applied Physiology. 2013;113(8):2039-46.

164. Truskey G, Barber K, Rinker K. Factors influencing the nonuniform localization of monocytes in the arterial wall. Biorheology. 2002;39(3):325-9.

165. Tse JR, Engler AJ. Preparation of Hydrogel Substrates with Tunable Mechanical Properties. Current Protocols in Cell Biology. John Wiley & Sons, Inc.; 2001.

166. Tzima E, Irani-Tehrani M, Kiosses W, Dejana E, Schultz D, Engelhardt B et al. A mechanosensory complex that mediates the endothelial cell response to fluid shear stress. Nature. 2005;437:426–31.

167. Ungvari Z, Bagi Z, Feher A, Recchia FA, Sonntag WE, Pearson K et al. Resveratrol confers endothelial protection via activation of the antioxidant transcription factor Nrf2. American Journal of Physiology. 2010;299(1):H18-H24.

168. van den Berg BM, Spaan JAE, Rolf TM, Vink H. Atherogenic region and diet diminish glycocalyx dimension and increase intima-to-media ratios at murine carotid

artery bifurcation. American Journal of Physiology - Heart and Circulatory Physiology. 2006;290(2):H915-H20.

169. van der Loo B, Fenton MJ, Erusalimsky JD. Cytochemical Detection of a Senescence-Associated β-Galactosidase in Endothelial and Smooth Muscle Cells from Human and Rabbit Blood Vessels. Experimental Cell Research. 1998;241(2):309-15.

170. van Popele NM, Grobbee DE, Bots ML, Asmar R, Topouchian J, Reneman RS et al. Association Between Arterial Stiffness and Atherosclerosis: The Rotterdam Study. Stroke. 2001;32(2):454-60.

171. van Thienen JV, Fledderus JO, Dekker RJ, Rohlena J, van IJzendoorn GA, Kootstra NA et al. Shear stress sustains atheroprotective endothelial KLF2 expression more potently than statins through mRNA stabilization. Cardiovascular Research. 2006;72(2):231-40.

172. Voyvodic PL, Min D, Liu R, Williams E, Chitalia V, Dunn AK et al. Loss of Syndecan-1 Induces a Pro-inflammatory Phenotype in Endothelial Cells with a Dysregulated Response to Atheroprotective Flow. Journal of Biological Chemistry. 2014;289(14):9547-59.

173. Wachtel M, Frei K, Ehler E, Fontana A, Winterhalter K, Gloor SM. Occludin proteolysis and increased permeability in endothelial cells through tyrosine phosphatase inhibition. Journal of Cell Science. 1999;112(23):4347-56.

174. Wallace CS, Champion JC, Truskey GA. Adhesion and function of human endothelial cells co-cultured on smooth muscle cells. Annals of biomedical engineering. 2007;35(3):375-86.

175. Wallace CS, Strike SA, Truskey GA. Smooth muscle cell rigidity and extracellular matrix organization influence endothelial cell spreading and adhesion formation in coculture. Am J Physiol-Cell Ph. 2007;293(3):H1978-H86.

176. Wallace CS, Strike SA, Truskey GA. Smooth muscle cell rigidity and extracellular matrix organization influence endothelial cell spreading and adhesion formation in coculture. vol 3. 2007.

177. Wallace CS, Truskey GA. Direct-contact co-culture between smooth muscle and endothelial cells inhibits TNF-α-mediated endothelial cell activation. American Journal of Physiology - Heart and Circulatory Physiology. 2010;299(2):H338-H46.

178. Walsh TG, Murphy RP, Fitzpatrick P, Rochfort KD, Guinan AF, Murphy A et al. Stabilization of brain microvascular endothelial barrier function by shear stress involves VE-cadherin signaling leading to modulation of pTyr-occludin levels. Journal of Cellular Physiology. 2011;226(11):3053-63.

179. Wang Y-L, Pelham Jr RJ. [39] Preparation of a flexible, porous polyacrylamide substrate for mechanical studies of cultured cells. In: Richard BV, editor. Methods in Enzymology. Academic Press; 1998. p. 489-96.

180. Wang Y-L, Pelham Jr RJ. Preparation of a flexible, porous polyacrylamide substrate for mechanical studies of cultured cells. Methods in Enzymology. 1998;298:489-96.

181. Wann AKT, Ingram KR, Coleman PJ, McHale N, Levick JR. Mechanosensitive hyaluronan secretion: stimulus–response curves and role of transcription–translation–translocation in rabbit joints. Experimental Physiology. 2009;94(3):350-61.

182. Warboys CM, de Luca A, Amini N, Luong L, Duckles H, Hsiao S et al. Disturbed Flow Promotes Endothelial Senescence via a p53-Dependent Pathway. Arteriosclerosis, Thrombosis, and Vascular Biology. 2014;34(5):985-95.

183. Ward BJ, Donnelly JL. Hypoxia induced disruption of the cardiac endothelial glycocalyx: implications for capillary permeability. Cardiovascular Research. 1993;27(3):384-9.

184. Wen JH, Vincent LG, Fuhrmann A, Choi YS, Hribar KC, Taylor-Weiner H et al. Interplay of matrix stiffness and protein tethering in stem cell differentiation. Nat Mater. 2014;13(10):979-87.

185. Wind S, Beuerlein K, Eucker T, Müller H, Scheurer P, Armitage ME et al. Comparative pharmacology of chemically distinct NADPH oxidase inhibitors. British Journal of Pharmacology. 2010;161(4):885-98.

186. Wojciak-Stothard B, Potempa S, Eichholtz T, Ridley AJ. 9Rgr; and Rac but not Cdc42 regulate endothelial cell permeability. Journal of Cell Science. 2001;114(7):1343-55.

187. Wu W, Xiao H, Laguna-Fernandez A, Villarreal G, K-C. W, Geary G et al. Flow-Dependent Regulation of Kruppel-Like Factor 2 Is Mediated by MicroRNA-92a. Circulation. 2011;124:633-41.

188. Xia L, Wang XX, Hu XS, Guo XG, Shang YP, Chen HJ et al. Resveratrol reduces endothelial progenitor cells senescence through augmentation of telomerase activity by Akt-dependent mechanisms. Br J Pharmacol. 2008;155:387-94.

189. Xia WH, Yang Z, Xu SY, Chen L, Zhang XY, Li J et al. Age-Related Decline in Reendothelialization Capacity of Human Endothelial Progenitor Cells Is Restored by Shear Stress. Hypertension. 2012;59(6):1225-31.

190. Xu Q, Zhang Z, Davison F, Hu Y. Circulating Progenitor Cells Regenerate Endothelium of Vein Graft Atherosclerosis, Which Is Diminished in ApoE-Deficient Mice. Circulation Research. 2003;93(8):e76-e86.

191. Yang H, Zhang W, Pan H, Feldser HG, Lainez E, Miller C et al. SIRT1 Activators Suppress Inflammatory Responses through Promotion of p65 Deacetylation and Inhibition of NF-κB Activity. PLoS ONE. 2012;7(9):e46364.

192. Yao Y, Rabodzey A, Dewey CF. Glycocalyx modulates the motility and proliferative response of vascular endothelium to fluid shear stress. American Journal of Physiology - Heart and Circulatory Physiology. 2007;293(2):H1023-H30.

193. Yeung T, Georges PC, Flanagan LA, Marg B, Ortiz M, Funaki M et al. Effects of substrate stiffness on cell morphology, cytoskeletal structure, and adhesion. Cell Motility and the Cytoskeleton. 2005;60(1):24-34.

194. Zarzuelo MJ, López-Sepúlveda R, Sánchez M, Romero M, Gómez-Guzmán M, Ungvary Z et al. SIRT1 inhibits NADPH oxidase activation and protects endothelial function in the rat aorta: Implications for vascular aging. Biochemical Pharmacology. 2013;85(9):1288-96.

195. Zeng Y, Ebong EE, Fu BM, Tarbell JM. The Structural Stability of the Endothelial Glycocalyx after Enzymatic Removal of Glycosaminoglycans. PLoS ONE. 2012;7(8):e43168.

196. Zeng Y, Tarbell JM. The Adaptive Remodeling of Endothelial Glycocalyx in Response to Fluid Shear Stress. PLoS ONE. 2014;9(1):e86249.

197. Zhang L, Freedman NJ, Brian L, Peppel K. Graft-Extrinsic Cells Predominate in Vein Graft Arterialization. Arteriosclerosis, Thrombosis, and Vascular Biology. 2004;24:470-6.

198. Zhang Q-j, Wang Z, Chen H-z, Zhou S, Zheng W, Liu G et al. Endothelium-specific overexpression of class III deacetylase SIRT1 decreases atherosclerosis in apolipoprotein E-deficient mice. Cardiovascular Research. 2008;80(2):191-9.

199. Zu Y, Liu L, Lee MYK, Xu C, Liang Y, Man RY et al. SIRT1 Promotes Proliferation and Prevents Senescence Through Targeting LKB1 in Primary Porcine Aortic Endothelial Cells. Circulation Research. 2010;106(8):1384-93.

Biography

TRACY MELISSA CHEUNG
Date of Birth: January 22, 1988
Place of Birth: Orlando, Florida

Academic Degrees

Duke University, Durham, North Carolina
- Ph.D. in Biomedical Engineering, December 2014

Cornell University, Ithaca, NY
- B.S. in Biological Engineering, May 2010

Publications

1. Cheung TM, Fu JJ, and Truskey GA. "SIRT1 Regulates Glycocalyx and VE-cadherin to Modulate Response of Senescent Endothelial Cells to Shear Stress." (in submission)
2. Cheung TM, Yan JB, Fu JJ, Huang J, Yuan F, and Truskey GA. " Endothelial Cell Senescence Increases Traction Forces due to Age-Associated Changes in the Glycocalyx and SIRT1." (in submission)
3. Zhao K, Reinhart M, Cheung TM, Wax A, and Truskey GA. "Optimization of Endothelial Seeding in Microfluidic Devices to Create Physiologically-Sized *In vitro* Microcapillaries for High Magnification Visualization Techniques." (in submission)
4. Tracy M. Cheung and George A. Truskey. "Environmental Factors that Influence the Response of the Endothelium to Flow." *Mechanobiology of the Endothelium*. CRC Press. 2014.
5. Cheung TM*, Ganatra MP*, Fu JJ, and Truskey GA. "The Effect of Stress-Induced Senescence on Aging Human Cord Blood-Derived Endothelial Cells." *Cardiovascular Engineering and Technology*. 2013. 4(2): 220-230 (cover art).
6. Cheung TM, Ganatra MP, Peters EB, and Truskey GA. "Effect of Cellular Senescence on the Albumin Permeability of Blood-Derived Endothelial Cells." *American Journal of Physiology – Heart and Circulatory Physiology*. 2013. 303: H1374–H1383.

Awards

Research Awarded Grants

- NIH NRSA F31 Predoctoral Fellowship for "Role of Glycocalyx in Regulating the Aging Endothelial Cell Response to Shear Stress." September 2014-present.
- Duke University McChesney Graduate Fellowship. September 2013-August 2014.
- National Science Foundation Graduate Research Fellowship. August 2010-August 2013.

Travel Awards

- Duke Graduate School Conference Travel Award. July 2014.
- Duke Biomedical Engineering Conference Travel Award. July 2014.
- Duke Graduate School Conference Travel Award. June 2013.
- Duke Biomedical Engineering Conference Travel Award. June 2013.
- Women in Science and Engineering Symposium Best Molecular Podium Presentation Award. December 2012.

Teaching Awards
- Graduate Outstanding Teaching Assistant Award. Duke University. Durham, NC. June 2012.
- Graduate Outstanding Teaching Assistant Award – Honorable Mention. Duke University, Durham, NC. June 2011.